FACTORS AFFECTING THE PHOTODEGRADATION RATES OF POLYMERS

THAT CONTAIN ($-C_5H_4(CO)_3Mo-Mo(CO)_3C_5H_4-$) IN THE BACKBONE

by

BEVIN COLLEEN DAGLEN

A DISSERTATION

Presented to the Department of Chemistry
and the Graduate School of the University of Oregon
in partial fulfillment of the requirements
for the degree of
Doctor of Philosophy

September 2008

University of Oregon Graduate School

Confirmation of Approval and Acceptance of Dissertation prepared by:

Bevin Daglen

Title:

"FACTORS AFFECTING THE PHOTODEGRADATION RATES OF POLYMERS THAT CONTAIN (-C5H4(CO)3MO-MO(CO)3C5H4-) IN THE BACKBONE"

This dissertation has been accepted and approved in partial fulfillment of the requirements for the degree in the Department of Chemistry by:

Catherine Page, Chairperson, Chemistry
David Tyler, Advisor, Chemistry
David Johnson, Member, Chemistry
Darren Johnson, Member, Chemistry
Miriam Deutsch, Outside Member, Physics

and Richard Linton, Vice President for Research and Graduate Studies/Dean of the Graduate School for the University of Oregon.

September 6, 2008

Original approval signatures are on file with the Graduate School and the University of Oregon Libraries.

An Abstract of the Dissertation of

Bevin Colleen Daglen   for the degree of   Doctor of Philosophy

in the Department of Chemistry   to be taken   September 2008

Title: FACTORS AFFECTING THE PHOTODEGRADATION RATES OF

POLYMERS THAT CONTAIN ($-C_5H_4(CO)_3Mo-Mo(CO)_3C_5H_4-$) IN THE

BACKBONE

Approved: _____
Prof. David R. Tyler

There are compelling economic and environmental reasons for using degradable

plastics in selected applications and considerable research is now devoted to devising new

photodegradable polymers with improved performance. Controlling the degradation of

these materials in a prescribed fashion is still a difficult problem because the parameters

that influence degradation rates are not completely understood. In order to predict polymer

lifetimes, to manipulate when a polymer starts to degrade, and to control the rate of

degradation, it is necessary to identify the experimental parameters that affect polymer

degradation rates and to understand how these parameters affect degradation.

This dissertation describes the results of experiments designed to gain fundamental

insight into the factors that affect the rate of polymer photodegradation. The key

experimental strategy employed was the incorporation of organometallic dimers into the

backbone of the polymer chains, specifically, $[CpRMo(CO)_3]_2$ (CpR = a substituted cyclopentadienyl (η^5-C_5H_4R)). Incorporating these organometallic units into a polymer chain make the polymer photodegradable because the metal-metal bond can be cleaved with visible light. The photogenerated metal radicals can then be trapped by O_2 or chlorine, resulting in degradation of the polymer. Another benefit from incorporating this chromophore into the polymer backbone is that it provides the experimentalist with a convenient spectroscopic handle to monitor degradation rates.

Using these model polymers, several experimental factors that can affect polymer photodegradation rates have been explored. For example, experiments showed that radical trap concentration affects degradation rates below, but not above, the polymer glass transition temperature. In addition, degradation rates as a function of irradiation temperature, tensile stress, and time-dependent morphology changes were explored for various polymers. The results of these studies suggest that the ability of the photogenerated radicals to escape the radical cage is the dominant factor in determining photodegradation efficiencies.

This dissertation includes previously published and unpublished co-authored material.

CURRICULUM VITAE

NAME OF AUTHOR: Bevin Colleen Daglen

PLACE OF BIRTH: Camp Lejeune, North Carolina

DATE OF BIRTH: 25 September 1977

GRADUATE AND UNDERGRADUATE SCHOOLS ATTENDED:

> University of Oregon, Eugene, Oregon
> Boise State University, Boise, Idaho

DEGREES AWARDED:

> Doctor of Philosophy in Chemistry, 2008, University of Oregon
> Master of Science in Chemistry, 2005, University of Oregon
> Bachelor of Science in Chemistry, 2003, Boise State University

AREAS OF SPECIAL INTEREST:

> Physical Polymer Chemistry
> Photochemistry
> Organometallic Chemistry
> Science Education

PROFESSIONAL EXPERIENCE:

> Polymer Program Volunteer, Materials Science Institute, University of Oregon, 2004–2007
>
> Graduate GK-12 Fellow, Materials Science Institute, University of Oregon, 2004–2007
>
> Graduate Teaching Fellow, Materials Science Institute, University of Oregon, 2003–2004 & 2007

Women in Graduate Science Past President and Founding Member, University of Oregon, 2004–2008

Adjunct Faculty, Department of Chemistry, Boise State University, 2003

GRANTS, AWARDS AND HONORS:

NSF-IGERT Fellowship, University of Oregon, 2007

Women in Graduate Science Travel Award, University of Oregon, 2007

NSF Debating Science Program, University of Montana, 2007

NSF-GK12 Fellowship, University of Oregon, 2004–2007

ACS Summer School on Green Chemistry, The Johnson Family Foundation, 2006

PUBLICATIONS:

Daglen, B. C.; Tyler, D. R. Application of a Perrin-like Model to Explain the Biphasic Photochemical Degradation Rates of Polymers. *Macromolecules* submitted.

Tyler, D. R.; Daglen, B. C.; Shultz, G. V. Polymers with Metal-metal Bonds as Models in Mechanistic Studies of Polymer Photodegradation. In *Macromolecules Containing Metal and Metal-like Elements: Photochemistry and Photophysics*; Abd-El-Aziz, A. S., Eds.; Wiley-Interscience: Hoboken, NJ, 2008 under review.

Daglen, B. C.; Harris, J. D.; Dax, C. D.; Tyler, D. R. Measuring Solid-state Quantum Yields: The Conversion of a Frequency-doubled Nd:YAG Diode Laser Pointer Module into a Viable Light Source. *Rev. Sci. Instr.* **2007**, *78*, 074104/1-074104/4.

Daglen, B. C.; Harris, J. D.; Tyler, D. R. Factors Controlling the Rate of Photodegradation in Polymers; the Effect of Temperature on the Photodegradation Quantum Yield in a PVC Polymer Containing Metal-metal Bonds in the Polymer Chain. *J. Inorg. Organomet. Polym. Mat.* **2007**, *17*, 267-274.

Daglen, B. C.; Tyler, D. R. Factors Controlling the Rate of Photodegradation in Polymers. In *Degradable Polymers and Materials*; Khemani, K. C.; Scholz, C., Eds.; ACS Symposium Series 939; American Chemical Society: Washington, DC, 2006; pp 384-397.

Chen, R.; Meloy, J.; Daglen, B. C.; Tyler, D. R. Photochemically Reactive Polymers. Identification of the Products Formed in the Photochemical Degradation of Polyurethanes that Contain $(C_5H_4R)(CO)_3Mo$-$Mo(CO)_3(C_5H_4R)$ Units Along their Backbones. *Organometallics* **2005**, *24*, 1495-1500.

ACKNOWLEDGMENTS

I wish to express my sincere appreciation to my research advisor, Prof. David R. Tyler, for supporting my research endeavors and enduring my numerous extracurricular activities. I am thankful to have studied in a laboratory that tackles a diversity of difficult scientific questions. I am equally honored to have been a part of the team of talented individuals who have shared in the frustration and elation experienced while attempting to answer those challenging scientific questions (Team Tyler pushing back the forefront of science). I would like to extend an honorable mention to those who have collaborated on the polymer project during my tenure in the Tyler lab: Rui Chen, John Harris, Ginger Shultz, Katherine Klug, and Jennifer Zemke. This is not the space to acknowledge all lab members individually but there are two in particular I must mention for their inspiration, their laughter, and their courage: Takiya J. Ahmed and Ginger V. Shultz. Thank you. My life is more consequential for having spent these years in your company.

More appreciation for those who enriched my Graduate School experience: David Senkovich and Kris Johnson were instrumental in maintaining the O_2-free atmosphere in our dryboxes. David and Kris along with John Bossinger and Jeffrey Garman of the machine shop also counseled me in numerous trouble-shooting and repair projects. (They are the cornucopia of knowledge and skill that keeps the University scientists' experiments going.) Clifford Dax was critical in the improvements of the irradiation source used in the degradation experiments. Clarisse Heinhorst and Jim Rasmussen were useful for the timely acquisition of needed materials. Thanks to the assistance of the

faculty and staff of the university's Materials Science Institute, I was able to accomplish my GK-12 and IGERT responsibilities. Lastly, critical to my education and career development was my involvement in the UO Women in Graduate Science founded by my dear friend Sara J. Staggs. I will never underestimate the power of a mentor.

As for mentors: Prof. Michael Haley recruited me to the University of Oregon for graduate school and I am very grateful. My committee, Darren Johnson, Dave Johnson, and Miriam Deutsch, was also a great resource over the years. To my committee chair, Cathy Page, I appreciate you taking on the extra load of chair, I especially enjoyed the opportunity to teach Inorganic Chemistry, and I learned much from you imparting your teaching and research experiences. I also had a series of great instructors, David Tyler, Mark Lonergan, Jim Hutchison, and Cathy Page, who all inspired me to become an even more enthusiastic teacher.

To my family: I am thankful for your support. My mother has forever encouraged me to continue my education which was the beginning really. My grandmother showed me the usefulness of thrift and creativity, which is handy in the research lab. My grandfather taught the importance of voice projection and a firm handshake. My mother- and father-in-law are wonderful role models and have proved very useful in solving calculus problems. And finally, I cannot express the extent to which my husband, Michael Daglen, has contributed to the success of my graduate career. Life is just more fun with you in it.

To Michael Todd Daglen, my Judo partner, my friend, my love.

"The harmonious development
and eventual perfection
of the human character."
– Jigoro Kano

TABLE OF CONTENTS

LIST OF FIGURES

Figure   Page

Figure
Page

LIST OF TABLES

LIST OF SCHEMES

CHAPTER I

PHOTODEGRADABLE POLYMERS AND SOLID-STATE PHOTOCHEMISTRY

1.1 Introduction

According to the Society of the Plastics Industry, the United States produces over $379 billion worth of plastic annually, making plastics the third largest manufacturing industry in the United States. Furthermore, the industry has grown at a rate of 3.2% annually since the 1980's. The reason for the resilience of this industry is the numerous benefits plastics have had and continue to have on our lives. A couple examples include providing a protective barrier from pathogens in the medical and food industries and making cars lighter by using plastic in lieu of metal parts, and consequently, making vehicles more fuel efficient. Because plastics are so ubiquitous, scientists have made great advances in the development and improvement of polymeric materials. This year alone, over 38,000 publications on polymers have appeared in the scientific literature. This particular piece of literature will address a niche in the plastics industry that deals with the photodegradation of polymers.

Photochemically reactive polymers are of significant interest for two main reasons: their use as degradable plastics for a variety of applications and for the study of polymer degradation. In regards to the former, photodegradable polymers are extensively used for photolithography and biomedical applications.[1-5] Another niche for photodegradable polymers is in the 'green' plastics market. In the environmental area, photodegradable plastics are finding increased use as packaging materials for items that

have a high probability of becoming litter. Photodegradable consumer plastics have also

found their way into homes as degradable trash bags and plastic kitchenware. Another

area that is experiencing increasing utility in photodegradable polymers is plasticulture.

In this application, the ground is covered with plastic sheeting (typically a polyolefin);

this acts as a mulch to prevent the growth of weeds (thus requiring the use of fewer

herbicides), decreases water demand, and extends the growing season by keeping the

ground warmer. By making these agricultural films out of degradable plastics,

considerable labor and money can be saved in the plastics recovery phase of the

technique.[6-9]

The second reason photochemically reactive polymers are of significant interest is

for use in the study of polymer degradation. In order for photodegradable polymers to be

suitable in the applications mentioned above, the performance of these polymers must be

well understood before they are incorporated into materials. The ideal photodegradable

polymer has (at least) three ideal properties (illustrated in Figure 1).[8, 10] First, the onset of

degradation should be reliably predictable. Although it is obvious why this property is

desirable for practical applications, it is noted that it is difficult to predict polymer

lifetimes in practice because light intensities vary, as do temperatures and a host of other

mechanistic variables that control degradation rates and degradation onsets. Second, the

onset of degradation should be tunable. Photodegradable polymers have different

applications and each application will generally require different polymer lifetimes.

Methods must be found for manipulating polymer lifetimes. Third, the polymer should

degrade completely and quickly once degradation starts. This characteristic is important

for practical reasons because most polymer mechanical properties are related to

molecular weight. Small amounts of degradation can drastically decrease the molecular

weight (and thus mechanical properties) of a plastic, yet to all appearances the plastic

piece is visually unchanged. In essence, the plastic is still present but it is not structurally

sound and hence useless and perhaps dangerous. Under such circumstances, it may as

well be completely degraded. Photochemically reactive polymers are studied in an effort

to understand and control the life cycle of materials. This includes not only polymers that

are engineered to degrade but also those that are meant to last indefinitely in the case of

structural plastics.
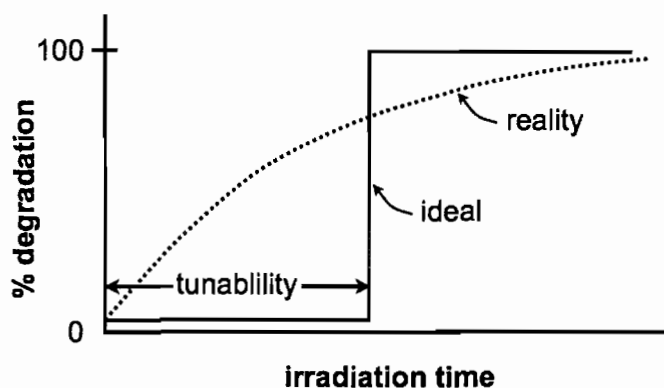
Figure 1. The properties of both a typical polymer and an ideal photochemically
degradable polymer demonstrating tunable onset of degradation and rapid degradation.

Controlling the degradation of a material in a prescribed fashion, so that the rate

and onset of degradation is both tunable and predictable for the particular application, is

of immense interest. In order to achieve this goal, it is necessary to understand how

environmental parameters and specific polymer properties affect photodegradation. For

example, it is important to understand the effect of temperature because of the range of temperatures plastic materials experience in their diverse applications. Specifically, it is known that many polyolefins as well as polyethers, polyketones, and polysulphones have accelerated degradation rates at elevated irradiation temperatures.[11-16] Temperature dependence also has extensive implications in service lifetime predictions where accelerated rate testing is the industry standard. Temperatures employed in these types of tests are typically greater than the intended application conditions because it is often impractical to perform real time testing on plastics whose expected use is over several decades. In these cases and in general, polymer thermal transitions must be taken into consideration in elucidating the effects of temperature on degradation rates. Specifically, the rates of polymer photodegradation above and below the polymer glass transition have been shown to vary significantly.[12, 17-19]

There are several challenging experimental problems that hinder the rigorous mechanistic exploration of polymer photodegradation. One of the primary difficulties is that polymer degradation is mechanistically complicated. This is not to say that the mechanisms are not understood; in fact, they are understood in detail. Rather, the mechanisms are intricate, often involving multiple steps, cross-linking, and side-reactions; this makes pinpointing the effects of various experimental parameters difficult. This chapter will discuss methods for designing photodegradable polymers and exploring their corresponding degradation mechanisms. In addition, several factors that influence photodegradation rates as well as specific models that describe the reaction kinetics will also be explored.

1.2 Photodegradable Polymer Design

Photodegradable polymers are typically designed for commercial use in one of two ways: 1) by incorporating a photosensitive chromophore into in the backbone of the polymer chain or 2) by physically combining 'non-degradable' polymers with small molecule photosensitizers that absorb light and initiate photochemical degradation reactions with the polymer.[20, 21] The first strategy is accomplished primarily by incorporation of a carbonyl group into the backbone of the polymer.[22] The most commercially successful polymer of this type is E-CO, which was generated by the copolymerization of ethylene and carbon monoxide in the presence of a catalyst to produce a polyketone.[23] This polymer has been used since the 1970's to make the Hi-Cone[TM] six-pack rings following environmental concerns and is still used today. The photochemistry of these types of polymers were first studied by Guillet and Hartley and their findings made the advancement of these materials a commercial possibility.[24, 25] They discovered that the primary mode of photodegradation of polymers containing carbonyls as the chromophore occurs by the Norrish type reactions upon irradiation with UV light as illustrated in Scheme 1. The primary experimental evidence for support of such a mechanism was the formation of terminal alkenes. It is also worth mentioning that the Norrish type II reaction is also a significant contributor to the degradation of polyesters and polyacrylates owing the presence of the carbonyl group.[1, 25]

a.

b.
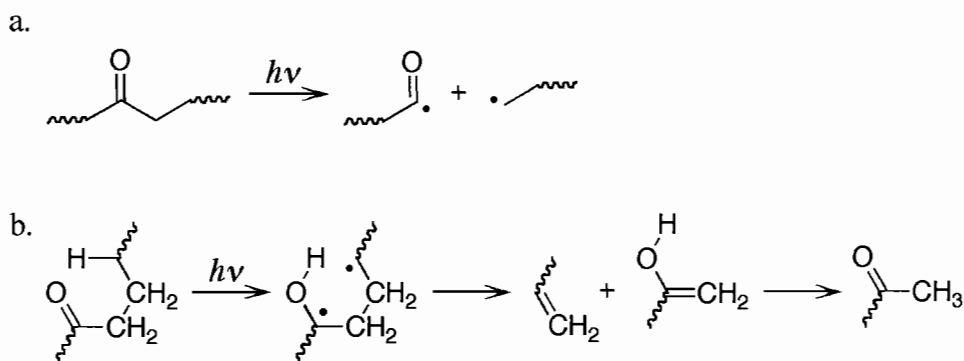
Scheme 1. Mechanism of the Norrish type I (a) and II (b) reactions in a ketone-containing polymer.

The second design for making photodegradable polymers is to add small molecule radical initiators to otherwise light stable carbon-based polymers. Some common initiators include peroxides, metal oxides (e.g. TiO_2, CuO, ZnO), metal chlorides (e.g. cobalt(II), lithium, iron(III), nickel(II), copper(II)), M(acac)$_n$ and M(stearate)$_n$ complexes, benzophenone, and quinines.[23, 26-30] These systems degrade by a complex system of reactions that starts when the photosensitive additive absorbs a photon and begins the autooxidation process shown in Scheme 2. This results in the formation of peroxide and organic radical species. (It is interesting to note that the autooxidation process is autocatalytic because another carbon radical is generated during the hydrogen abstraction step). Organic peroxide species generated in the autooxidation mechanism can lead to polymer main chain cleavage via two routes: direct cleavage by β-scission or through a more circuitous route by formation of carbonyl carbons in the backbone and subsequent Norrish type reactions. Some photoreactions of peroxides are shown in Scheme 3.

Initiation

Initiator $\longrightarrow$ $R_i\cdot$

$R_i\cdot$ + O_2 $\longrightarrow$ $R_iOO\cdot$

$R_iOO\cdot$ + R–H $\longrightarrow$ R_iOOH + R$\cdot$

Propogation

R$\cdot$ + O_2 $\longrightarrow$ ROO$\cdot$

ROO$\cdot$ + R–H $\longrightarrow$ ROOH + R$\cdot$
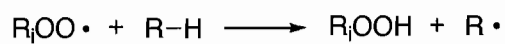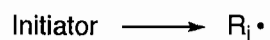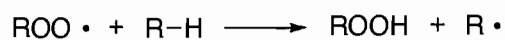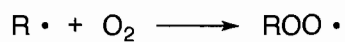
Termination

Radical coupling or diproportionation reactions

Scheme 2. The autooxidation process, where R is some carbon species.
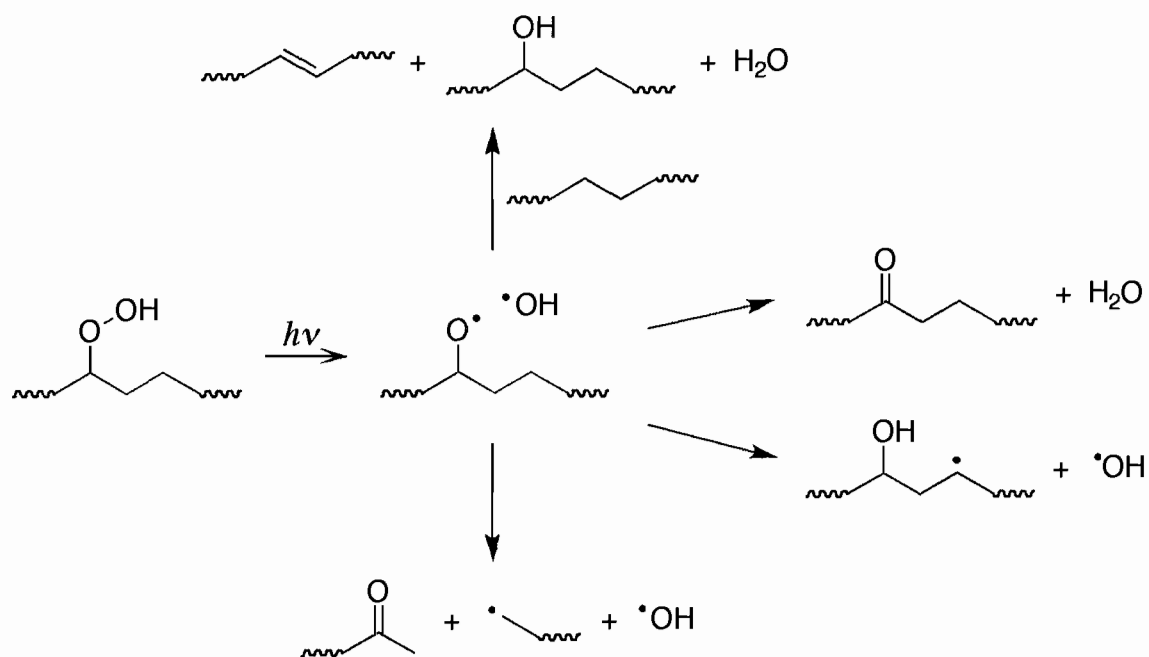
Scheme 3. Examples of organic peroxide reactions.

Other examples of the two strategies discussed above are noteworthy for both their relevance to inorganic and organometallic containing polymers genre and for their innovative attributes. For example, a novel synthetic strategy is currently being explored to covalently link commonly used inorganic photosensitizers to polymer pendent groups using sol-gel synthesis techniques (Figure 2 polymers **1** and **2**).[31, 32] Polymers containing pendant radical initiators have the advantage of discouraging large inorganic aggregates in the solid-state. Polysilanes (Figure 2 polymers **2** and **3**) are another class of photodegradable polymers which are primarily developed for photolithography applications, given their transparent nature and photoconductivity.[32, 33] Recent progress in this area has been made toward elucidating the mechanism of photodegradation. It was shown, for the case of polyurea containing silane units, that the photodegradation pathway involves a single-electron transfer between the silyl and carbonyl groups, silyl group migration, and solvolysis.[33]
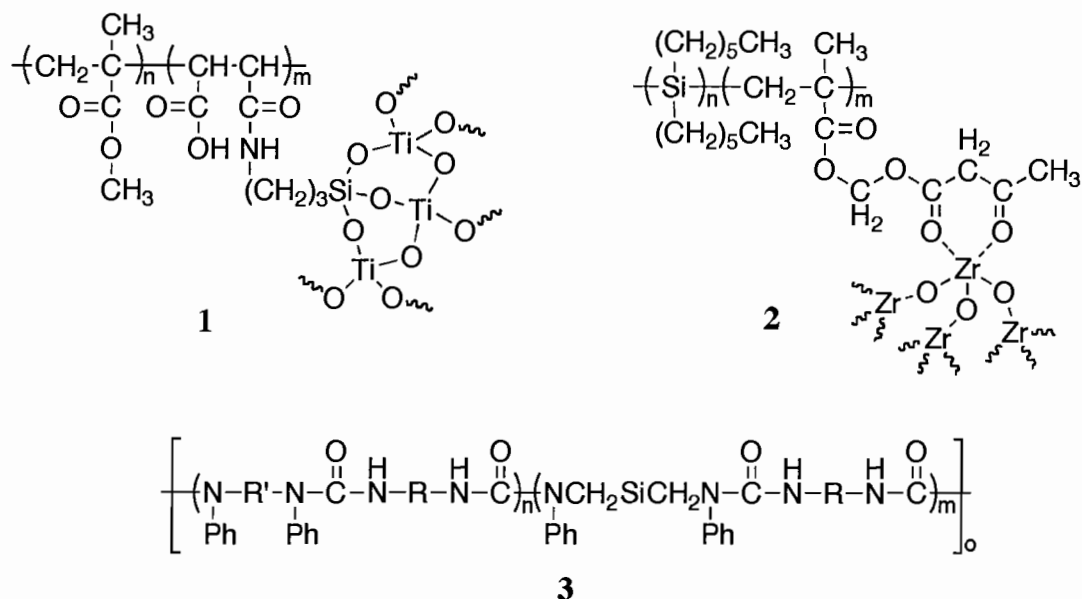
Figure 2. Example of an inorganic photosensitizer attached to a polymer chain through the pendant groups.

Another method for generating photodegradable polymers that utilizes the first strategy of building in photosensitive groups into the backbone is the incorporation of organometallic dimer complexes into the backbone of the polymer chain.[10] A general synthetic route for incorporating metal-metal bonds into polymer backbones is based on the step polymerization techniques used to integrate ferrocene into polymer backbones.[34-36] This was accomplished by functionalization of the cyclopentadienyl ligands creating the necessary difunctional monomer unit for step polymerization and reacting the ferrocene monomer with an appropriate difunctional organic molecule (Scheme 4). An analogous strategy for synthesizing metal-metal bond containing polymers also utilizes the functionalization of cyclopentadienyl ligands. A sample polymerization reaction is shown in Scheme 5, which illustrates the reaction of a metal-metal bonded 'diol' with

hexamethylene diisocyanate (HMDI) to form polyurethane. Other synthetic strategies also have been utilized to incorporate metal dimers into polymer backbones including (Figure 3): 1) the chain copolymerization of styrene and an iron dimer with vinyl cyclopentadiene ligands, **5**, 2) acyclic diene metathesis polymerization of a molybdenum dimer with α,ω-alkene substituents, **6**, and 3) cross-linking of a functionalized prepolymer with a disubstituted molybdenum dimer species, **7**.[10, 37-40]
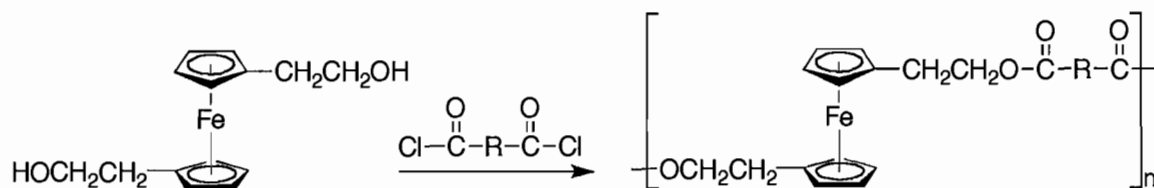
Scheme 4. Synthesis of a ferrocene-containing polymer using step polymerization techniques.

4
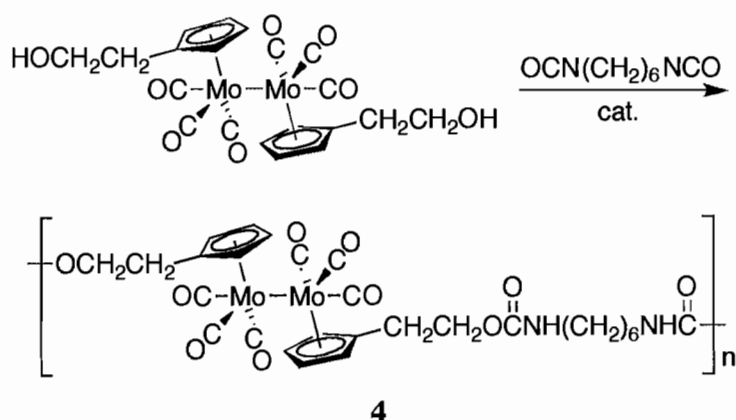
Scheme 5. Example synthesis of a metal-metal bond-containing polymer using step polymerization techniques.
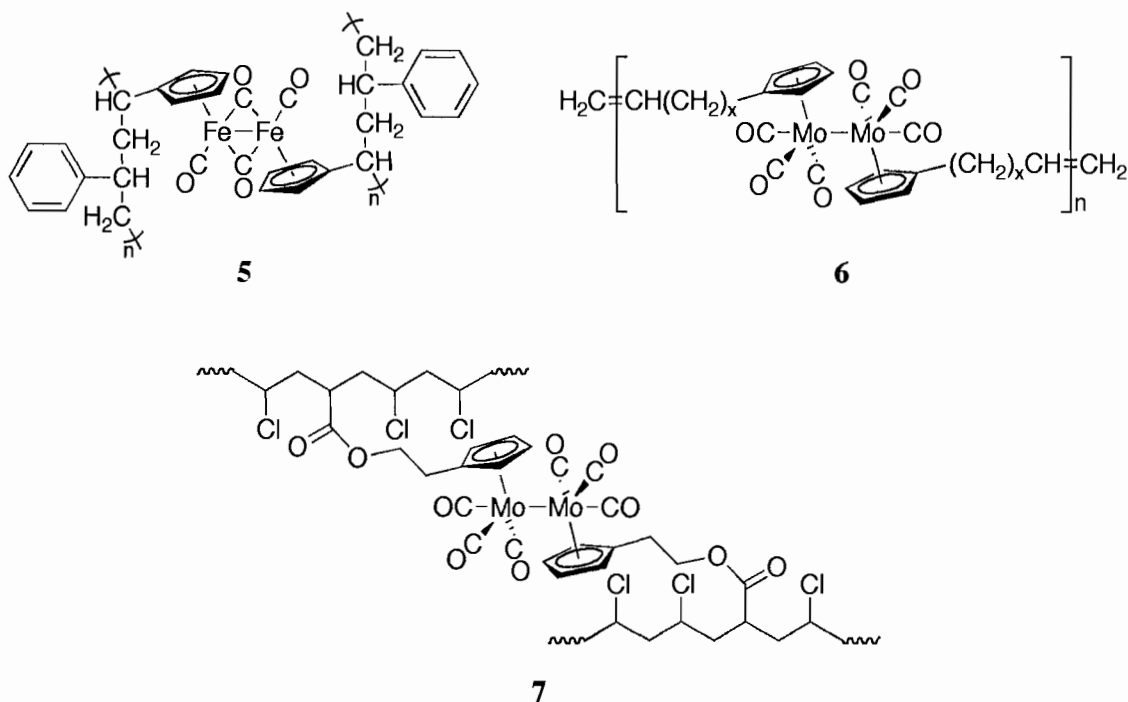
Figure 3. Examples of polymers with transition metal dimers in the backbone of the polymer.

Polymers that contain metal-metal dimers in the backbone of the polymer chain, for example polymers **4-7**, will photodegrade in the presence of visible light (Scheme 6). This occurs because of the photoreactivity of the metal-metal bond which homolyizes upon irradiation resulting in the generation of two metal radical species.[41, 42] In the absence of a radical trap, these two metal radicals will recombine for no net reaction. However, in the presence of a radical trap, for example oxygen or chlorine atom, the photogenerated metal radical can be trapped before recombination occurs. This results in an overall reduction in polymer molecular weight.

$$\text{LnM—MLn} \quad \text{LnM—MLn} \quad \text{LnM—MLn}$$

$$\Updownarrow h\nu$$

$$\text{LnM—MLn} \quad \text{LnM}\cdot \quad + \quad \cdot\text{MLn} \quad \text{LnM—MLn}$$

$$O_2 \diagdown \qquad \diagup Cl$$

$$\text{metal oxides} \qquad \text{Cl-MLn} \quad \text{LnM—MLn}$$

$$(ML_n = CpMo(CO)_3, CpW(CO)_3, Mn(CO)_5, Re(CO)_5,$$
$$\text{or } CpFe(CO)_2 \text{ and } Cp = \eta^5\text{-}C_5H_4)$$
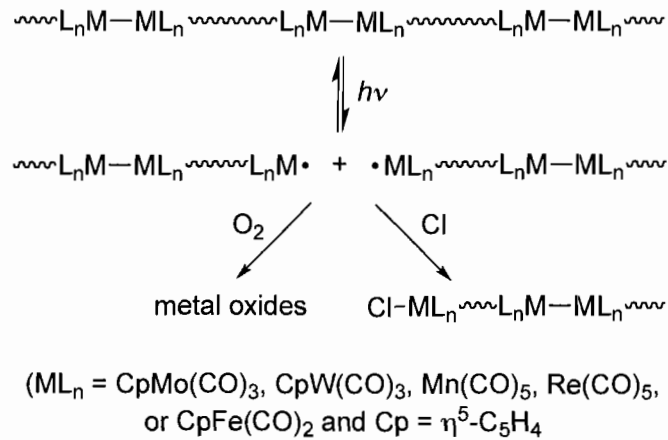
Scheme 6. Photochemical degradation of a generic polymer with metal-metal bonds in the backbone.

A more complete list of photodegradable polymers and polymer photodegradation reactions can be found in the many monographs that exist in the literature.[26, 43-47]

1.3   Factors Affecting Degradation Rates

1.3.1   *Effect of Radical Trap Concentration*

The radical trap concentration has been shown to influence the degradation rate of polymers both in the solid-state and in solution. In the case of the autooxidative degradation pathway of carbon-based polymers shown in Scheme 2, the carbon free-radical species that is formed in the initiation step must be trapped by an oxygen molecule for degradation to proceed. (Note, it is true that the carbon free radical may abstract a hydrogen atom in lieu of reacting with oxygen but that would result in no net reaction). In the solid-state, oxygen diffusion is often the rate limiting step in the autooxidative degradation of polymers. This is contingent on the sample thickness, morphology, and permeability of the polymer toward oxygen).[48, 49] For example, by sampling the molecular weight of a photochemically degraded polystyrene sample as a

function of depth, it was found that there was variability in the degradation efficiency that could only be explained by depletion in oxygen at greater sample depths.[48, 50] For this polymer, samples with thicknesses greater than 0.1 mm will experience rate limiting oxygen diffusion.

Radical cage effects are of particular importance to the radical trapping reaction in polymer photodegradation (see Scheme 7 for a simplified example of a cage reaction.) It is known that when a bond is homolyzed in the solid or liquid phase, the two radicals that are formed (termed geminate radicals) exist inside a solvent cage.[51-53] It is the ability of this geminate radical pair to escape the solvent cage that determines whether the two radicals will either recombine for no net reaction or escape the radical cage and become free radicals. When free radicals form, they will either react with another species (a radical trapping molecule) or react with another non-geminate radical for no net reaction. Because of the cage effect, the photodegradation efficiencies of photosensitive molecules can be manipulated by changing the concentration of the radical trapping agent.[54] For example, by adjusting the concentration of CCl_4 (radical trapping agent) in the photolysis reaction of $(C_5H_5)_2Mo_2(CO)_6$, the quantum yield can be varied from zero (no radical trap present) to 0.6 (> 0.1 M CCl_4 in hexanes). Radical trap concentration affects the probability of non-geminate radical recombination; at high concentrations of trap, any radical that escapes the cage is trapped.

$$R{-}R \underset{k_c}{\overset{h\nu}{\rightleftharpoons}} \underset{\text{cage pair}}{[R\cdot,\cdot R]} \overset{k_d}{\longrightarrow} \underset{\text{free radicals}}{2\,R\cdot} \overset{T = \text{trap}}{\underset{k_t}{\longrightarrow}} 2\,R{-}T$$
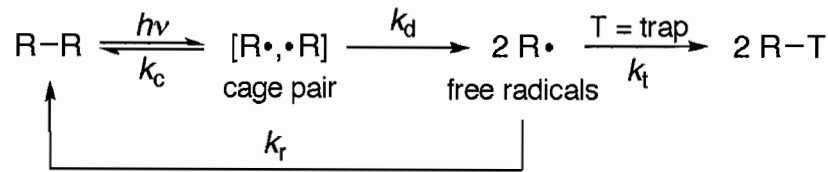
Scheme 7. Homolysis of a bond and subsequent trapping reaction depicting the radical cage intermediate where k_c is for the geminate recombination, k_d is for the diffusion from the radical cage, k_r is for non-geminate recombination, and k_t is for the radical trapping step.

1.3.2 *Effect of Temperature*

The effect of temperature on the thermal degradation rates of polymer has been extensively explored because of the need to predict the service lifetime of consumer plastics. However, only a few studies have probed the effect of temperature on the photochemical degradation rates of polymers. These studies are rather inconclusive with respect to a general model for predicting the dependence of photodegradation rates on temperature. Several studies found that the results are consistent with an Arrhenius relationship, but other studies have found non-Arrhenius behavior.[11, 55-58] There is some indication that the non-Arrhenius behavior is due to the complex degradation pathways referred to in the proceeding sections. For this reason, interpreting Arrhenius plots of photochemical reactions can be non-trivial. Balzani notes that the relationship between the temperature and the activation parameters in a photochemical reaction is a complex one, and the "apparent activation energies" obtained should be regarded with care.[59]

Another hypothesis regarding non-Arrhenius is that the behavior is caused by changes in the molecular mobility of the polymer chains. Several groups have observed non-linearity in Arrhenius plots that coincide with the polymer's thermal transitions, most

notably, the glass transition.[15, 17, 18] One stark example is the photodegradation of

poly(vinyl ketone) (PVK). In that study, Guillet found that the quantum yields of

degradation below the glass transition temperature, T_g, increased gradually with

increasing temperature ($\Delta\Phi = 0.04$ for T = 20–100 °C. To explain this behavior, Guillet

noted that PVK degrades by a Norrish type II mechanism, which proceeds via formation

of a six-membered ring intermediate (Scheme 8). He proposed that, because the

degradation pathway required substantial rearrangement of the polymer chain to form the

six-membered ring intermediate, the slight increase in quantum yields with increase

temperature below T_g was a reflection of the increase in free-volume of the solid-state

polymer. A larger free-volume allows for easier rearrangement of the chain to the six-

membered ring intermediate. It is interesting to note that at T_g, Guillet observed a

dramatic increase in the quantum yield to a value similar to that in solution (Φ_{PVK} =

0.24). The sudden increase in Φ at the glass transition temperature was attributed to the

ability of the polymer chains to easily form the intermediate because of facile chain

movement above T_g. These findings can be summarized by stating that increasing the

photoreaction temperature can have several effects (both direct and indirect) on the rate

of polymer degradation, notably increases in kinetic energy, free-volume, and molecular

mobility.
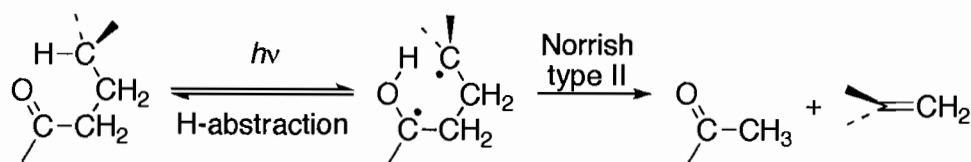
Scheme 8. Mechanism for the photochemical Norrish type II reaction showing the formation of the 6-membered ring intermediate.

1.3.3 *Effect of Stress*

An interesting outcome of polymer degradation studies is the discovery that tensile and shear stress can accelerate the rate of photochemical degradation. For example, recent studies of this phenomenon have shown that tensile stress will accelerate the photodegradation of numerous polyolefins as well as polycarbonates, nylon, and acrylic-melamine coatings.[60-73] Currently, there are three prevailing theories that attempt to explain this phenomenon: the Plotnikov, the Decreased Radical Recombination, and the Zhurkov Hypotheses (Figure 4). Each of the hypotheses refer to the different rate constants in Scheme 9 to explain the occurrence of increased degradation rates with applied tensile stress. The overall rate, or quantum efficiency, of the photoreaction is defined by eq 1,

$$\Phi = \frac{k_{trap}[RX]}{k_{homolysis} + k_{trap}[RX]} \tag{1}$$

where RX is the concentration of radical trapping species and k_t and k_r are the rate constants for recombination and trapping steps, respectively.
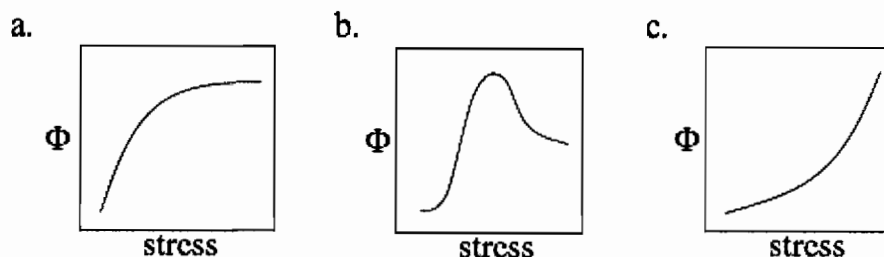
Figure 4. Graphical representation of the three hypotheses for the effect of tensile stress on the quantum efficiency of polymer photodegradation as postulated by the: a. Plotnikov, b. Decreased Radical Recombination Efficiency, and c. Zhurkov hypotheses.

Scheme 9. Simplified polymer photodegradation mechanism showing bond homolysis.

Plotnikov Hypothesis

Plotnikov theorized that tensile stress affects the activation barrier of the excited state of the individual bond involved in homolysis.[74] The photophysical phenomenon can be represented by a linear perturbation of the Lennard-Jones potential as shown in Figure 5, which compares an unstressed bond to a stressed bond in a photochemical reaction. The mathematical perturbation results in a lower activation barrier for bond homolysis in the case of a stressed bond. The predicted consequence is that the lowered activation energy for homolysis would increase the quantum yield for disappearance of the starting material as shown in Figure 4a. There is a mathematical limitation on the extent of perturbation, which causes the increasing quantum yield to level off at high stresses. Another consequence of the perturbation is that it results in the potential well taking on a negative

slope (not shown in Figure 5) as the atom distance approaches infinity, which suggests that the photogenerated radicals become more thermodynamically stable at infinite separation. The negative slope is a mathematical artifact and is not meant to imply thermodynamic stability at infinite distance.
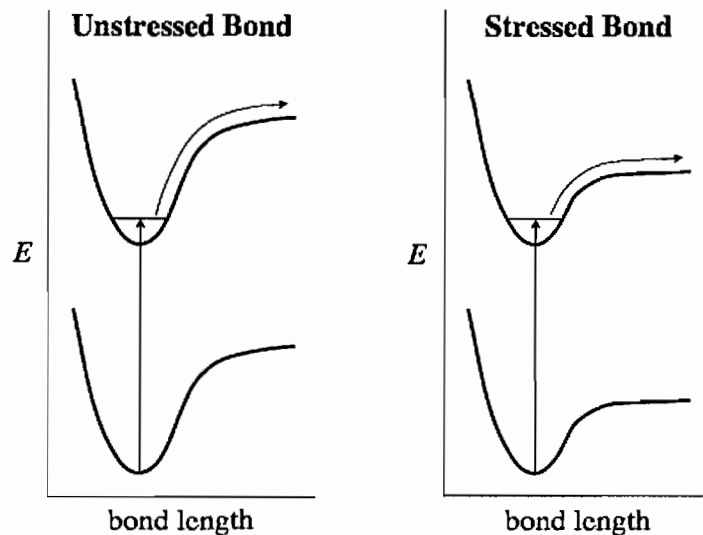
Figure 5. The photophysical description of the Plotnikov hypothesis.

Decreased Radical Recombination Efficiency Hypothesis

The Decreased Radical Recombination Efficiency hypothesis postulates that the degradation efficiency is affected by the ability of the geminate radical to recombine.[75-78] This hypothesis is shown in Figure 6 as a series of conditions under which radical recombination can occur. The first condition is at zero or minimal stress levels where an amorphous polymer has an intrinsic quantum yield. When tensile stress is applied to a polymer, the chains, which are primarily in a random coil state, become elongated and

straightened. In this case, the radicals generated during bond homolysis recoil to resume the more entropically favored random coil. This results in an increase in radical distance, and increase in the likelihood of radical trapping and consequently an increase in degradation efficiency. An increase in applied tensile stress also has other consequences that predict a deviation from a continued increase in degradation efficiency with increased stress. It is well known, and often utilized in plastic production, that tensile stress can impart a high degree of polymer strand orientation and induce the formation of crystalline regions in some polymer systems. Bonds homolyzed in these regions of high thermodynamic stability are unlikely to recoil into a random coil configuration. This would result in an enhanced rate of radical recombination and a general decrease in degradation efficiency. The qualitative illustration of the effect of stress on the quantum yield is shown in Figure 4b.

| no stress (amorphous) | applied stress (amorphous) | applied stress (crystalline) |

$h\nu$ $h\nu$ $h\nu$
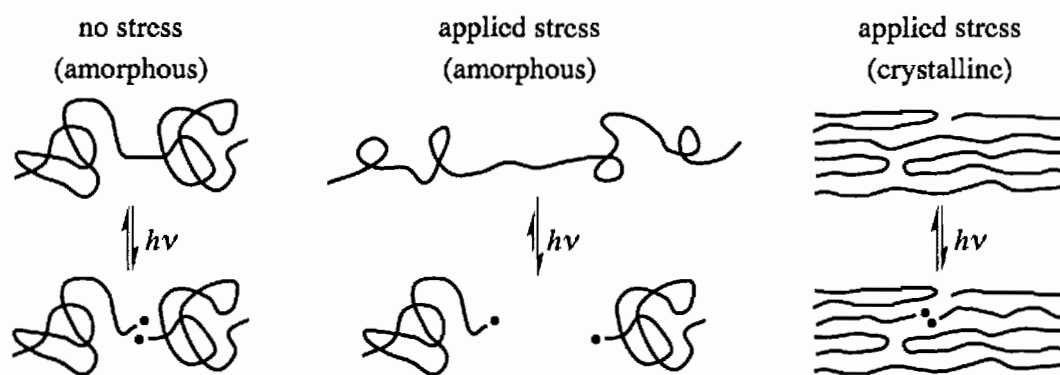
Figure 6. An illustration of the Decreased Radical Recombination Efficiency hypothesis regarding the effect of tensile stress on polymer photodegradation.

<u>Zhurkov Hypothesis</u>

The Zhurkov hypothesis is an extension of the research performed to investigate the thermal degradation of polymers under tensile stress and is empirical in nature.[79] It was observed that the degradation efficiency increased as a function of stress in an exponential fashion. This can be quantitatively described by eq 2, where τ is the lifetime of a polymer under stress (σ) at a given temperature (T), τ_0 is the period of thermal oscillation of the bond, γ is a 'structural coefficient which defines the actual loads in a stressed body', and U_0 is the 'apparent' activation energy for bond scission (the 'apparent' activation energy is a composite of $k_{homolysis}$, $k_{recombination}$, and $k_{trapping}$). It is hypothesized that the same trend would hold true for photochemical degradation of a polymer under stress and have the same general equation:[74]

$$\tau = \tau_0 e^{U_0 - \gamma\sigma / RT} \tag{2}$$

The qualitative illustration of the effect of stress on the quantum yield is shown in Figure 4c.

<u>Evidence Supporting the DRRE Hypothesis</u>

There is one prevailing set of experiments that tested the hypotheses listed above. The work was performed by evaluating the quantum efficiency of a model photodegradable polymer (**PVC-Mo** is shown in Figure 7) as a function of stress and comparing the results to the possible outcomes illustrated in Figure 4.[80] The model polymer system does not degrade by the typical photooxidative mechanism but rather by a simplified mechanism shown in Scheme 10. Using this system, the degradation

efficiency was measured as a function of tensile stress and found to follow the Decreased

Radical Recombination Efficiency hypothesis.
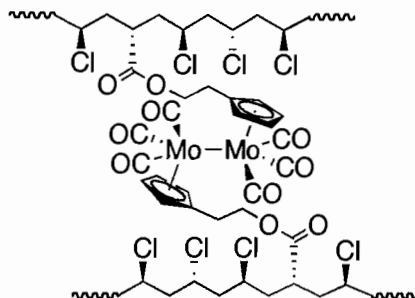
Figure 7. Photodegradable polymer (**PVC-Mo**) made by crosslinking poly(vinyl chloride) with a metal-metal bond chromophore.
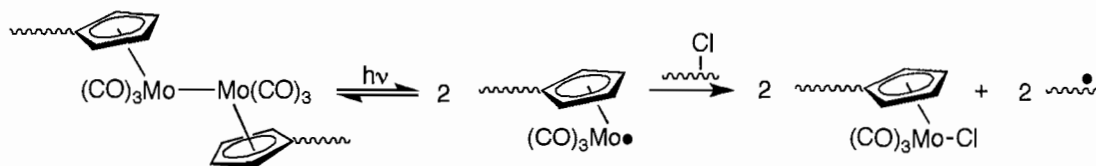
Scheme 10. Degradation pathway of **PVC-Mo** used in studying the effect of stress on photochemical quantum yields.

There are a number of factors not discussed in this section that can affect the

photodegradation efficiencies of polymers. A brief list includes light intensity,

chromophore concentration, irradiation wavelength, molecular weight, tacticity, moisture,

etc. Monographs on these subjects can be found in other references.[45, 81-83]

1.4   Kinetic Models of Polymer Photodegradation

To devise a photodegradable polymer with a tunable onset of degradation and

with a specific degradation rate, it is necessary to identify the experimental parameters

that affect degradation rates and to determine how those parameters affect the degradation mechanism. A typical first step toward this goal is to determine the kinetics of the degradation reaction. An interesting observation from kinetic studies of the photodegradation rates of solid-state polymers is that the plots of degradation versus irradiation time are often biphasic, showing a relatively fast rate during the initial period of irradiation but a slower rate at longer times.[33,44] Several hypotheses have been proposed to explain this observation but no definitive explanation has come forth.

One hypothesis is that the photodegradation reaction is a simple number-ordered reaction: zeroth, first, or second order. Owing to the fact that the plots are not linear, a simple zeroth-order reaction, which is typical for many photochemical reactions, is not feasible in the case of a biphasic plot. First-order reactions however do yield biphasic plots and have been appropriately fit to the data. For example, photooxidative degradation in the presence of excess oxygen has been shown in several cases to exhibit first-order kinetics.[84-87] In all cases, which include polyethers, conjugated polymers, and poly(vinyl chloride), the main chain scission results from formation of a carboxyl carbon, usually an ester linkage, which is subsequently involved in β-scission. (A more detailed description of the formation of carbonyl groups in polymers is given in the preceding section and in the associated references.) Second-order kinetics in polymer photodegradation is less prevalent in the literature. To site one example, second-order kinetics were observed for the photodegradation of neoprene in the presence of $FeCl_3$.[88] However, no definitive explanation was offered as to the origin of this behavior.

Other hypotheses used to explain the biphasic behavior exhibited in polymer photodegradation attribute the unique reactivity to solid-state diffusion kinetics. A possible explanation is that the reaction rate is not solely determined by a specific chemical transformation but rather by diffusion processes. One representation of diffusion behavior is simple-diffusion.[76] Simple-diffusion models are often used to describe diffusion processes involving metal-metal interfaces but they have also been employed in polymeric systems. For example, simple-diffusion kinetics were used to describe the degradation of solid-state polyolefins where the decay of photogenerated radicals were hypothesized to be controlled either by oxygen diffusion into the polymer material or by radical diffusion via hydrogen abstraction to the crystalline surfaces where radical-trapping oxygen was present.[89] Another diffusion model to describe the biphasic kinetic behavior of polymer photodegradation was developed by Waite. His hypothesis was a modification of the simple-diffusion model called the diffusion-controlled model.[90-92] This model describes bimolecular reactions in the solid-state or in highly viscous solutions where both diffusion and spatial distribution of the reactive species are taken into account. The diffusion-controlled model has been used to fit the radical decay kinetics of several photodegradation reactions of polyolefins and polyethers as monitored by electron spin resonance spectroscopy.[13,14,76,93]

1.5   Dissertation Outline

This dissertation is composed of advances made on the front of understanding polymer photodegradation using unique polymer models that contain the chromophore $(-CH_2C_5H_4(CO)_3Mo-Mo(CO)_3C_5H_4CH_2-)$. Chapter II describes the reactivity of these

model polymers in the solid-state in the presence and absence of oxygen and identifies the photochemical products. Chapter III discusses the reactivity of these polymers in the presence of various radical trapping agents and provides insights into the relationship between degradation efficiencies and both the radical trapping concentration and glass transition temperature. Chapters IV and V describe the effect of temperature on two different polymer systems and the effect that secondary thermal transitions have on polymer degradation below the glass transition temperature. Further findings on the relationship between tensile stress and photodegradation efficiencies are discussed in Chapter VI. Finally, an investigation into the biphasic nature of the kinetic traces of polymer degradation as a function of irradiation time is presented in Chapter VII. Included in the appendix are the synthetic details for the polymer films and solutions employed and the experimental instrumentation for the photochemical studies.

1.6   Acknowledgments

This dissertation contains my co-authored material. Chapter II contains co-authored material with R. Chen, J. Meloy, and D. R. Tyler. The manuscript was primarily written by R. Chen with myself and J. Meloy as contributors. My specific contribution was the oxygen free experimentation and corresponding write-up as well as editorial responsibilities. The experiments were performed by myself, R. Chen, and J. Meloy. Tyler provided editorial assistance. Chapter III contains co-authored material with D. R. Tyler. The experiments were performed by myself. D. R. Tyler and B. C. Daglen being the co-contributors to the writing. Chapter IV contains co-authored material with J. Harris and D. R. Tyler. The solid-state experiments were performed by myself and the solution data was collected with the assistance of Harris. The manuscript was prepared by myself with

editorial assistance provided by D. R. Tyler. Authorship of chapters V, VI, VII, and VIII are shared with D. R. Tyler who acted as my advisor. The experiments were performed by myself. Appendix I was co-authored with J. Harris, C. Dax and D. R. Tyler. The experiments were performed by myself and J. Harris. C. Dax was critical in the design and assembly of the instrumentation. D. R. Tyler provided editorial assistance.

CHAPTER II

PHOTOCHEMICALLY REACTIVE POLYMERS. IDENTIFICATION OF THE

PRODUCTS FORMED IN THE PHOTOCHEMICAL DEGRADATION OF

POLYURETHANES THAT CONTAIN $(C_5H_4R)(CO)_3Mo–Mo(CO)_3(C_5H_4R)$ UNITS

ALONG THEIR BACKBONES

Chen, R.; Meloy, J.; Daglen, B. C.; Tyler, D. R. *Organometallics* **2005**, *24*, 1495-1500.

2.1   Introduction

Our synthesis of metal-metal bond containing polymer uses metal-metal bonded

organometallic dimers with functionally substituted cyclopentadienyl ligands, a synthetic

method borrowed from earlier work on polyferrocenes.[1-5] An example of a polyurethane

synthesis is shown in Scheme 1.[6] Thus far, polyurethanes, polyureas, polyethers,

polyvinyls, polyamides, and several types of copolymers with metal-metal bonds along

the backbone have been synthesized.[7] As predicted, all of these polymers are

photodegradable, both in solution and in the solid state, provided that a radical trap is

present to capture the metal radicals and prevent reformation of the metal-metal bond by

radical-radical recombination. In solution, organic halides such as CCl_4 are excellent

traps, while ambient oxygen serves that purpose in the solid-state reactions.
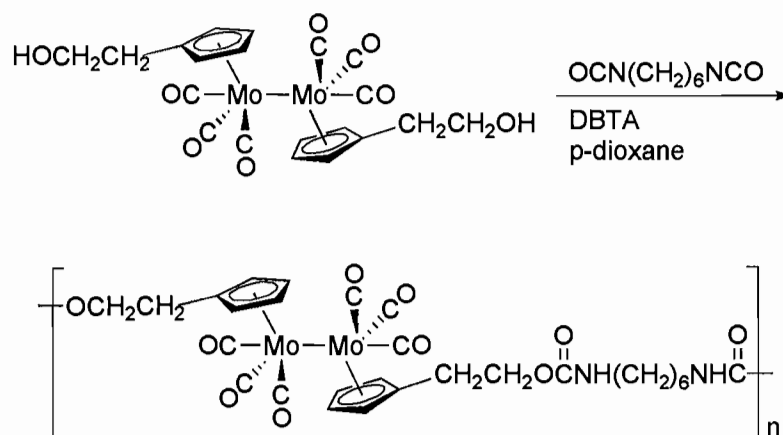
Scheme 1. Example of a polyurethane synthesis used to incorporate molybdenum dimers into the backbone of a polymer chain. (DBTA = dibutyltin diacetate)

In the case of the CCl_4 radical traps in solution, the organometallic portion of the product that forms is $(\eta^5\text{-}C_5H_4R)Mo(CO)_3Cl$ (Scheme 2).[7] Previously, the product formed when oxygen was the radical trap had not been identified. Discussed in this chapter are the results of experiments designed to identify the metal product that forms when oxygen is the radical trap. Also described is the synthesis of a new polymer that is capable of degrading in the absence of oxygen (or any other exogenous trap) because it has Cl atoms "built-in" along the polymer backbone.
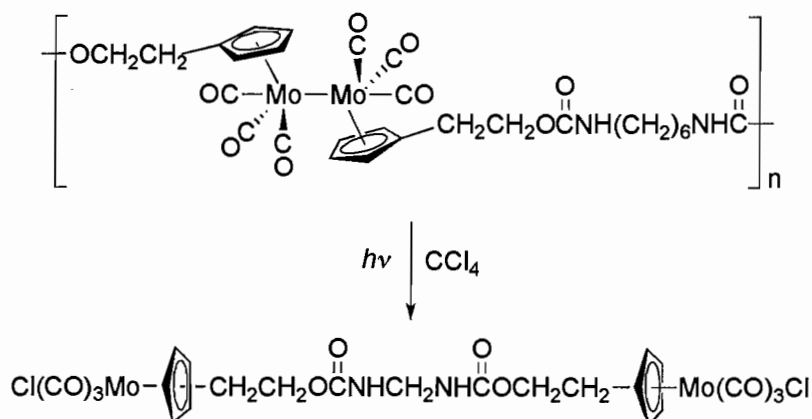
Scheme 2. Example photodegradation reaction of polyurethane containing molybdenum dimers with a halide radical trap in solution.

This work is published in Volume 24 of the journal Organometallics in 2005. The work on the photodegradation in the presence of oxygen was performed by R. Chen and J. Meloy, with the anaerobic work being performed by myself. D. R. Tyler and R. Chen prepared the manuscript with myself providing editorial assistance as well as the written experimental portion of the manuscript that coincided with my work.

2.2   Results and Discussion

2.2.1   *Syntheses and Photochemical Reactions of Polymers Hypol-Mo and Hypol-PEG-Mo*

The polyurethane **Hypol-Mo** was prepared by reacting (η^5-$C_5H_4CH_2CH_2OH)_2Mo_2(CO)_6$ with Hypol 2000 in THF solution at 50 °C (Scheme 3). As mentioned in the Experimental Section, Hypol 2000 is a toluene diisocyanate endcapped, lightly branched poly(ethylene glycol). The structure was analyzed and reported in a prior paper.[8] (Note the branching feature of the prepolymer structure is not shown in Scheme 3.)
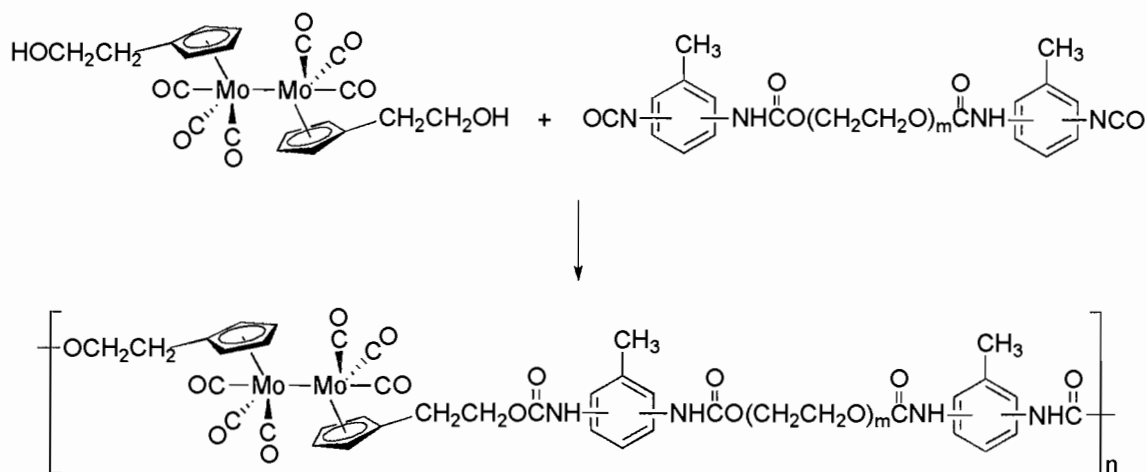
Scheme 3. Synthesis of the polyurethane **Hypol-Mo**.
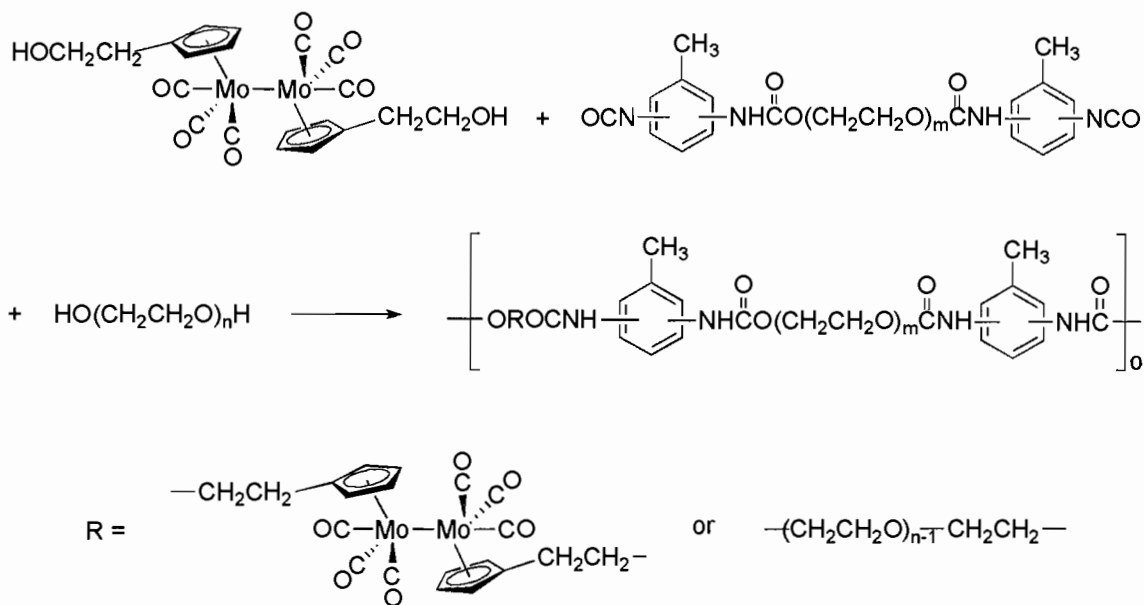
Scheme 4. Synthesis of the polyurethane **Hypol-PEG-Mo**.

The polyurethane copolymer **Hypol-PEG-Mo** was prepared in a similar fashion, except that PEG-1000 was also present (Scheme 4). Both polymers retain the deep red color of the $(\eta^5\text{-}C_5H_4CH_2CH_2OH)_2Mo_2(CO)_6$ complex (λ_{max} 389 and 512 nm), and both

polymers form films suitable for irradiation in the solid-state.[6] Samples of such films were prepared on glass microscope slides, and then separate samples were exposed to one of four different conditions: (1) ambient light in air, (2) ambient light under a nitrogen atmosphere, (3) air but no light, and (4) neither light nor air. Only the samples exposed to both light and air degraded, as monitored by UV-vis spectroscopy. ("Ambient light" in this instance refers to the normal light present in the laboratory from the overhead fluorescent lights and from the windows but not from direct sunlight.) These results are consistent with the results found for other polymers with metal-metal bonds along their backbones and are interpreted as showing that both light and a radical trap are necessary in order for degradation to occur; i.e., a net photochemical reaction only occurs if a radical trapping agent is present (in this case, O_2).[7] In the absence of a trapping agent, it is proposed that the geminate (Mo,Mo) radical cage pair recombines, leading to no net reaction: $L_nMo–MoL_n \leftrightarrows (L_nMo\bullet,\bullet MoL_n)$.[7]

Thin films of the samples exposed to light and air showed interesting changes in their physical appearance. After 3-5 hours of light exposure, numerous small bubbles appeared in the polyurethane films (Figure 1). On further exposure to light, the bubbles continued to grow, eventually merging with each other to form larger bubbles. Ultimately, polymers turned into a viscous liquid and dripped from the (vertical) glass microscope slide. (Note that both Hypol 2000 and PEG-1000 are viscous liquids; thus, as the Mo-Mo bonds are photochemically cleaved, the prepolymer units are effectively regenerated, hence the formation of a liquid product.) As shown in Figure 1, the polyurethane films turned from red to brown-green during the photochemical reactions.[a]

(a)   (b)   (c)
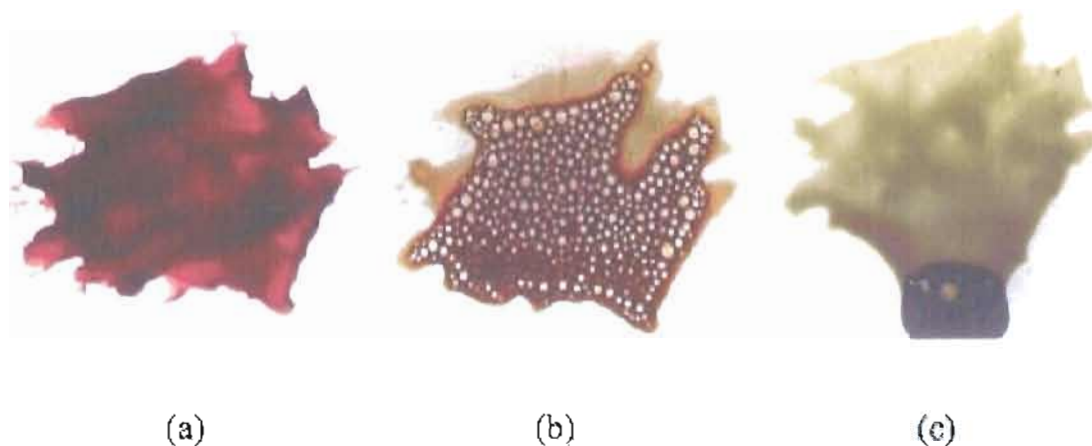
Figure 1. Photos of the photooxidative degradation of **Hypol-PEG-Mo** under ambient light and atmospheric temperature and pressure. (a) unexposed sample; (b) sample exposed to light for 5 h; (c) sample exposed for 3 days.

To gain more insight into what is happening during the photodegradation reaction, the photochemical reaction of **Hypol-Mo** in air was monitored by infrared spectroscopy using a film prepared on a NaCl salt plate. During the reaction, two new bands appeared at 2170 and 2110 cm^{-1} and increased in intensity as the bubbles grew in (Figure 2). These bands agree well with those reported for gaseous CO (see Figure 2, insert), and it is logical to suggest that the bubbles are formed by CO released from the Mo center during the degradation reaction.[b] Consistent with this interpretation, the spectra show the decrease in intensity of the $\nu(C\equiv O)$ bands of the $(-OCH_2CH_2C_5H_4)(CO)_3Mo-Mo(CO)_3(C_5H_4CH_2CH_2O-)$ unit at 1900, 1947, and 2004 cm^{-1} as irradiation progressed (see Figure 2).[9] Accompanying the decrease of these bands, new bands appeared at 1771, 1865, and 2046 cm^{-1}, but continued irradiation eventually caused these bonds to disappear (Figure 2). The $\nu(C\equiv O)$ bands at 1771, 1856, and 2046 cm^{-1} are tentatively assigned to disproportionation products of the $(\eta^5-C_5H_4CH_2CH_2O-)Mo_2(CO)_6$ unit. This

assignment is based on the fact that, in solution, the $(\eta^5\text{-}C_5H_5)Mo_2(CO)_6$ species readily

photochemically disproportionates in the presence of virtually any ligand (L) to form $(\eta^5\text{-}$

$C_5H_5)(CO)_3Mo^-$ and $(\eta^5\text{-}C_5H_5)(CO)_3MoL^+$ products. The anionic product has bands at

1771 and 1890 cm^{-1}, while the cationic species has a band located in the 2025-2060 cm^{-1}

region, depending on the identity of L.[10] In the photochemical reaction of the polymer,

the ligand L may possibly be an oxygen donor from the polyether segment or an oxygen

of a C=O group in the urethane linkage. The ionic disproportionation products are air-

sensitive, and the disappearance of these bands is consistent with the eventual reaction of

the ions with oxygen to form metal oxide final products that do not contain CO ligands.
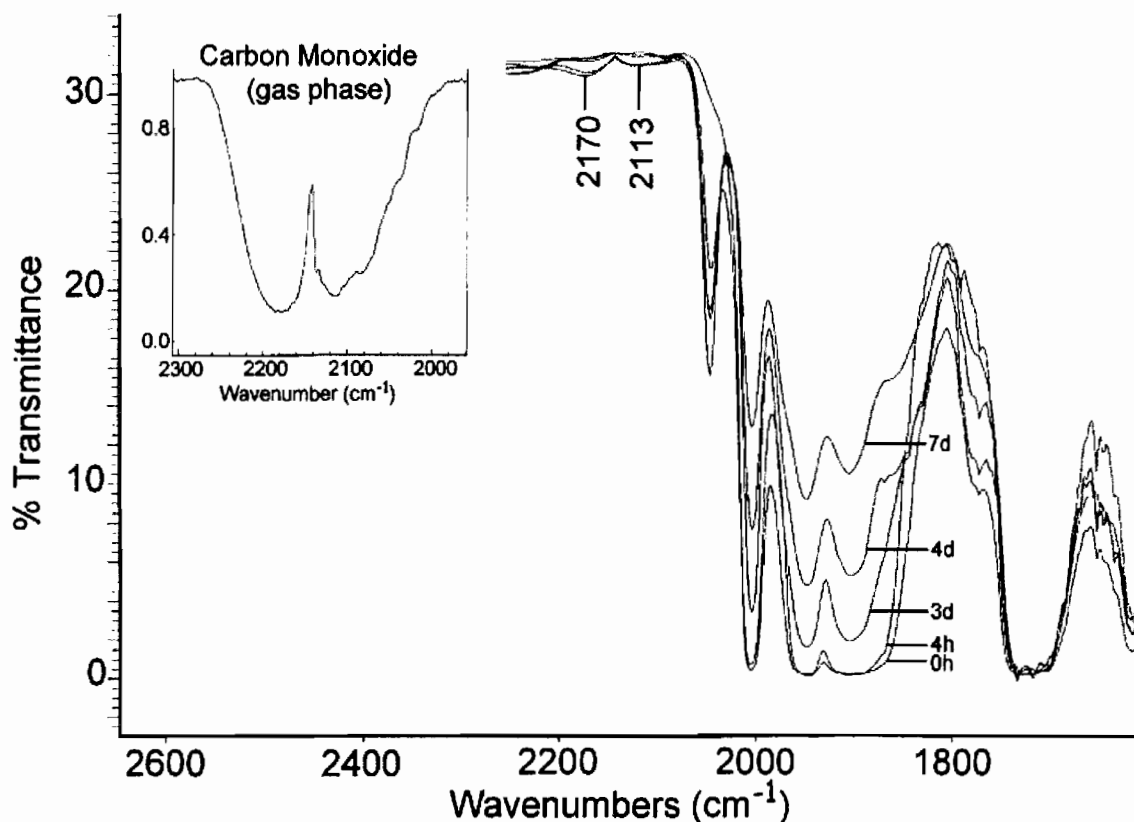
Figure 2. Infrared spectra showing the changes that occur when a film of **Hypol-Mo** on a NaCl plate was exposed to ambient light. The intensity of the two bands at 2170 and 2113 cm^{-1} (attributed to CO(g)) appeared and grew in intensity, the ν(C≡O) bands of the ($-$OCH$_2$CH$_2$C$_5$H$_4$)(CO)$_3$Mo$-$Mo(CO)$_3$(C$_5$H$_4$CH$_2$CH$_2$O$-$) unit at 1900, 1947, and 2004 cm^{-1} disappeared, and bands at 1771, 1856, and 2046 cm^{-1} transiently appeared and then disappeared with prolonged exposure. The inset shows the spectrum of CO gas for reference.

2.2.2 *X-ray Photoelectron Spectroscopic Investigation*

To identify the fate of the Mo in the photochemical degradation reactions of the polyurethanes, samples of polymers were analyzed by X-ray photoelectron spectroscopy (XPS). XPS spectra were also obtained for (η^5-C$_5$H$_5$)Mo$_2$(CO)$_6$ and MoO$_3$ for comparison. The Mo 3d core level presents two peaks, 3d$_{3/2}$ and 3d$_{5/2}$, due to spin-orbit

splitting, and accordingly the spectra were fit to two peaks. The binding energy difference between $3d_{3/2}$ and $3d_{5/2}$ peaks (3.1 eV) and peak intensity ratios $(I(3d_{5/2})/I(3d_{3/2}) = 3/2)$ were kept constant for all of the fits. The Mo $3d_{5/2}$ binding energies and the corresponding content in the sample surface are listed in Table 1. (The $3d_{5/2}$ peak is listed in the table because it is the more intense of the two peaks.) The values have been corrected for the effects of charge neutralization.

Table 1. Mo $3d_{5/2}$ binding energies of different materials.[a]

Material	Mo $3d_{5/2}$ binding energies (eV)[b]				
	Mo(0)	**Mo(I)**	**Mo(IV)**	**Mo(V)**	**Mo(VI)**
Pure Mo (Mo(0))	227.8				
MoO_2 (Mo(IV)			229.7		
MoO_3 (Mo(VI))					232.7
$(\eta^5\text{-}C_5H_4(CH_2)_2OH)_2Mo_2(CO)_6$ (Mo(I))		228.9			
Hypol-Mo ($t_{irradiation}$ = 0 min)		229.1			
Hypol-Mo ($t_{irradiation}$ = 10 min)		229.1 (74%)		231.5 (26%)	
Hypol-Mo ($t_{irradiation}$ = 120 min)				231.7 (20%)	232.9 (80%)

[a] C 1s hydrocarbon = 285.0 eV. [b] The percentages listed under the binding energies are the percentages of the total $3d_{5/2}$ peak area accounted for by that peak.

Note that the unexposed polymer **Hypol-Mo** has essentially the same binding energy (229.1 eV) as $(\eta^5\text{-}C_5H_4CH_2CH_2OH)_2Mo_2(CO)_6$ (228.9 eV), consistent with the unexposed polymers still having intact $(-OCH_2CH_2C_5H_4)(CO)_3Mo-$ $Mo(CO)_3(C_5H_4CH_2CH_2O-)$ units with Mo in the +1 oxidation state. (The slight shift in

binding energies between the two samples may be attributed to a slightly different chemical environment of Mo in the polymer compared to that in the solid microcrystals.) After exposure to ambient light for 10 minutes, a sample of the polymer showed $3d_{5/2}$ peaks at 229.1 (Mo(I) in the undegraded polymer) and at 231.5 eV. On the basis of literature data, the oxidation state of Mo in the latter species is likely +5.[11, 12] The ratio of Mo(I) to Mo(V) is 74% to 26%. After further exposure to ambient light for 2 hours, the XPS spectrum showed a major peak at 232.9 eV (assigned to a Mo(VI) species) and a smaller peak at 231.7 eV. The latter peak is again assigned to undegraded Mo(I). The ratio of Mo(VI) to Mo(V) was 80% to 20%.

2.2.3 *Photochemical Reactivity of the Polyurethanes in Air*

The key results in the sections above are (1) the Mo-Mo bond disappears in the photochemical reaction of the polymers (as demonstrated by the disappearance of the $v(C{\equiv}O)$ bands for the $(-OCH_2CH_2C_5H_4)(CO)_3Mo-Mo(CO)_3(C_5H_4CH_2CH_2O-)$ unit and by the color change of the films), (2) CO is released in the photochemical reactions (as demonstrated by the appearance of bubbles in the films and the presence of free CO in the infrared spectrum), (3) no other Mo-carbonyl species is formed as a final product, (4) O_2 is necessary to obtain a net photochemical reaction, (5) the ultimate fate of the Mo is a Mo(VI) species, and (6) the fate of the organic portion of the polymers is low-molecular-weight liquid, likely PEG units. Taken together, these results suggest the photochemical reaction shown in Scheme 5 (shown for **Hypol-Mo**, but an analogous reaction applies for **Hypol-PEG-Mo**).
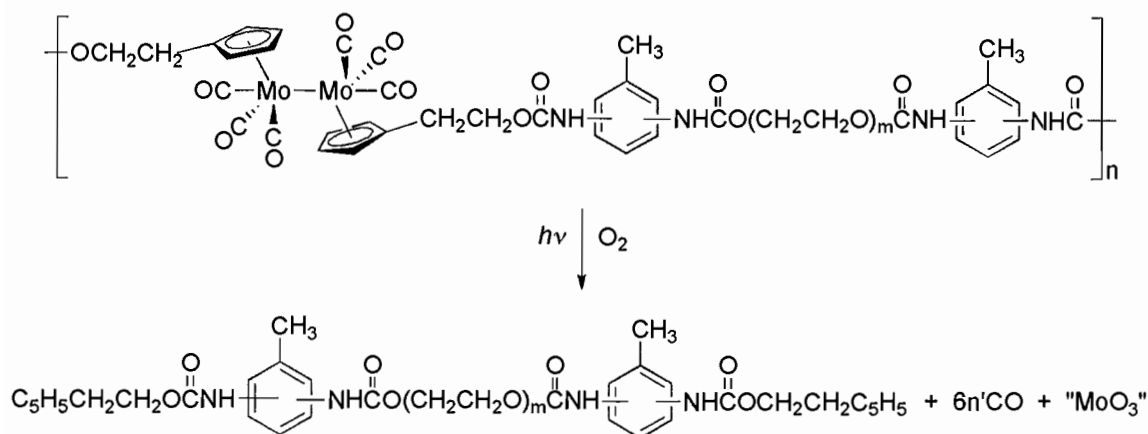
Scheme 5. Photodegradation of **Hypol-Mo** under ambient conditions.

2.2.4 *Photodegradation of PU-70 Under a Nitrogen Atmosphere*

A long-range goal is to develop ways to control the rate of degradation in photodegradable polymers. One approach is to control the efficiency with which any photogenerated metal radicals are captured. (The capture efficiency will affect the rate of degradation, because the non-trapped radicals can back-react to reform the metal-metal bond.) To control the rate of the radical trapping reaction, we are designing polymers with radical traps built into the backbone. It is suggested that it should be possible to control more easily the degradation of polymer with built-in radical traps, because the concentration of the trap can be manipulated. In a prior paper, we reported the photochemical degradation reactions of a PVC polymer modified with Mo-Mo bonds that has an abundance of chlorine atoms to act as radical trapping agents (Figure 7 of Chapter I).[13] To explore the effect of a lower concentration of Cl, polymer **PU-70** was synthesized (Scheme 6).
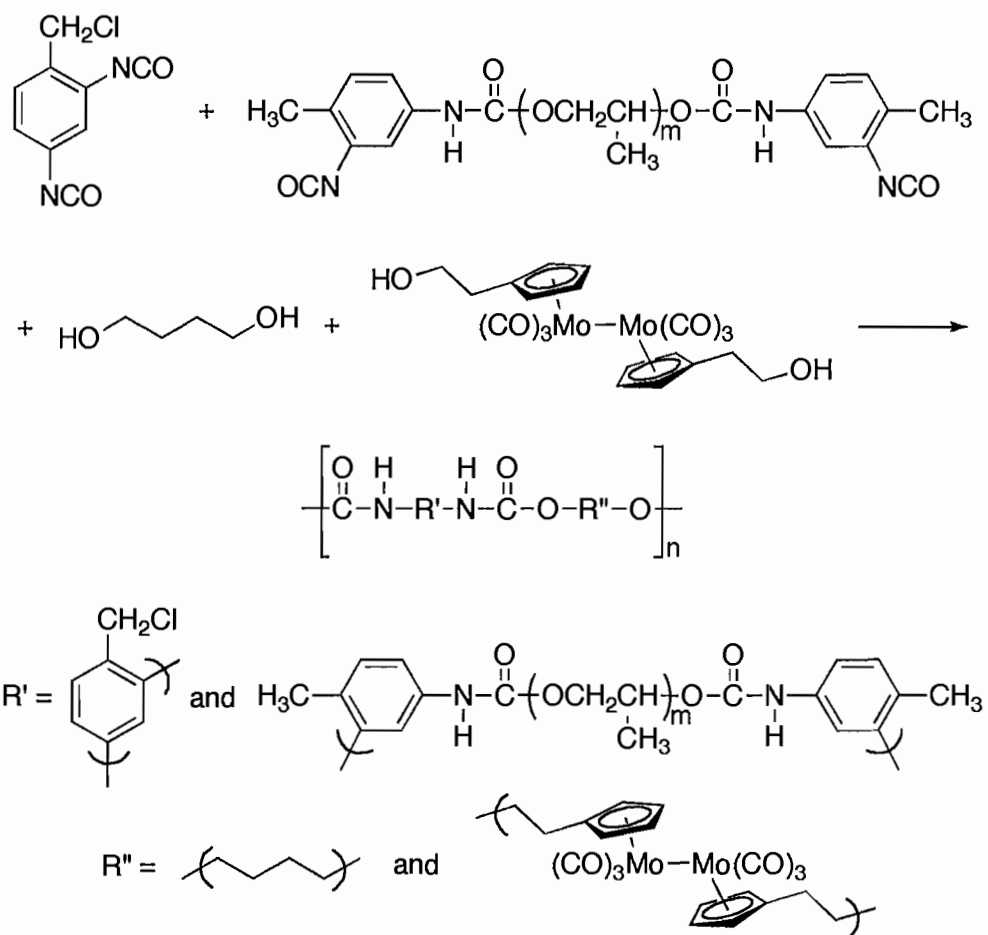
Scheme 6. Synthesis of polymer **PU-70**.

The photochemical reaction of polymer **PU-70** ($\lambda_{irradiation}$ 546 nm) under a nitrogen atmosphere was monitored by infrared and electronic absorption spectroscopy. The latter method showed the disappearance of the absorption band at 512 nm, and infrared spectroscopy showed the disappearance of the $\nu(C\equiv O)$ bands in the ($-OCH_2CH_2C_5H_4)(CO)_3Mo-Mo(CO)_3(C_5H_4CH_2CH_2O-$) unit at 2005, 1950, and 1907 cm^{-1} and the appearance of new bands at 2048 and 1972 cm^{-1}, attributable to the

(–OCH$_2$CH$_2$C$_5$H$_4$)(CO)$_3$Mo–Cl component.[c] The reaction is the same as in solution and an example of the photochemistry is illustrated in Scheme 2.

The quantum yield for the reaction of polymer **PU-70** was determined to be 0.35. (The quantum yield, Φ, is defined as the rate of a photoreaction divided by the absorbed light intensity; i.e., Φ = reaction rate/absorbed intensity.) Perhaps surprisingly, this quantum yield is higher than the quantum yield (0.15) for the similar reaction for the modified PVC polymer **PVC-Mo**, which has a considerably high concentration of C–Cl bonds for metal-radical trapping.[13] These values can also be compared to the quantum yield (0.36) of plasticized PVC, **PPVC-Mo**.[114] One possible explanation is the difference in the glass transition temperature, T_g, values of the polymers. The irradiation of the polymers was performed at 25 °C, which is below the T_g volume of polymer **PVC-Mo** (65 °C) and above the T_g value of polymer **PU-70** (-44 °C) and plasticized polymer **PPVC-Mo** (20 °C). It is suggested that chain movement to achieve proper orientation for radical capture and C–Cl concentration are both important factors in determining the efficiency of photochemical degradation.

2.3 Key Insights and Conclusions

Films of polymers containing the (–OCH$_2$CH$_2$C$_5$H$_4$)(CO)$_3$Mo– Mo(CO)$_3$(C$_5$H$_4$CH$_2$CH$_2$O–) unit along their backbones react photochemically with visible light in the presence of oxygen to form Mo(V) and Mo(VI) oxides, CO(g), and lower molecular weight organic-backbone polymer species. In the absence of metal-radical traps (e.g., O$_2$), no net photochemical reaction occurs, because the photogenerated Mo radicals recombine. **PU-70** contains built-in radical traps (C–Cl bonds), and this

polymer efficiently degrades in the absence of oxygen, because the Mo radicals abstract the Cl atoms to form Mo-Cl bonds, thus preventing the recombination reactions of Mo radicals. Despite the relatively low concentration of Cl in polymer **PU-70**, it degrades more efficiently at room temperature than polymers containing considerably higher concentrations of Cl. It is proposed that, because T_g of polymer **PU-70** is lower than the reaction temperature, chain movement to achieve the proper orientation for the abstraction reaction is relatively facile, resulting in a relatively efficient photochemical reaction. In Chapter III, data is presented that provides greater insight into the role of radical trapping concentration and the glass transition temperature.

2.4   Endnotes

a.   Mixtures of Mo(V) and Mo(VI) oxides are frequently highly colored. See for example: Siokou, A.; Leftheriotis, G.; Papaefthimiou, S.; Yianoulis, P. Surf. Sci. 2001, 482-485 (Part 1), 294.

b.   NIST Mass Spec Data Center, S. E. Stein, director, "Infrared Spectra" in NIST Chemistry WebBook, NIST Standard Reference Database Number 69, Eds. P. J. Linstrom and W. G. Mallard, March 2003, National Institute of Standard and Technology: Gaithersburg, MD, 20899 (http://webbook.nist.gov).

c.   The band at 1972 cm^{-1} was merged into the strong absorption from the parent dimer.

CHAPTER III

FACTORS CONTROLLING THE RATE OF PHOTODEGRADATION IN

POLYMERS

Daglen, B. C.; Tyler, D. R. In *Degradable Polymers and Materials*; Khemani, K. C.;
Scholz, C., Eds.; ACS Symposium Series 939; American Chemical Society: Washington,
DC, 2006; pp 384-397.

3.1   Introduction

In order to predict polymer lifetimes, control when a polymer starts to degrade,

and control the rate of degradation, it is necessary to identify the experimental parameters

that affect polymer degradation rates and to understand how these parameters affect

degradation. Among the parameters that have been identified as affecting polymer

lifetime are temperature, exposure to ultraviolet radiation, light intensity and wavelength,

oxygen diffusion rates in the polymer, tensile stress, compressive stress, chromophore

concentration, molecular weight, humidity, and polymer morphology.[1-4] In this chapter,

we report how the glass transition temperature and the radical trap concentration also

affect polymer photodegradation rates.

This work was published in Volume 939 of the American Chemical Society

Symposium Series on Degradable Polymers and Materials in 2006. All the experiments

in this chapter were performed by myself. D. R. Tyler and myself were co-authors of the

manuscript.

3.2   Results and Discussion

3.2.1   *Experimental Approach to the Problem*

Several challenging experimental problems hinder the rigorous experimental mechanistic exploration of polymer photodegradation. One of the difficulties is that polymer degradation is mechanistically complicated.[5] This is not to say that the mechanisms are not understood; in fact, they are understood in detail.[5] Rather, the mechanisms are intricate, often involving multiple steps, cross-linking, and side-reactions; this makes pinpointing the effects of stress difficult. Another complication is that oxygen diffusion is the rate-limiting step in photooxidative degradations, the primary degradation mechanism in most polymers.[6, 7] This can add to the intricacy of the kinetics analysis because cracks and fissures develop in the polymer as degradation proceeds; these fractures provide pathways for direct contact of the polymer with oxygen, which will then no longer degrade at a rate controlled by oxygen diffusion. To circumvent these experimental and mechanistic complexities and therefore make it less difficult to interpret data and obtain fundamental insights, we use three key experimental strategies in our investigations. First, we study the problem using special photodegradable polymers of our own design that contain metal-metal bonds along the backbone.[8-13] These polymers are photodegradable because the metal-metal bonds can be cleaved with visible light and the resulting metal radicals captured with an appropriate radical trap, typically and organic halide or molecular oxygen (the reaction is discussed in more detail in Chapter II).

By studying these "model" systems, we are able to extract information without the mechanistic complications inherent in the degradation mechanisms of organic radicals. (For example, metal radicals do not lead to cross-linking, so we can avoid this complicating feature found with organic radicals.) The second key experimental strategy is to use polymers that have built-in radical traps, namely C–Cl bonds.[14, 15] By eliminating the need for external oxygen to act as a trap, we exclude the complicating kinetic features of rate-limiting oxygen diffusion. The third experimental strategy is to use the distinctive M–M bond chromophore to spectroscopically monitor the photodegradation reactions of the polymers. This allows us to compare the efficiencies of the photodegradations by measuring the quantum yields of the reactions. (The quantum yield, Φ, is defined as the rate of a photoreaction divided by the absorbed light intensity; i.e., Φ = reaction rate/absorbed intensity.) The use of quantum yields to quantify and compare the various degradation rates is a crucial advance because polymer degradation reactions have typically been monitored by stress testing, molecular weight measurements, or attenuated total reflection (ATR) spectroscopy, all of which can be laborious and time consuming.[16] Relative to these techniques, quantum yield measurements are straightforward. (Note that quantum yields in regular carbon-chain polymers cannot be measured conveniently by UV-vis spectroscopy because there are generally no suitable chromophores.) To further expedite our quantum yield measurements, we use a computerized apparatus that automatically measures the quantum yields on thin film polymer samples.[17, 18]

3.2.2 *Polymer Synthetic Strategy*

Our general synthetic route for incorporating metal-metal bonds into polymer

backbones is based on the step polymerization techniques for incorporating ferrocene into

polymer backbones.[19-21] Step polymers of ferrocene can be made by substituting the

cyclopentadienyl (Cp) rings with appropriate functional groups followed by reaction with

appropriate difunctional organic monomers (Scheme 1).[22-24]
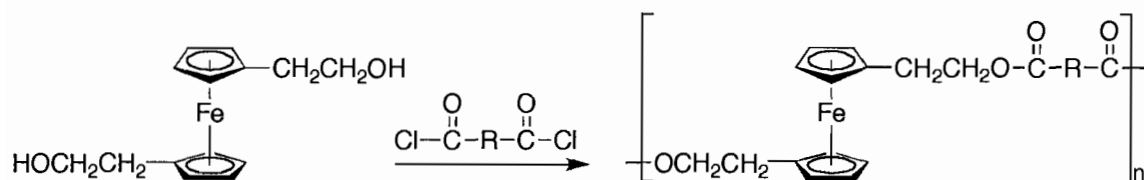
Scheme 1. Example of a step polymerization technique used to incorporate an
organometallic complex into a polymer backbone.

The analogous strategy for synthesizing metal-metal bond-containing polymers

also used difunctional, cyclopentadienyl-substituted metal dimers. A sample

polymerization reaction is shown in Scheme 2, which illustrates the reaction of a metal-

metal bonded "diol" with a hexamethylene diisocyanate (HMDI) to form a polyurethane.

This step polymerization strategy is quite general, and a number of metal-metal bond-

containing polymers have been made from monomers containing functionalized Cp

ligands.
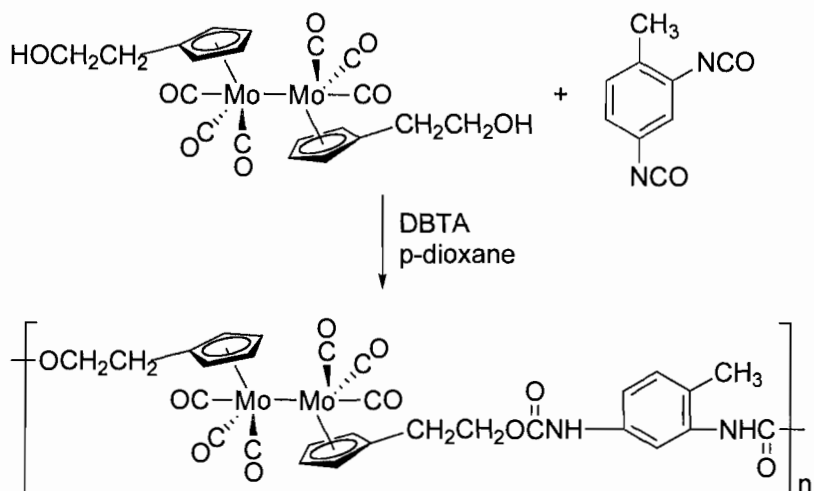
Scheme 2. Example of a polyurethane synthesis used to incorporate molybdenum dimers into the backbone of a polymer chain.

3.2.3 *Synthesis of the PU-XX Polymers*

Using the synthetic strategy in Schemes 1 and 2, the polymers for this study were synthesized by the route shown in Scheme 3. Note that the amount of Cl-containing aromatic diisocyanate was varied, which gave polymers with different glass transition temperatures as well as polymers that have different radical trap to metal atom ratios. For example, **PU-90** has a T_g of 35 °C and a 9:1 [C–Cl]:[Mo] ratio, and **PU-70** has a T_g of -44 °C and a 7:1 [C–Cl]:[Mo] ratio. (The XX number in the **PU-XX** nomenclature indicates the mole fraction of aromatic diisocyanate in the overall amount of diisocyanate used in the formulation.)
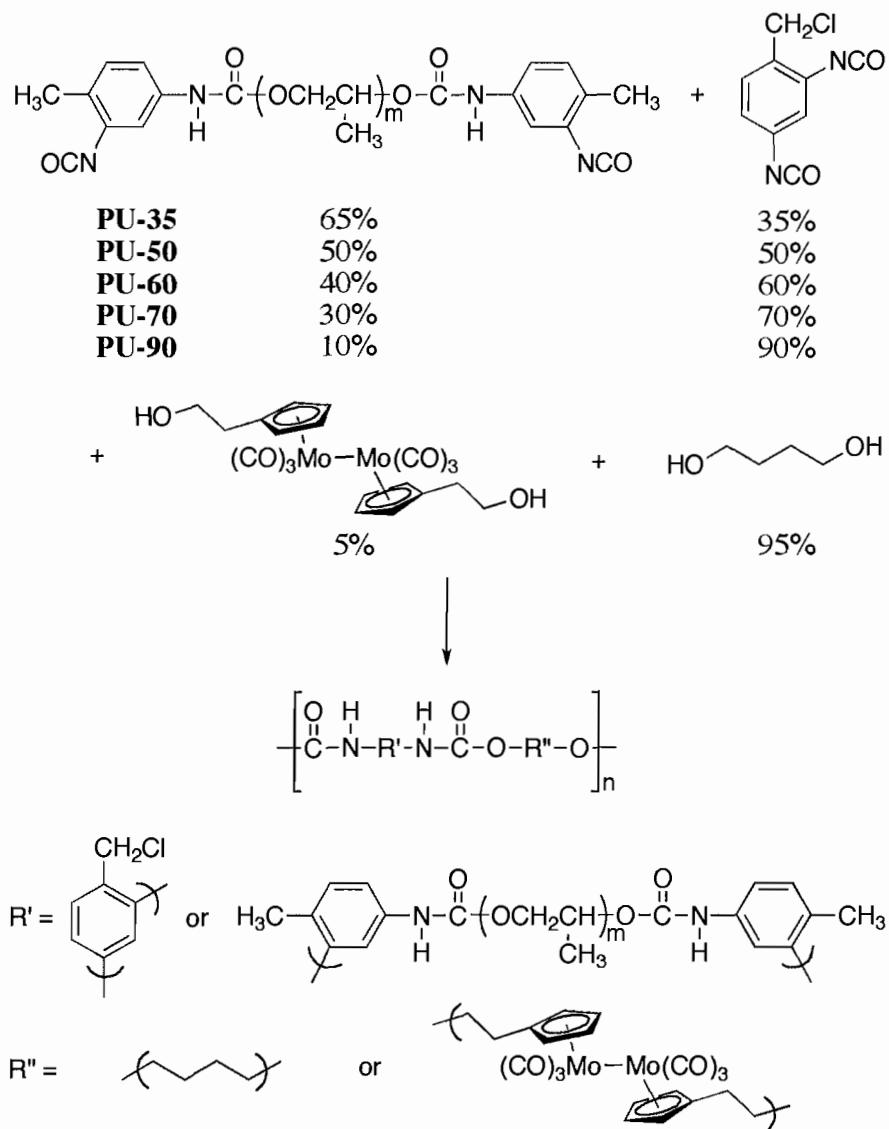
Scheme 3. Syntheses of **PU-XX** polymers.

3.2.4 *Photodegradation Occurs in the Absence of O₂*

As expected, polymers containing C-Cl bonds photochemically degraded in the absence of oxygen. Spectroscopic monitoring of the reactions showed the disappearance of the $Cp_2Mo_2(CO)_6$ chromophore (λ_{max} = 390 and 510 nm; ν(C≡O) 2009, 1952, and 1913 cm^{-1}) and the appearance of the $CpMo(CO)_3Cl$ unit (ν(C≡O) 1967 and 2048 cm^{-1}).

In addition, the number average molecular weight decreased steadily during the course of the reaction. The reaction in Scheme 4 is suggested.
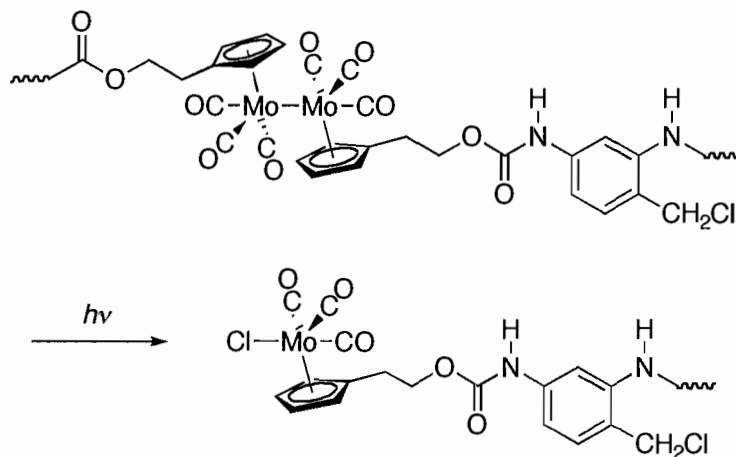
Scheme 4. Photochemical reaction of the **PU-XX** polymers.

3.2.5 *Effect of T_g on the Efficiency of Photodegradation*

The quantum yields for **PU-90** and **PU-70** at 26 °C are shown in Table 1. In addition, the quantum yields for **PVC-Mo** and PVC-Mo plasticized with DOP (**PPVC-Mo**) (20%) are provided.

Table 1. Quantum yields for various polymers with different glass transition temperatures and for a model complex.

Polymer	T_g (°C)	Quantum Yield (Φ) at 26 °C
PVC-Mo	75	0.15 ± 0.03
PU-90	35	0.05 ± 0.02
PU-70	-44	0.35 ± 0.04
PPVC-Mo	<< RT	0.35 ± 0.07
model complex **1**	solution phase	0.43 ± 0.03

The quantum yields were measured at 26 °C. Note in the table that the quantum yields are 0.35 for the two polymers with T_g < 26 °C, while the two polymers with T_g > 26 °C have considerably lower quantum yields.

The quantum yields for the polymers with T_g < 26 °C are close to the quantum yields for model complexes (e.g., Φ = 0.43 for model complex **1** at 0.38 cP; Scheme 5.) This result suggests that when the irradiation takes place above T_g, chain mobility is facile enough that a radical trap (i.e., a C–Cl bond) is encountered before metal-radical-metal-radical recombination occurs. In contrast, when irradiation takes place below T_g, chain mobility is limited and metal-radical-metal-radical recombination occurs in many instances before a metal-radical encounters a C–Cl bond. The quantum yields above T_g are similar to those in solution because, in solution, chain mobility is quite facile and radical traps are readily encountered.
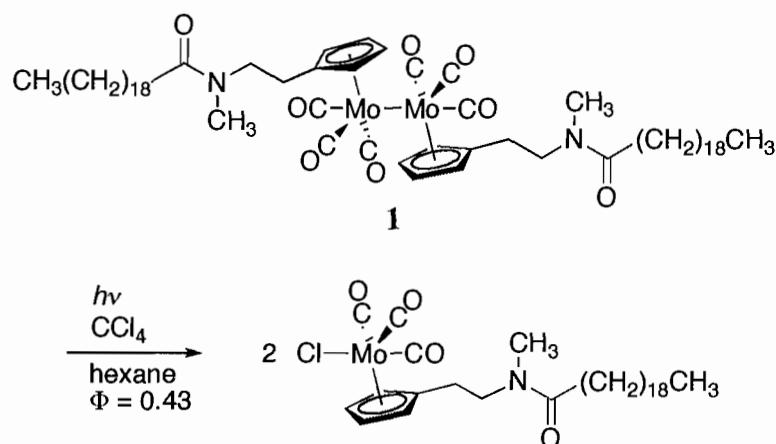
Scheme 5. Photodegradation of a model complex, **1**, in solution with CCl$_4$ as the radical trapping agent.

3.2.6 *Effect of Radical Trap Concentration*

The effect of radical trap concentration on the quantum yields of polymer degradation was studied using the polymers **PU-35**, **PU-50**, **PU-60**, **PU-70**, and **PU-90**. The results are shown in Table 2 and can be summarized as follows: If $T_g < T_{irradiation}$ then the quantum yield (Φ) is independent of trap concentration. Thus, $\Phi = 0.35$ for **PU-35**, **PU-50**, **PU-60**, and **PU-70**. In contrast, if $T_g > T_{irradiation}$ then the quantum yield is dependent on trap concentration. Thus, $\Phi = 0.05$ for **PU-90** ($T_g = 35$ °C) under an N$_2$ atmosphere but $\Phi = 0.10$ for **PU-90** under an O$_2$ atmosphere. (The O$_2$ is a radical trap so the experiment performed under an O$_2$ atmosphere has a larger concentration of radical trap.) The explanation for these observations again lies in chain mobility. When the irradiation takes place above T_g, the radical chain ends are relatively mobile, and the reaction of the metal radicals with the radical traps is kinetically saturated with trap at the concentrations of trap used in these experiments. In contrast, when irradiation occurs below the glass transition temperature, because of limited chain mobility, the reaction

kinetics are not saturated in trap concentration and the quantum yields depend on the concentration of radical trap.

Table 2. Quantum yields for polymer degradation for polymers with different concentrations of metal-radical trap.

Polymer (atmosphere)	T_g (°C)	Quantum Yield (Φ) at 26 °C
PU-35 (N_2)	-47	0.35 ± 0.04
PU-50 (N_2)	-46	0.35 ± 0.01
PU-60 (N_2)	-46	0.35 ± 0.02
PU-70 (N_2)	-44	0.35 ± 0.04
PU-90 (N_2)	35	0.05 ± 0.02
PU-90 (O_2)	35	0.10 ± 0.03

3.3   Summary and Conclusions

The photochemical reactivity of polymers is of considerable interest because photodegradable plastics have a number of applications. Additional interest in polymer photoreactivity stems from the need to limit and control "weathering" in polymer materials. Photodegradation is an important component of polymer weathering, and a proper understanding of degradation processes and of the experimental factors that affect degradation is necessary for the accurate estimation of polymer lifetime and for the development of stabilizing systems.

Among the experimental parameters that have been shown to affect polymer degradation rates are light intensity, temperature, oxygen diffusion, chromophore concentration, polymer morphology and stress. This study added two more experimental

parameters to this list, namely the glass transition temperature, T_g, and the concentration of radical trap. To investigate the effects of T_g and trap concentration on degradation efficiencies, specially designed polymers with metal-metal bonds along their backbones were synthesized. These polymers degrade by a straightforward mechanism that makes it possible to extract meaningful information. Using these polymers, it was shown that when polymers are irradiated above their glass transition temperature their quantum yields of degradation are similar to their quantum yields in solution. When irradiated below their glass transition temperatures, the quantum yields of photodegradation are small, i.e., the degradation reactions are inefficient. The explanation suggested is that when the irradiation takes place above T_g, chain mobility is facile enough that a metal-radical trap is encountered before radical-radical recombination occurs. In contrast, when irradiation takes place below T_g, chain mobility is limited and metal-radical-metal-radical recombination occurs in many instances before a metal-radical encounters a trap. The quantum yields above T_g are similar to those in solution because, in solution, chain mobility is facile and radical traps are easily encountered. Chain mobility also explains the affect of radical trap concentration on the efficiency of photodegradation. When the irradiation takes place above T_g then the radical chain ends are relatively mobile, and the reaction of the metal radicals with radical traps is kinetically saturated with trap at the concentrations of trap used in these experiments. In contrast, when irradiation occurs below the glass transition temperature then, because of limited chain mobility, the reaction kinetics are not saturated in trap concentration and the quantum yields are dependent on the concentration of radical trap. In Chapter IV, the photodegradation

efficiencies of a polymer as a function of temperature are evaluated and compared to two model systems.

CHAPTER IV

THE EFFECT OF TEMPERATURE ON THE PHOTODEGRADATION QUANTUM

YIELDS OF POLYMERS CONTAINING METAL-METAL BONDS IN THE

POLYMER CHAIN

4.1   Introduction

The effect of temperature on the thermal degradation rates of polymers has been

extensively explored because of the need to predict the service lifetime of consumer

plastics. However, only a few studies have probed the effect of temperature on the

photochemical degradation rates of polymers. These studies are rather inconclusive with

respect to a general model for predicting the dependence of photodegradation rates on

temperature. Several studies found that the results are consistent with an Arrhenius

relationship, but other studies have observed non-Arrhenius behavior.[1-5] There is some

indication that the non-Arrhenius behavior is due to the complex degradation pathways

referred to above, and therefore the relatively straightforward degradation process in

polymers with metal-metal bonds might provide some fundamental insights that are not

obtainable with standard carbon-chain polymers. Accordingly, we began a study to

investigate the effect of temperature on the degradation efficiencies of metal-metal bond

containing polymers. In this chapter we report data showing the effect of temperature on

the degradation efficiencies of a PVC polymer that has metal-metal bonds incorporated in

its chain.

This chapter was published in volume 17 in the Journal of Inorganic and Organometallic Polymers and Materials in 2007. (With the exception of the experiments in section 4.2.4 which were performed by myself subsequent to the publication.) The solution studies were performed with the assistance of J. Harris and the solid-state experiments were performed by myself. D. Tyler and I were the co-authors of the manuscript.

4.2   Results and Discussion

4.2.1   *Polymer Preparation and Characterization*

PVC-Mo was prepared by reacting acyl chloride-substituted poly(vinyl chloride) with diol $(\eta^5\text{-}C_5H_4CH_2CH_2OH)_2Mo_2(CO)_6$, as shown in Scheme 1. The polyurethane, **PU-70** was prepared by reacting two diisocyanates: a poly(propylene glycol) prepolymer and radical trap containing monomer, and two diols: $(\eta^5\text{-}C_5H_4CH_2CH_2OH)_2Mo_2(CO)_6$ and 1,4-butanediol. Previous work showed that thin films of **PVC-Mo** are photochemically reactive ($\lambda = 532$ or 546 nm) in the absence of oxygen.[6] Infrared spectroscopic monitoring of the polymer chemical reaction showed the disappearance of the $\nu(C\equiv O)$ bands of the $[Cp_2Mo_2(CO)_6]$ unit at 2005, 1950, and 1970 cm^{-1} and the appearance of bands attributed to the $[CpMo(CO)_3Cl]$ unit at 2048 and 1976 cm^{-1}. The reaction is thus similar to the photochemical radical trapping reactions of the $Cp_2Mo_2(CO)_6$ dimer that takes place in solution in the presence of an alkyl halide, and an analogous mechanism is proposed (Scheme 1).[7]
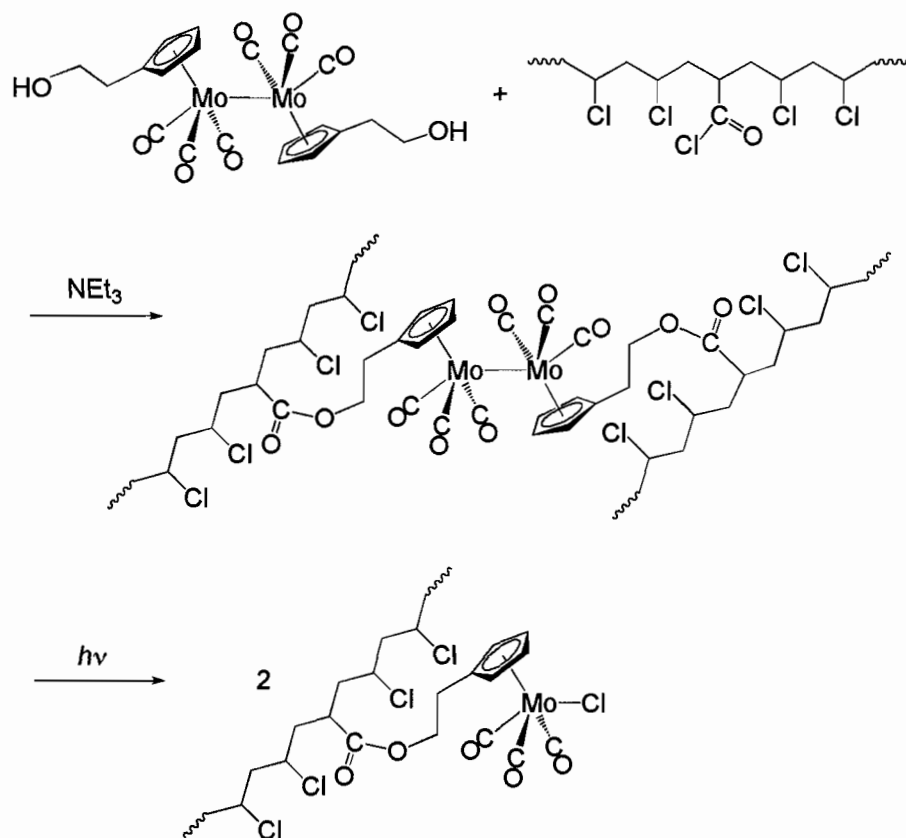
Scheme 1. Synthesis and photodegradation of **PVC-Mo**.

4.2.2 *Temperature Dependence on the Degradation of PVC Polymer and Model Systems*

The temperature dependence of the quantum yields for the degradation of polymer **PVC-Mo** could depend on: (1) the inherent temperature dependence of the photolysis and radical trapping reaction of the $[Cp_2Mo_2(CO)_6]$ unit: (2) the temperature dependent behavior of the polymer morphology, or (3) a temperature-dependent dynamical property of the photogenerated radicals in the polymer. To differentiate between these possibilities, two control experiments were carried out, namely the photolysis of $Cp'_2Mo_2(CO)_6$ dispersed in a PVC polymer matrix and the photolysis of

$Cp'_2Mo_2(CO)_6$ in hexane/CCl_4 solution. The quantum yields for the disappearance of the $Cp_2Mo_2(CO)_6$ unit in **PVC-Mo,** for $Cp'_2Mo_2(CO)_6$ dispersed in PVC, and for $Cp'_2Mo_2(CO)_6$ in hexane/CCl_4 solution are plotted versus temperature in Figure 1. Note that all of the solid-state data were collected below the glass transition temperature of the polymer films (T_g = 65–72 °C). The plots show that there is a significant increase in the quantum yields for the polymer **PVC-Mo** with increasing temperature. In contrast, for $Cp'_2Mo_2(CO)_6$ dispersed in PVC and for $Cp'_2Mo_2(CO)_6$ in hexane/CCl_4 solution (in which the Mo-Mo chromophores are unattached to the polymer chains) there are only slight increases in the quantum yields over this temperature range. An immediate conclusion is that the large increase in the quantum yields with temperature for **PVC-Mo** is not attributable to an inherent temperature dependence of the photolysis and subsequent radical trapping reaction of the $Cp_2Mo_2(CO)_6$. (Otherwise, the quantum yields for $Cp'_2Mo_2(CO)_6$ in the hexane/CCl_4 solution would also show a sizeable temperature dependence.) Also, because the quantum yields for $Cp'_2Mo_2(CO)_6$ dispersed in PVC show only a slight temperature dependence, the temperature dependence observed for **PVC-Mo** cannot be ascribed solely to changes in PVC morphology. (Otherwise, the $Cp'_2Mo_2(CO)_6$ dispersed in PVC and **PVC-Mo** would show a similar temperature dependence because the morphologies of PVC and **PVC-Mo** are similar in regard to crystallinity, modulus (1300 ± 100 vs. 1200 ± 50 MPa), and glass transition temperature (65 ± 4 vs. 72 ± 3 °C).
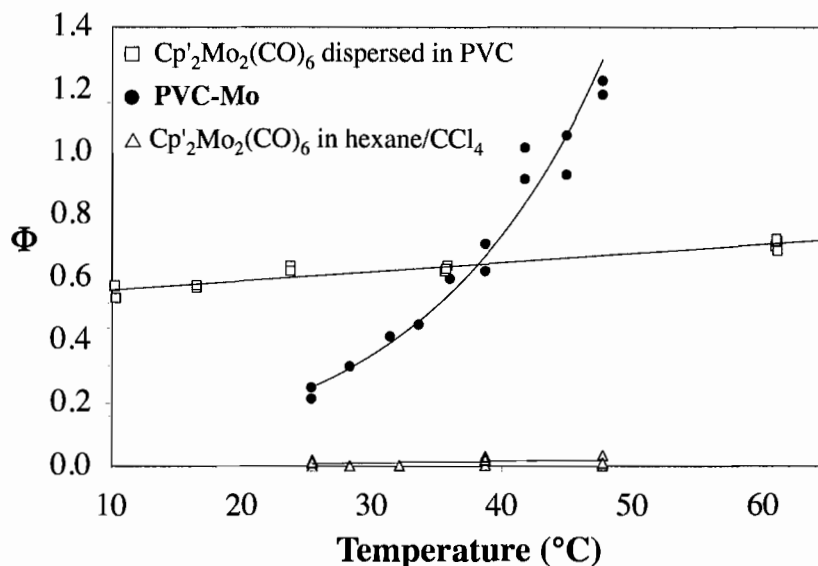
Figure 1. Plots of the quantum yields for the disappearance of the $Cp_2Mo_2(CO)_6$ unit in **PVC-Mo**, $Cp'_2Mo_2(CO)_6$ dispersed in PVC, and $Cp'_2Mo_2(CO)_6$ in hexane/CCl_4.

As an aside, it is noted that the small increase in the quantum yield for $Cp'_2Mo_2(CO)_6$ in the hexane/CCl_4 solution is attributed to the slight decrease in the viscosity of the solution with the increase in temperature. It is well established that the quantum yields for photolysis and subsequent trapping reactions of metal-metal bonded dimers are viscosity dependent because of the cage effect, and the temperature dependence of the quantum yields observed in this study is likely just an example of this phenomenon.[8] To check the validity of this statement, two experiments were performed: 1) observe the change in viscosity of the solution over the temperature range evaluated and 2) observe the effect of viscosity on the quantum efficiency of this reaction using a viscogen rather than variable temperature to change the viscosity. The results of these two experiments are shown in Figure 2. Figure 2a shows the change in viscosity for the $Cp'_2Mo_2(CO)_6$ in the hexane/CCl_4 solution over the temperature range of the

photochemical experiments. The viscosity ranged from about 1.6 cP at 25 °C to 0.8 cP at 50 °C. Solutions of $Cp'_2Mo_2(CO)_6$ in the hexane/CCl_4 were prepared with varying amounts of squalene to represent the range of viscosities observed in the variable temperature experiment illustrated in Figure 2a. The photochemical quantum yields for those solutions with variable viscosities obtained at room temperature are shown in Figure 2b. A crude linear relationship can be fit to both of these plots and an equation extracted. (The fit is crude because the overall relationship between temperature and viscosity and viscosity and quantum yield is not linear but a linear relationship can be approximated over this small range.) These two equations, with viscosity as the common variable, can be combined to solve for an equation that represents the change in quantum yield as a function of temperature as predicted from changes in viscosity with temperature. (Note again that the resulting equation is derived only for this particular temperature range and is not applicable outside of it.) Shown in Figure 2c is the plot for the experimentally determined quantum yield versus temperature for the $Cp'_2Mo_2(CO)_6$ in the hexane/CCl_4 solution and the predicted values from the calculated relationship. The experimental and calculated values are similar and it is therefore concluded that the temperature affects the viscosity of the solution and subsequently the ability of the metal radicals to escape the radical cage.
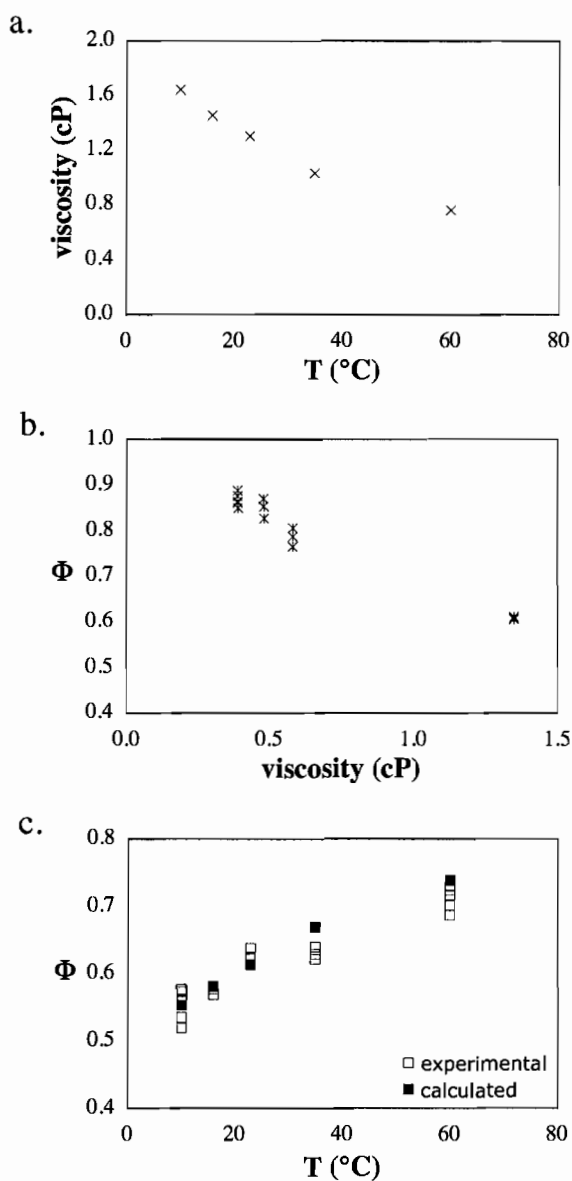
Figure 2. Illustrated are the relationships between: a) the viscosity of a solution of $Cp'_2Mo_2(CO)_6$ in hexane/CCl_4 at variable temperature, b) the quantum efficiency of $Cp'_2Mo_2(CO)_6$ photolysis in hexane/CCl_4 at a constant temperature and variable viscosity, and c) the quantum efficiency of $Cp'_2Mo_2(CO)_6$ in a hexane/CCl_4 solution at variable temperature.

For the $Cp'_2Mo_2(CO)_6$ dispersed in PVC, the small increase in quantum yields with increasing temperate is attributed to an increase in the free-volume.[9] This

explanation is based on a suggestion by Guillet to explain a similarly small temperature dependence in the quantum yields for degradation of poly(vinyl ketone), PVK.[10] In that study, Guillet found that the quantum yields of degradation below the glass transition temperature, T_g, increased gradually with increasing temperature ($\Delta\Phi = 0.04$ for T = 20–100 °C. To explain this behavior, Guillet noted that PVK degrades by a Norrish type II mechanism, which proceeds via formation of a six-membered ring intermediate. He proposed that, because the degradation pathway required substantial rearrangement of the polymer chain to form the six-membered ring intermediate, the slight increase in quantum yields with increased temperature below T_g was a reflection of the increase in free-volume of the solid-state polymer, which allows for easier rearrangement of the chain to the six-membered ring intermediate. It is interesting to note that, at T_g, Guillet observed a dramatic increase in the quantum yield to a value similar to that in solution ($\Phi_{PVK} = 0.24$). The sudden increase in Φ at the glass transition temperature was attributed to the ability of the polymer chains to easily form the intermediate because of facile chain movement above T_g. (The experimental apparatus used in the present study was not able to attain the temperatures required to study this phenomenon with **PVC-Mo**.)

In contrast to PVK, the degradation of polymer **PVC-Mo** does not require the polymer chains to extensively reorganize, and consequently some parameter other than free-volume is likely responsible for the observed temperature dependence of the quantum yield. In order to get better insight into what parameter is controlling the temperature dependence of Φ in **PVC-Mo**, it is necessary to look in more detail at the

mechanism of $Cp'_2Mo_2(CO)_6$ photolysis and the subsequent radical capture reaction. (Recall from the discussion above that the increase in Φ with increasing temperature in **PVC-Mo** cannot be attributed to either an intrinsic temperature-dependent reactivity property of the $Cp'_2Mo_2(CO)_6$ molecule or to changes in PVC morphology.) At 25.4 °C, the quantum yields for disappearance of the Mo-Mo chromophore are as follows: **PVC-Mo**, $\Phi = 0.20$; $Cp'_2Mo_2(CO)_6$ dispersed in PVC, $\Phi = 0.07$; and $Cp'_2Mo_2(CO)_6$ in the hexane/CCl_4 solution, $\Phi = 0.35$. As expected, the quantum yield in solution is considerably higher than that for $Cp'_2Mo_2(CO)_6$ dispersed in PVC polymer because the solution state is considerably less viscous that the solid state. Perhaps surprising, however, is the much larger quantum yield for **PVC-Mo** (0.20) compared to $Cp'_2Mo_2(CO)_6$ dispersed in PVC polymer (0.07). The substantial difference in the two quantum yields is proposed to be attributable to a difference in the radical-radical recombination efficiencies (the "cage effect") in the two polymers.[11] The cage effect is illustrated in Scheme 2, which shows the elementary steps involved in the photochemical generation of metal radicals and their subsequent capture reaction with a trapping molecule.
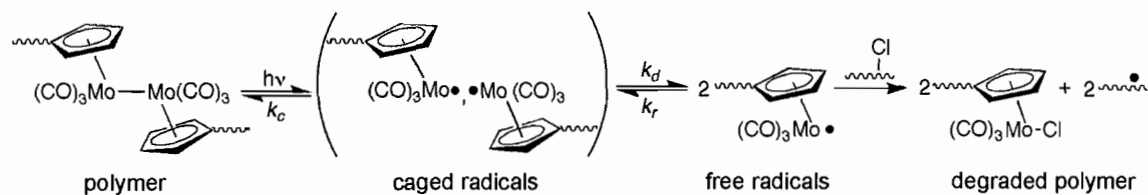
Scheme 2. Reaction of a photoreactive species to form a caged radical pair followed by escape of the radicals from the cage and subsequent radical trapping reaction.

4.2.3 *Secondary Thermal Transitions Hypothesis*

It is proposed that the temperature dependence of **PVC-Mo** arose from the temperature dependence of the k_d step. Specifically, it is suggested that the polymer segments to which the radicals are attached are conformationally stressed. There are two possible modes for the newly formed radicals to relax and become separated: they can rotate or recoil away from each other (Scheme 3). These secondary motions of the polymer arise from the relaxation of unfavorable bond conformations that are formed during the polymer casting process. The increased thermal energy facilitates the rotation and recoil relaxation processes, which effectively increases the rate constant for diffusion of the radicals out of the cage, k_d. This leads to decreased radical-radical recombination and consequently an increase in photodegradation efficiency.
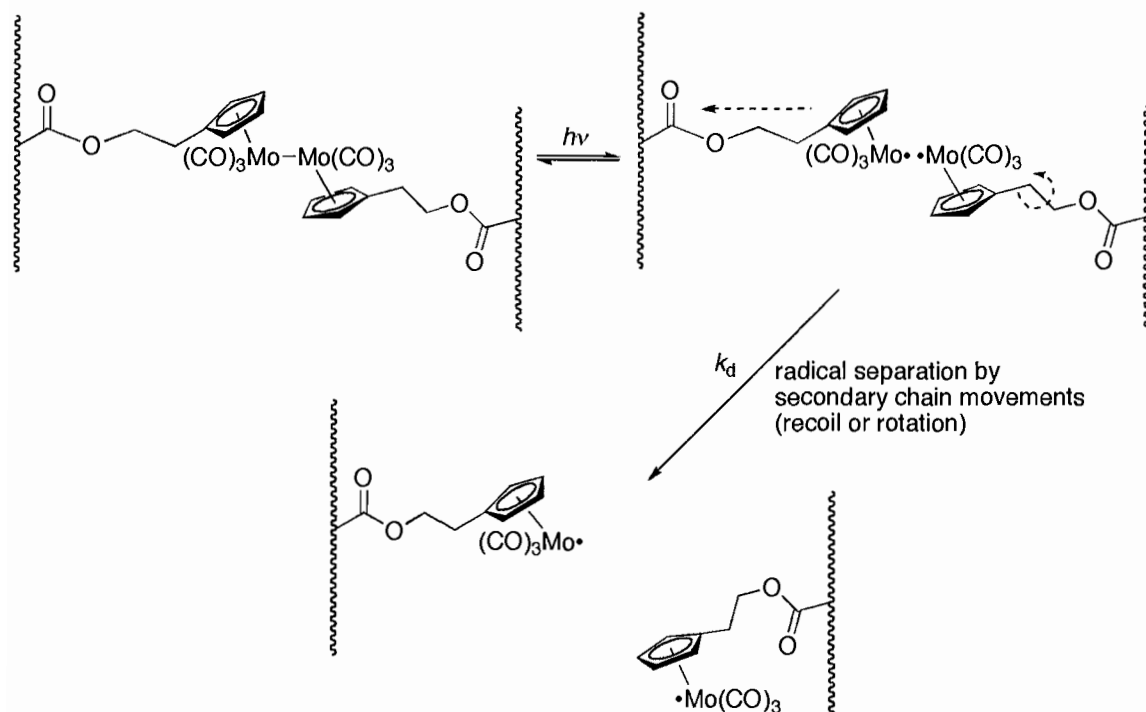
Scheme 3. Pathway for the increased separation efficiency of the radicals formed by irradiation of **PVC-Mo**. A rotation process is shown but radical recoil will also lead to increased radical-radical separation. Relaxation of the polymer chains leads to an increase in k_d and a subsequent increase in the quantum yield for degradation.

The quantum yield data for **PVC-Mo** in Figure 3 has an exponential dependence on the inverse temperature, and it is therefore tempting to extract activation parameters from the natural log plots of quantum yield vs. inverse temperature. Balzani, however, has cautioned that the relationship between the temperature and activation parameters in a photochemical reaction is a complex one, and the "apparent activation energies" thus obtained must be interpreted with care.[12] With that disclaimer in mind, the activation energy obtained from the ln Φ vs. T^{-1} plot (Figure 3) is 14.1 ± 0.3 kcal mol^{-1}. This value is typical for secondary relaxation chain movements in polymers (which generally fall in the range of 5–20 kcal mol^{-1}) and is consistent with the proposal that the temperature

dependence of Φ results from chain movements involved in recoil and rotation processes.[13]
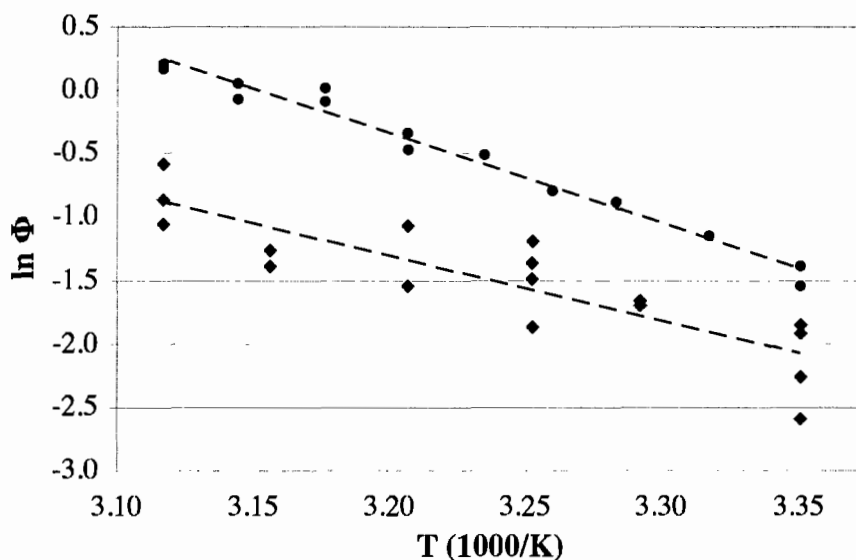
Figure 3. Plot of the lnΦ versus T^{-1} for for **PVC-Mo** (shown as ●) and **PU-70** (shown as ◆).

To further investigate this hypothesis, a second polymer system, **PU-70**, containing the $Cp_2Mo_2(CO)_6$ subunit was evaluated as a function of temperature. It was found that the quantum efficiency of **PU-70** also exhibited exponential dependence on temperature. The activation energy obtained from the ln Φ vs. T^{-1} plot (Figure 3) is 10 ± 1 kcal mol^{-1} for **PU-70**. This data is also in line with the hypothesis that the temperature dependence of Φ results from chain movements involved in recoil and rotation processes. To further support this hypothesis, it was also necessary to compare the activation barriers of the photochemical reaction obtained from the Arrhenius plots with the

activation energy for the molecular motions that are suspected to facilitate radical cage

escape for both polymer systems

4.2.4 *Activation Energies of Polymer Secondary Thermal Transitions*

The activation energies for polymer molecular motions that may facilitate escape

of the photogenerated metal radical species from the radical cage were determined by

dynamic mechanical analysis. First, however, the relevant molecular motions occurring

during the temperature range of the degradation experiments were determined. The glass

transition temperature, T_g, and the secondary thermal transition, T_β, for **PVC-Mo** and

PU-70 are shown in Table 1. The temperature range of data acquisition for the quantum

efficiency versus temperature was obtained below the polymer T_g and above T_β, so there

were no thermal transitions that occurred during the data acquisition of the experiment.

The values obtained also indicate that, during the experiments, there was no cooperative

segmental motion of the polymer backbone associated with the onset of the glass

transition. However, since the experiments were performed above the β-transition, there

were smaller segmental motions, i.e. polymer backbone corkscrewing or pendant chain

rotation (Figure 4).

Table 1. Thermal transitions and activation parameters for **PVC-Mo** and **PU-70**.

Polymer	T_g (°C)[a]	T_β (°C)[a]	photochemical reaction (kcal/mol)[b]	molecular motion (kcal/mol)[a]
PVC-Mo	65 ± 4	-120 ± 10	14.1 ± 0.3	14.7 ± 0.4
PU-70	55 ± 3	-40 ± 10	10 ± 1	8 ± 1

a – values were determined by dynamic mechanical analysis. b – values were determined from the Arrhenius plots
of the photochemical quantum yields versus temperature.
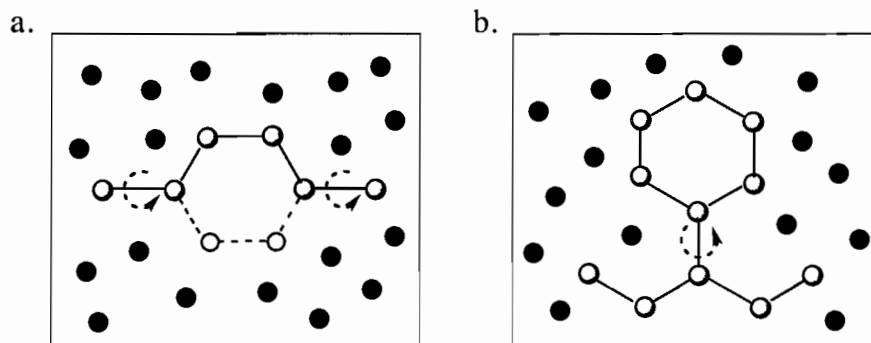
Figure 4. Two examples of molecular motion that result in secondary thermal transitions. a – corkscrew rotation in the polymer backbone. b – polymer pendent group rotation.

The activation energies of the photochemical reactions are shown in Table 1 along side the activation energies for the secondary thermal transitions for **PVC-Mo** and **PU-70**. It can be seen that the energies of activation for the photochemical reaction are equivalent within error to the energy of activation of the β-transition for both polymers. This evidence supports the hypothesis that polymer molecular motions, to which the photogenerated radical species are a part of, facilitate the escape of the radicals from the 'solvent' cage thus decreasing the radical-radical recombination efficiency and consequently increasing the photodegradation efficiency.

4.3   Conclusions

Control experiments show that the quantum yields for the photolysis and radical capture reactions of $Cp'_2Mo_2(CO)_6$ units in solution or dispersed in a polymer are normally not very sensitive to temperature. What little temperature dependence there is can be attributed to changes in viscosity of the solution or to small changes in the free-volume of the polymer. In contrast, when the $Cp_2Mo_2(CO)_6$ unit is incorporated into a polymer chain, the quantum yields of degradation are strongly temperature dependent. A

cage effect model is proposed to explain these results. When a polymer chain is cleaved, the chains will relax by secondary chain movements. It is proposed that increased thermal energy facilitates the rotation and recoil relaxation processes, which effectively increases the rate constant for diffusion of the radicals out of the cage, k_d. In effect, the cage recombination efficiency is decreased and this leads to an increase in the efficiency of degradation. In support of this proposal, the apparent activation energies obtained from the temperature dependence of the quantum yield of polymers **PVC-Mo** (14.0 ± 0.3 kcal mol^{-1}) and **PU-70** (10 ± 1 kcal mol^{-1}) are consistent with the secondary relaxation chain movements in polymers. In addition, these values coincide with the activation energies of the b-transitions of the polymers **PVC-Mo** (14.7 ± 0.4 kcal mol^{-1}) and **PU-70** (8 ± 1 kcal mol^{-1}).

This chapter summarizes the effect of temperature on polymer photodegradation. In the next chapter, Chapter V, two more factors that affect polymer photodegradation efficiencies will be discussed: time-dependent morphology changes and tensile stress.

CHAPTER V

THE EFFECT OF MORPHOLOGY CHANGES ON POLYMER

PHOTODEGRADATION EFFICIENCIES. A STUDY OF TIME-DEPENDENT

MORPHOLOGY AND STRESS INDUCED CRYSTALLINITY

Daglen, B. C.; Tyler, D. T. *J. Inorg. Organomet. Polym. Mat.* **2008**, submitted.

5.1   Introduction

The previous chapters have discussed several parameters that affect polymer

photodegradation rates including glass transition temperature, radical trap concentration,

and temperature. This chapter will focus on two additional parameters: time-dependent

morphology changes and tensile stress. First, the time-dependent morphology changes in

the segmented polyurethane, **PU-35**, will be discussed as well as how these changes

affect degradation efficiencies. Segmented polyurethanes are defined as polyurethane

copolymers that possess hard and soft segments in the polymer backbone (Figure 1).[1]

Soft segments are typically oligomers of polyol and hard segments can be aromatic rings

or regions were extended hydrogen bonding can occur (i.e. urethane or urea groups).

These segmented polyurethanes have distinct environments in the solid-state where the

soft segments form amorphous regions and the hard segments form highly crystalline

regions. An interesting phenomenon in these polymers is not just the formation of these

regions, but also the expansion of these domains in the solid-state over days or even

weeks.[2] The thermodynamic driving force for the change in morphology is relaxation of

residual conformational strain from either the film casting process or foam formation

which results in an increase in thermodynamically stable regions of randomly coiled

polymer segments (soft) and extended hydrogen-bonding networks (hard). The time-

dependent morphology changes that occur may affect the rates of polymer degradation.

Accordingly, the investigation of time-dependent morphology changes in our model

polymers was investigated.
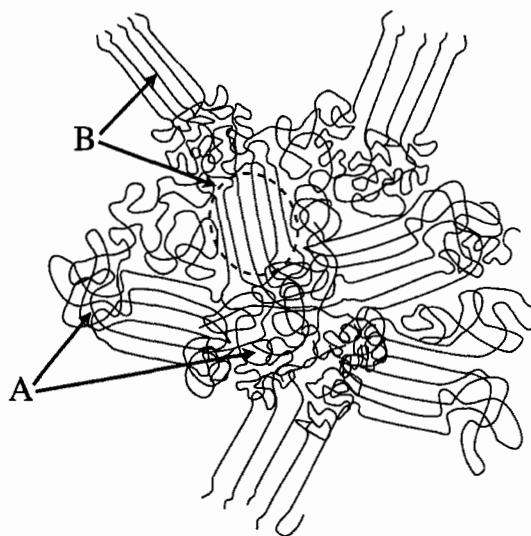
Figure 1. Illustration of the solid-state morphology of a polymer with soft (A) and hard (B) segments.

The second factor that affects polymer photodegradation efficiencies presented in

this chapter is tensile stress. An interesting outcome of polymer degradation studies is

the discovery that tensile stress can accelerate photochemical degradation.[3] There are

several theories to explain this phenomenon: Plotnikov hypothesis, decreased radical

recombination efficiency hypothesis, and Zhurkov hypothesis (Chapter I section 1.3.3).

Previous experiments on **PVC-Mo** testing these hypotheses support the idea that stress

affects the ability of the photogenerated geminate radical to recombine.[4-6] Additional results will be presented that investigate degradation efficiency as a function of tensile stress.

5.2 Results and Discussion

5.2.1 *Polymer Preparation and Characterization*

The crosslinked polymer, **PVC-Mo** and **PU-35** were prepared as described in Chapter IV. (Note **PVC-Mo-1** and **PVC-Mo-2** were prepared by different experimentalist but are chemically equivalent). The glass transition temperatures (T_g) and the secondary thermal transitions (T_β) were determined by dynamic mechanical analysis and the results are discussed below. The time-dependent morphology changes in the polyurethane, **PU-35** were monitored by infrared spectroscopy using 32 scans at 4 cm^{-1}. The deconvolution of overlapping peaks in the carbonyl region of the IR spectra were performed using IGOR Carbon Pro software. The changes in crystallinity as a function of tensile stress for **PVC-Mo** were monitored by infrared spectroscopy as well.

5.2.2 *Effect of Time-Dependent Morphology Changes on the Degradation Efficiency of a Segmented Polyurethane*

Quantum Yield as a Function of Time for **PU-35**

The photodegradation efficiency of a segmented polyurethane film was monitored over the course of several weeks. The quantum yield as a function of time are shown in Figure 2. The initial quantum yield was relatively high ($\Phi = 0.58 \pm 0.08$). Over the course of two weeks at 30 °C, the quantum efficiency decreased significantly and then leveled off at $\Phi = 0.35 \pm 0.06$. It was hypothesized that the segmented structure of **PU-**

35 caused the polymer to change morphology over time and consequently cause a change in the quantum efficiency of the photoreaction. (Recall that **PU-35** was synthesized using a 'soft' poly(propylene glycol) prepolymer and can form the 'hard' extended hydrogen bonding networks characteristic of polyurethanes). It was shown that increased crystallinity in the solid-state decreases the degradation rates of model polymers containing metal–metal bonds in the polymer backbone.[6] (Note that photooxidative degradation of polymers, in general, is retarded by increased crystallinity.) Infrared spectroscopy was used to identify and quantify any changes in crystallinity as a function of time.
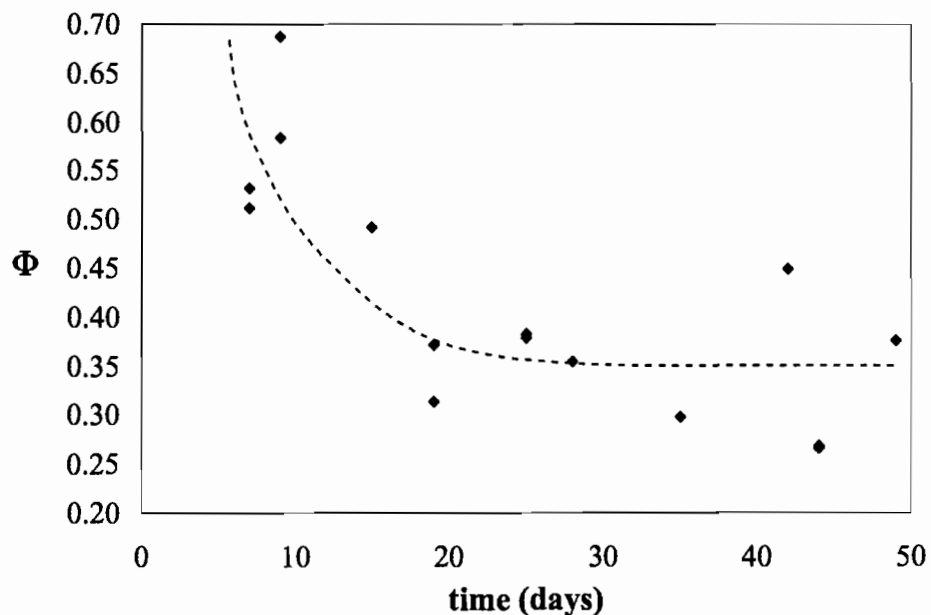
Figure 2. Quantum yield as a function of time for **PU-35**. The dashed line is meant to guide the eye and is not a quantitative fit.

<u>Identification of Peaks in the Infrared Spectrum of **PU-35**</u>

To probe the time-dependent morphology changes of **PU-35**, infrared spectra were analyzed as a function of time. To detect the formation or extension of a hydrogen bonding network, peaks associated with the urethane linkage, specifically the carbonyl stretch (C=O ν) and the N-H stretch (N-H ν), were identified using values found in the literature (shown in Table 1).[7-11]

Table 1. Literature values for the N-H and C=O stretching frequencies found in polyurethanes.[7-11]

Infrared transition	**H-bonded**	**wavenumber (cm^{-1})**
N-H ν	no	3350
N-H ν	yes	3300
C=O ν	no	1730 - 1740
C=O ν	yes (loosely)	1710
C=O ν	no (strongly)	1700

Figure 3 shows two example infrared spectra: a solution of **PU-35** in tetrahydrofuran (THF) and a polymer film of **PU-35** (5 days after casting). (Note that a solvent background spectrum was subtracted from the solution spectrum.) Figure 3a focuses on the N-H ν region, where peak a is the solution spectrum and peak b is the polymer film spectrum. Figure 3b focuses on the C=O ν region, where peak c is the solution spectrum and peaks d–e are the polymer film spectrum. In the solution spectrum, the N-H ν peak (a) at 3278 cm^{-1} is in the range of H-bonded amines and is assumed to be interacting with the hydrogen-bond accepting solvent, THF. The C=O ν

peak (c) at 1734 cm^{-1} was identified as non-hydrogen-bonding in solution. In the solid-state, the N-H ν peak (b) at 3308 cm^{-1} was identified as bound to a hydrogen; this hydrogen-bond is likely with a carbonyl oxygen of a urethane linkage. Four peaks were identified in the carbonyl region of the polymer film spectrum: d) non-hydrogen-bonded C=O ν peak at 1737 cm^{-1}, e) residual THF peak at 1727 cm^{-1}, f) hydrogen-bonded C=O ν peak at 1712 cm^{-1}, and g) strongly hydrogen bonded C=O ν peak as a shoulder at 1700 cm^{-1}.[12] To determine the relative peak contributions to the observed spectrum in the carbonyl region, it was necessary to perform a mathematical deconvolution.
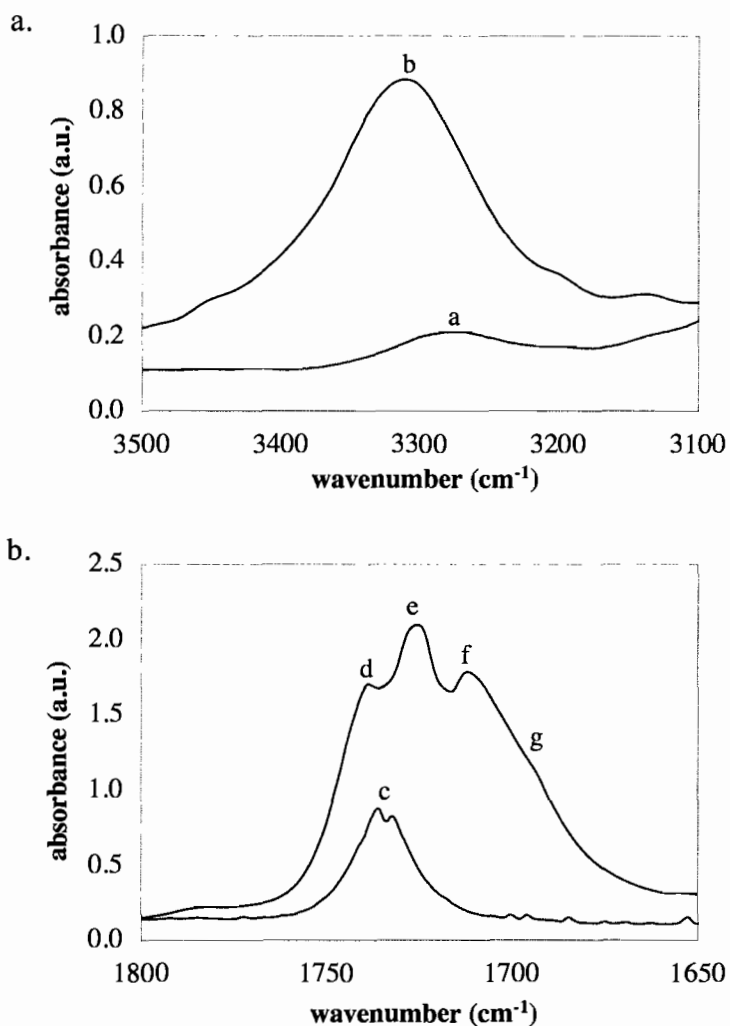
Figure 3. a) N-H stretching region and b) C=O stretching region of the infrared spectrum of a solution of **PU-35** in tetrahydrofuran (THF) and a polymer film of **PU-35** (5 days after casting).

Method of Infrared Peak Deconvolution

To quantify the contribution of the individual peaks in the carbonyl region of the spectrum, a deconvolution method was employed. First, it was assumed that the spectrum was composed of only the four peaks identified in the previous section and the observed spectrum was the linear combination of those four peaks (i.e.

$A_{observed} = A_1 + A_2 + A_3 + A_4$). It was further assumed that the vibrational modes associated with those peaks would yield a Lorentzian shaped curve. The Lorentzian equation was chosen because it accounts for line-broadening that occurs due to interactions of the vibrating species with the surrounding matrix.[13] The shape of a Lorentzian curve is defined in eq 1,

$$A = \frac{A_{max}}{4\left(\dfrac{\nu_{max} - \nu}{\Delta\nu^2}\right)^2 + 1} \tag{1}$$

where A is the absorbance at frequency, ν, A_{max} is the maximum absorbance for the particular vibrational mode, ν_{max} is the frequency at A_{max}, and $\Delta\nu$ is the full width at half maximum (FWHM). Using IGOR Carbon Pro, the infrared spectra were fit to a linear combination of eq 1.[a] The original data, the fit, and the contributing peaks are shown in Figure 4. It is interesting to note that the FWHM for the strongly hydrogen-bonded C=O ν peak is significantly greater than the other peaks. This is expected since the hydrogen-bonded species is often broader and lower in energy than the non-hydrogen-bonded species.[14]
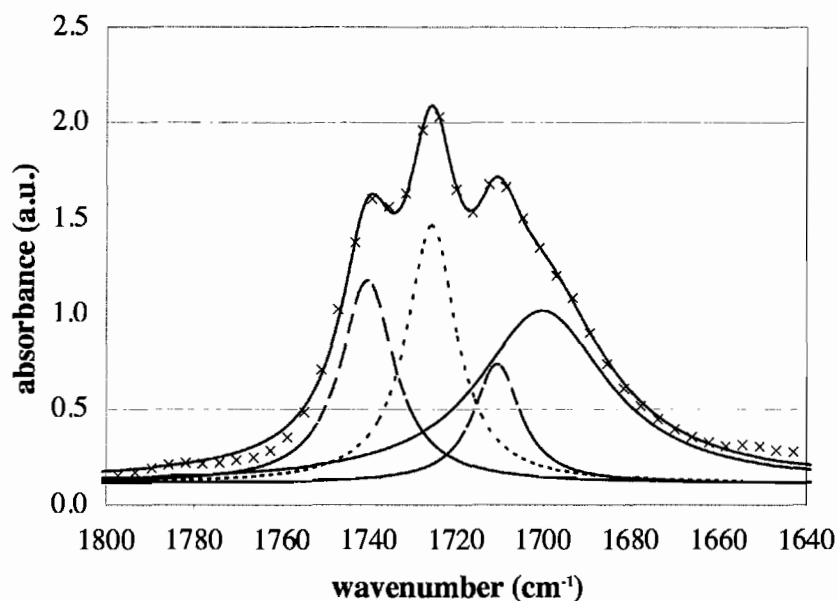
Figure 4. Carbonyl region of the infrared spectrum of a **PU-35** polymer film and the calculated contributions to the observed peaks using a linear combination of Lorentzian curves.

PU-35 Infrared Peak Areas as a Function of Time

To determine the changes in the spectra over time, the peak area was compared. The peak area was found by integrating the Lorentzian equation (eq 1) to generate eq 2.

$$\text{area(peak)} = \frac{\pi A_{max} \Delta v}{2} \qquad (2)$$

The change in crystallinity was monitored by observing the ratio of the areas of the hydrogen-bonded C=O v peaks at 1710 and 1700 cm^{-1} to the non-hydrogen-bonded C=O v peak at 1740 cm^{-1}. The ratio as a function of time is shown in Figure 5. According to the infrared data, **PU-35** increased in crystallinity as a function of time, which is characteristic of segmented polyurethanes. It is hypothesized that the corresponding decrease in quantum efficiency is a result of the photogenerated radicals being formed in

more thermodynamically stable regions of the polymer. Radicals generated in stable regions have no driving force for radical separation (relaxation of stressed conformations) and therefore the probability of radical cage escape is decreased.
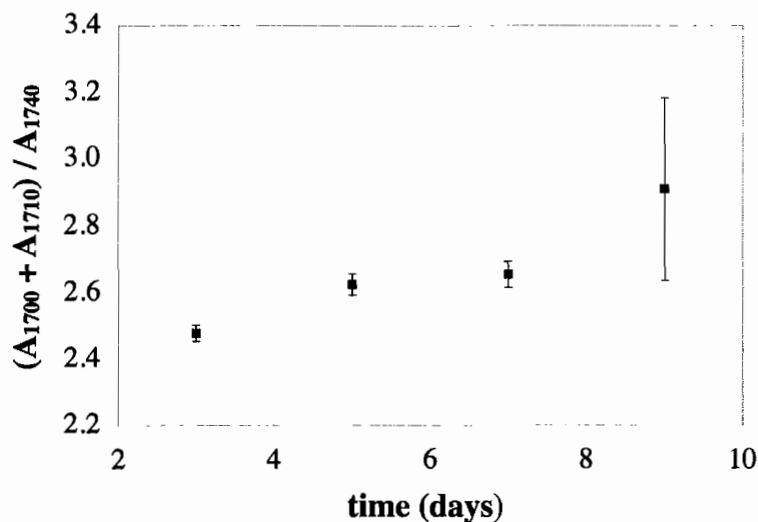
Figure 5. Ratio of the areas of the hydrogen-bonded C=O ν peaks (at 1710 and 1700 cm^{-1}) to the non-hydrogen-bonded C=O ν peak (at 1740 cm^{-1}) over time for **PU-35**.

5.2.3 *Effect of Tensile Stress on the Degradation Efficiencies of PVC-Mo*

Decreased Radical Recombination Efficiency Hypothesis

The Decreased Radical Recombination Efficiency (DRRE) hypothesis postulates that degradation efficiency is affected by the ability of the geminate radical to recombine ($k_{recombination}$ in Scheme 1).[15-18] This hypothesis, as discussed in Chapter I, outlines a series of conditions under which radical recombination can occur. To reiterate, at zero or minimal stress levels, the semi-crystalline polymer has an intrinsic quantum yield. When tensile stress is applied to a polymer, the chains which are in a random coil state become

elongated and taut. Under these conditions, the radicals generated during bond homolysis recoil to resume a more entropically favored random coil configuration. This results in an increase in radical distance. Greater radical separation increases in the likelihood of radical trapping and consequently increases the degradation efficiency. An increase in applied tensile stress may affect polymer morphology cause a deviation from a continued increase in degradation efficiency with increased stress. Tensile stress can impart a high degree of polymer strand orientation and induce the formation of crystalline regions in polymer systems. Bonds homolyzed in these regions of high thermodynamic stability are unlikely to recoil into a random coil configuration and thus remain in close proximity. This results in an enhanced rate of radical recombination and a decrease in degradation efficiency. (For a pictoral representation of this hypothesis, refer to section 1.3.3 in Chapter I.)

$$\sim\!\sim\!\sim\!\sim \underset{k_{recombination}}{\overset{k_{homolysis}}{\rightleftharpoons}} 2 \sim\!\sim\!\sim\bullet \xrightarrow[k_{trap}]{2\ RX} 2 \sim\!\sim\!\sim X\ +\ 2\,R\,\bullet$$
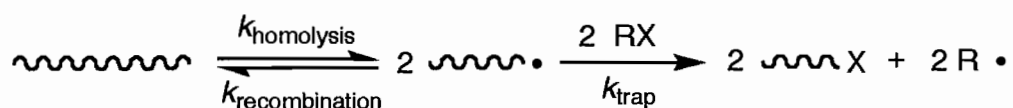
Scheme 1. Simplified polymer photodegradation mechanism showing bond homolysis.

Previous Data Supporting the DRRE Hypothesis

The DRRE hypothesis predicts a distinct quantum yield response to applied tensile stress: 1) an intrinsic quantum yield at low stress, 2) an increase in quantum yield due to polymer chain relaxation into a random coil following bond homolysis, then 3) a decrease in quantum yield from stress-induced crystallization. Figure 6 shows an example of this phenomenon from the literature (polymer **PVC-Mo-1**).[4, 6] The stress-

induced crystallization was monitored by observing the CH_2 bending mode (CH_2 δ) in the infrared spectra where the absorbance at 1425 cm^{-1} is the CH_2 δ mode in the crystalline region and the absorbance at 1436 cm^{-1} is the CH_2 δ mode in the amorphous regions.[19, 20] Figure 9 shows the ratio of the peak intensities as a function of tensile stress. The crystallinity of the polymer increased with applied tensile stress and the quantum yield versus tensile stress plot was characteristic of the DRRE hypothesis (Chapter 1, Figure 4b).
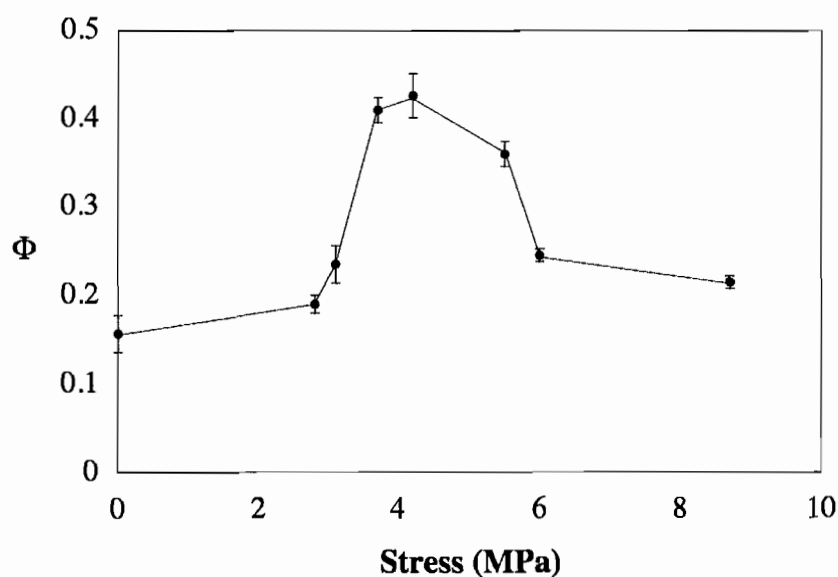
Figure 6. Literature data for the quantum yield versus tensile stress for **PVC-Mo-1**.[4]
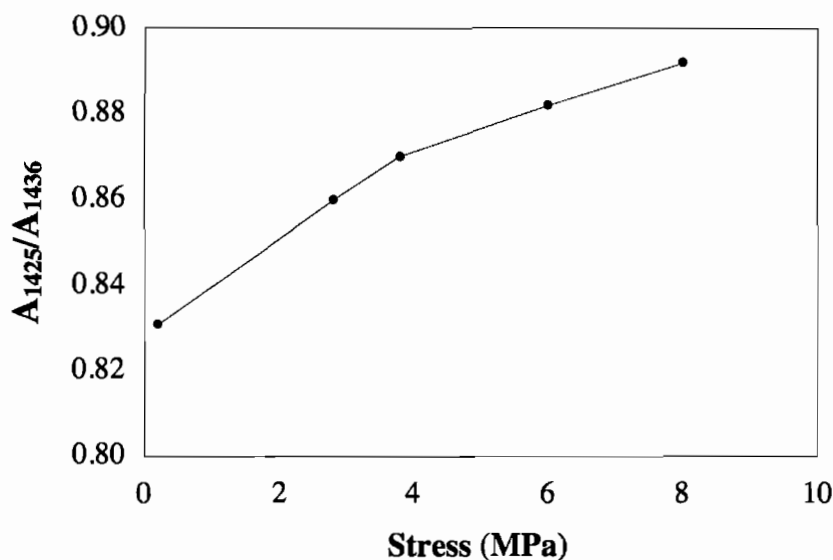
Figure 7. Literature data for the ratio of the infrared absorbances, A_{1425}/A_{1436}, for the bending modes of CH_2 in the amorphous (A_{1436}) and crystalline (A_{1425}) regions of **PVC-Mo-1** as a function of tensile stress.[4,6]

Recent Data for Quantum Yield versus Tensile Stress for **PVC-Mo-2**

To investigate the DRRE hypothesis and the role of crystallinity further, another sample of **PVC-Mo** (**PVC-Mo-2**) was investigated. Quantum yield data as a function of tensile stress for **PVC-Mo-1** and **PVC-Mo-2** are shown in Figure 8. The quantum yield responses to applied tensile stress were noticeably different for these two polymers. Both samples exhibited similar quantum efficiency at zero stress (Φ(**PVC-Mo-2**) = 0.15 and Φ(**PVC-Mo-1**) = 0.17). However, the quantum yield of **PVC-Mo-2** did not change as a function of increased stress, where as **PVC-Mo-1** quantum yield varied from 0.17 to 0.42 before decreasing to 0.21. The morphologies of these polymers were compared to investigate the discrepancy in response to tensile stress.
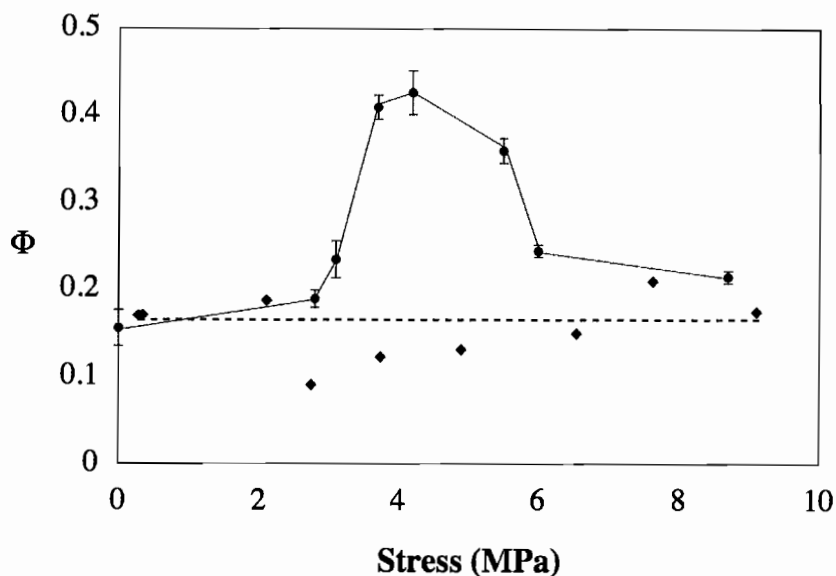
Figure 8. Quantum yield versus tensile stress for **PVC-Mo-1** and **PVC-Mo-2**.
● - Literature data for **PVC-Mo-1**. ◆ - Recent data for **PVC-Mo-2**.

Figure 9 shows the ratios of the infrared absorbances, A_{1425}/A_{1436}, for the CH_2 δ in

the amorphous (A_{1436}) and crystalline (A_{1425}) regions of **PVC-Mo-1** and **PVC-Mo-2** as a

function of tensile stress. The data indicate that the initial percent crystallinity (polymer

morphology before the application of tensile stress) of these polymers was markedly

different: A_{1425}/A_{1436}(**PVC-Mo-1**) = 0.83 and A_{1425}/A_{1436}(**PVC-Mo-2**) = 1.03. **PVC-**

Mo-2 was therefore more crystalline than **PVC-Mo-1** before tensile stress was applied.

Also, unlike **PVC-Mo-1**, the relative crystallinity in **PVC-Mo-2** did not change with

increased tensile stress. This result is consistent with the DRRE hypothesis. **PVC-Mo-2**

was a highly crystalline polymer that could be said to be in the third 'case' where stress-

induced crystallinity results in an increase in radical recombination and, consequently, a

low quantum yield. However, the crystallinity in **PVC-Mo-2** was formed during the

solvent casting process and not stress-induced as in the case of **PVC-Mo-1**. The infrared

data indicated that tensile stress did not affect the morphology of the polymer over the load applied. Since the environment experienced by the photogenerated radical species was equivalent throughout the experiment, the quantum yield was not predicted to change.
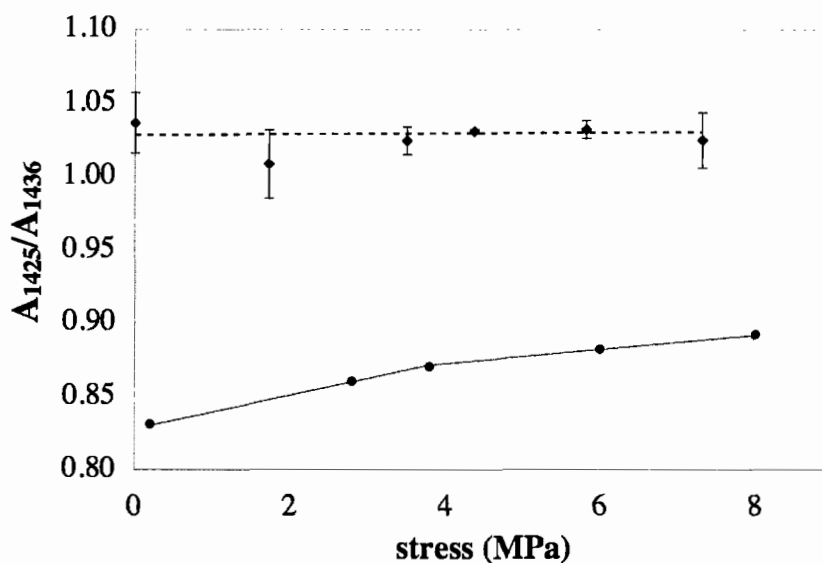
Figure 9. Ratio of the infrared absorbances, A_{1425}/A_{1436}, for the bending modes of CH_2 in the amorphous (A_{1436}) and crystalline (A_{1425}) regions of **PVC-Mo** as a function of tensile stress. ● - Literature data for **PVC-Mo-1**. (No error bars were provided in original publication.) ◆ - Recent data for **PVC-Mo-2**.

5.3   Conclusions

The effects of time-dependent morphology changes and tensile stress on photodegradation efficiencies were investigated. The photodegradation efficiency of a segmented polyurethane was observed to decrease over two weeks time. It was found that changes in polymer morphology, which are characteristic of polyurethanes, are the cause of the changes in quantum yield. It was also found that tensile stress may or may

not have an affect on photodegradation efficiencies depending on the initial morphology of the polymer. **PVC-Mo-1** exhibited variable quantum yield as a function of stress that was consistent with the DRRE hypothesis. **PVC-Mo-2**, which had a greater degree of crystallinity, was found to not change morphology with increased stress and consequently the applied stress did not affect the quantum yield. The results of the stress-induced and time-dependent morphology changes indicate that thermodynamic stability of the polymer affects the photodegradation efficiency. In the case of the polyurethane, the change in morphology decreased residual conformational strain from the initial casting process and created thermodynamically stable soft (random coil) and hard (hydrogen-bonded) regions which effectively increased the efficiency of the radical-radical recombination. In the case of PVC, external stress had two potential consequences. First, stress decreased the rate of radical-radical recombination by inducing recoil of the taut photogenerated radical polymer segments. Second, stress induces crystallinity, which effectively increased radical recombination efficiency. Restated, a thermodynamically stable polymer will have a slower degradation rate than a polymer that residual or applied stress.

Thus far, the following external parameters that affect polymer degradation have been discussed: radical trap concentration, glass transition temperature, reaction temperature, time-dependent morphology changes, and tensile stress. The next chapter, Chapter VI, explores the reaction kinetics of the photodegradation of **PVC-Mo** and **PU-70**. Several models found in the literature were evaluated and a new model based on Perrin kinetics is presented.

5.4 Endnotes

a.   The starting values of A_{max} were set to 1, ν_{max} was approximated from the spectra, and FWHM was approximated to be 20 cm^{-1}. Subsequent starting values were approximated from the initial fit.

CHAPTER VI

APPLICATION OF A PERRIN-LIKE KINETICS MODEL TO EXPLAIN THE

BIPHASIC PHOTOCHEMICAL DEGRADATION RATES OF POLYMERS

6.1   Introduction

A major goal in the field of polymer science is to devise photodegradable polymers with a tunable onset of degradation and with a specific degradation rate. In order to design polymers with these properties, it is necessary to identify the experimental parameters that affect degradation rates and to determine how those parameters affect the degradation mechanism. A necessary step toward this goal is to determine the kinetics of the degradation reaction. An interesting observation from these kinetic studies is that the photodegradation rates of solid-state polymers are often biphasic, showing a relatively fast rate during the initial period of irradiation but a slower rate at longer times, Figure 1.[1,2] Several hypotheses have been proposed to explain this observation but no definitive explanation has come forth. As part of our ongoing study of polymer photodegradation, we began an investigation into the origin of the biphasic behavior.
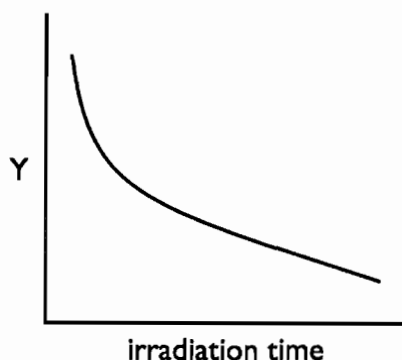
Figure 1. A plot illustrating the typical biphasic decay for the photodegradation of a polymer. The data represented on the y-axis will vary with the degradation monitoring technique; two examples are radical concentration in the case of electron spin resonance (ESR) experiments or number average molecular weight obtained from gel permeation chromatography (GPC).

In this chapter we present a new explanation for the biphasic photochemical degradation rates of polymers. Specifically, a mechanistic-based 4-parameter equation is presented and tested. The new model was assessed on two polymers that contain M–M bonds in their backbones, one a cross-linked poly(vinyl chloride) and the other a polyurethane with soft and hard segments. To investigate the range of application of this new model, literature data for the photodegradation of a polyoxymethylene was also tested.[3] The coefficients extracted from the fits were evaluated as a function of reaction temperature, which led to further mechanistic insights.

This work was recently accepted in the journal Macromolecules. All of the experiments in this chapter were performed by myself. D. R. Tyler and myself were co-authors of the manuscript.

6.2   Results and Discussion

6.2.1   *Fitting the Biphasic Photodegradation Data*

Concentration data for the photodegradation of polymers **1** and **2** as a function of irradiation time are shown in Figure 2.[a] (Note the data in Figure 2 were normalized by dividing the concentration values by the initial concentration.) The traces in Figure 2 exhibit biphasic character, showing a relatively fast rate during the initial period of irradiation but a slower rate at longer times. In an attempt to fit the data, several mechanistic models were evaluated. Owing to the fact that the plots are not linear, the reactions are not the usual simple zeroth-order photochemical reactions. (Note, however, that the slopes at long reaction times do appear linear.) To test for the potential origin of the biphasic kinetics, the data were fit to the expression $C/C_0 = Ae^{-kt}$, which represents first-order kinetics in the disappearance of starting material. In this case, the reaction kinetics would be dependent on the concentration of the molybdenum dimer chromophore. The first-order fits to the degradation data for polymers **1** and **2** are shown in Figures 2a and b. The fits clearly do not represent what is occurring at short reaction times. The second-order equation, $C/C_0 = (1 + Bt)^{-1}$, was also evaluated but the fits were no better (Figures 2a and b).
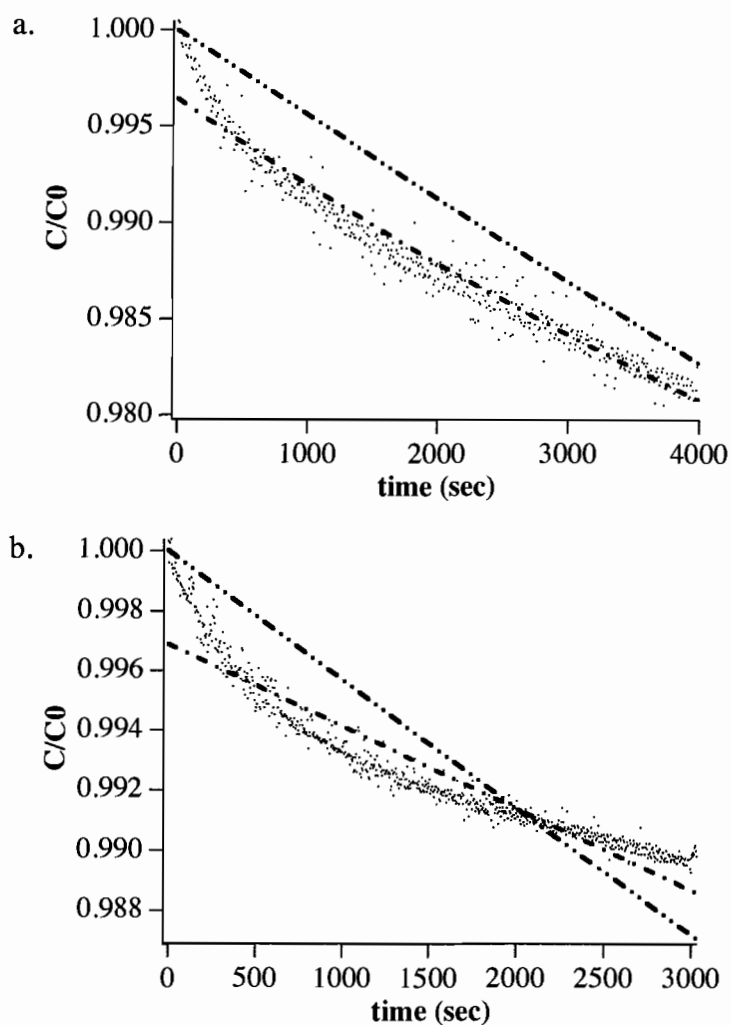
Figure 2. Relative $-CH_2C_5H_4(CO)_3Mo-Mo(CO)_3C_5H_4CH_2-$ concentration as function of irradiation time at room temperature for polymer **1** (a) and **2** (b) with fits for the 1st order (–·–··–) and 2nd order (–······–) equations.

It was hypothesized that the biphasic behavior exhibited by these polymers may be attributed to unique reactivity in the solid-state. One possible explanation is that the reaction rate is not solely determined by a specific chemical transformation but rather by diffusion processes. One representation of diffusion behavior, as observed for the disappearance of starting material, is the simple-diffusion equation, $C/C_0 = (1 + Dt^{1/2})^{-1}$.[4]

Simple-diffusion kinetics were used to describe the degradation of solid-state polyolefins where the decay of the photogenerated radicals was hypothesized to be controlled by either oxygen diffusion into the polymer material or by radical migration to the crystalline surfaces where radical-trapping oxygen was present.[5] The fits of the degradation data for polymers **1** and **2** to the simple-diffusion equation are shown in Figures 3a and c. Note that, although the simple-diffusion model is a more promising fit than a simple first- or second-order equation, it clearly overestimates the reaction rates at both short (see Figures 3b and d) and long reaction times and is consequently not a suitable description of this system.
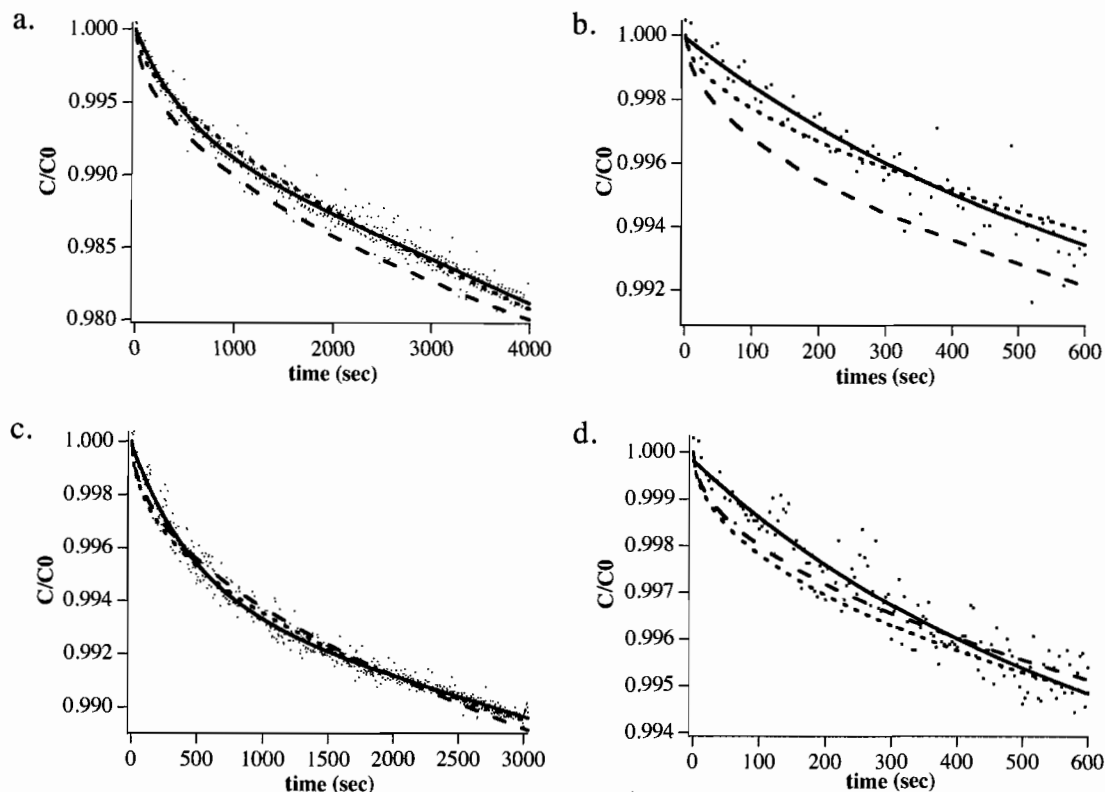
Figure 3. Relative –CH$_2$C$_5$H$_4$(CO)$_3$Mo–Mo(CO)$_3$C$_5$H$_4$CH$_2$– concentration as a function of irradiation time at room temperature for polymer **1** (a and b) and **2** (c and d) with fits for the simple diffusion (– – – –), diffusion-controlled (-----), and Perrin-like (———) equations. The plots in b and d show the initial data in plots a and c, respectively, on expanded axes.

Waite developed a modification of the simple-diffusion model called the diffusion-controlled model.[6-8] This model describes bimolecular reactions in the solid-state or in highly viscous solutions where both diffusion and spatial distribution of the reactive species are taken into account. The model (described by the equation, C/C$_0$ = (1 + Bt + Dt$^{1/2}$)$^{-1}$) has been used to fit the radical decay kinetics of several photodegradation reactions of polyolefins and polyethers as monitored by electron spin

resonance spectroscopy.[3,4,9,10] Figure 3 shows the fits for the diffusion-controlled model developed by Waite. Like the simple-diffusion model, it can be seen (particularly in Figures 3b and 3d) that the diffusion-controlled model overestimates the initial reaction rate. However, in contrast to the simple-diffusion model, Waite's model does more closely represent the data at longer reaction times. Be that as it may, none of these conventionally used models could adequately describe the kinetic behavior of polymers **1** and **2**; accordingly, a new model based on Perrin kinetics was developed to explain the biphasic behavior.

6.2.2   *Derivation of a Perrin-like Photochemical Model*

There are many instances in the literature where a chemical species is converted to a single product in the same reaction vessel by two or more mechanistically different routes that possess different observed rates. One example is heterogeneous catalysis, where a reactant may experience different catalytic sites on the reactive surface.[11,12] Another example, which is the focus of this paper, involves a photoreactive species embedded in a solid polymer matrix. Polymers can be classified morphologically as either amorphous or crystalline, but the majority of polymers are semi-crystalline (possessing both crystalline and amorphous regions). These polymers may visually appear to be homogeneous but, under the scrutiny of an electron microscope, are in fact heterogeneous with both crystalline and amorphous domains.[13] One consequence of this microheterogeneity is that a reactive species in a polymer matrix can reside in different molecular landscapes. For example, it is well known that oxidation reactions in highly crystalline polymers have different reaction rates at the crystal grain boundaries than

within the crystalline regions.[14] These two different environments result in an observed reaction rate that is a composite of two intrinsically different reaction pathways that result in the same product. The rate equation for such a reaction is derived from the model A → B, where reactant A can be described as two components, X and Y, as expressed in equation 1.

$$[A]_0 = [X]_0 + [Y]_0 \qquad (1)$$

Another case found in the literature where the observed reaction rate was the combination of two separate rates was described by Perrin in the early part of the twentieth century.[15] The Perrin model, shown in Figure 4, was established to explain the observed non-exponential fluorescence decay of small molecules in solid polymers.[15, 16] Perrin considered the microheterogeneity of solid-state polymers and the relative immobility of atoms in the solid-state. For fluorescence decay, he proposed that when an acceptor was in the quenching sphere of an electronically excited donor molecule, the fluorescence would be quenched. Therefore, the observed rate of fluorescence decay was the combination of the decay rate of excited molecules in the presence of a quencher and the natural decay rate of molecules in the absence of a quencher. A mechanistic analogy can be made for photogenerated radical species in solid-state polymers: the observed rate of radical decay will be the combination of the rate where a radical trapping agent is in the reactive sphere of the radical and where it is not. (The term "reactive sphere" is equivalent to the term "quenching sphere" used in the case of the original Perrin model.) This is represented pictorially in Schemes 1a and 1b.
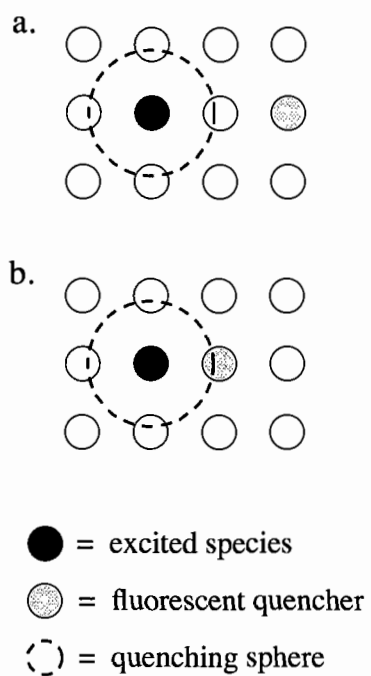
Figure 4. Perrin model used to describe the observed rates for the fluorescence decay of a chromophore in the solid-state.
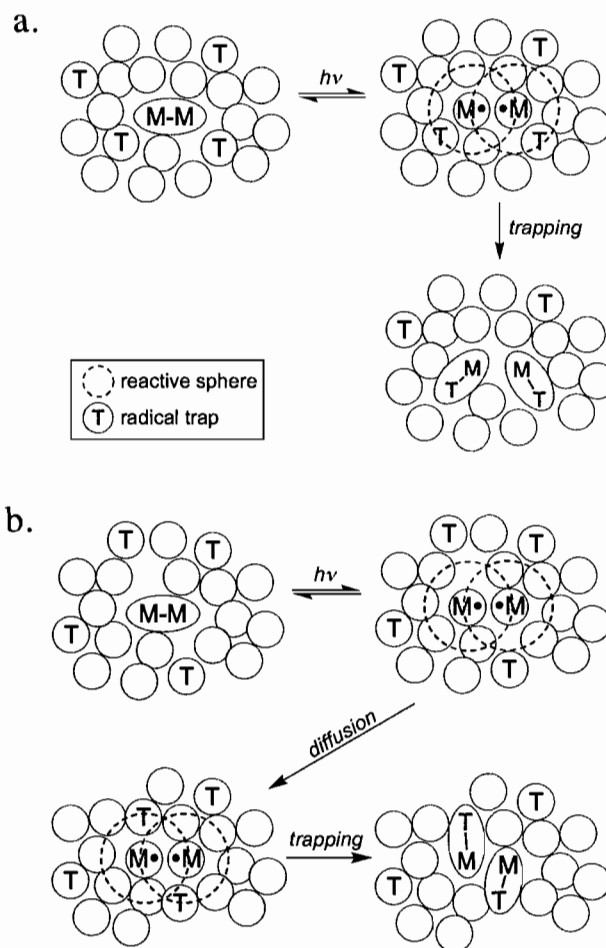
Scheme 1. Illustration of the reaction of photogenerated metal radicals with trapping atoms in a solid-state matrix. In one case (a), there is a trap in the reactive sphere of the metal radical. In the other case (b), the trap is initially outside of the reactive sphere.

To generate the observed rate equations for the disappearance of the starting material as illustrated in Scheme 1, one must consider the kinetics of the photoreaction and how the coinciding individual cases affect the kinetics. For the simple case where a photon causes a singular photoreaction, the rate equation for the conversion of A to B can be written as

$$-\frac{dA}{dt} = \phi I_m (1 - 10^{-\varepsilon c_A l}) \frac{S}{V} \tag{2}$$

where ϕ is the quantum yield of the reaction, I_m is the number of einsteins absorbed per unit volume per unit time, ε is the chromophore molar absorptivity, c_A is the concentration of the chromophore, and l is the path length, S is the surface area, and V is the volume of the irradiated sample.[17] Equation 2 can be simplified by considering the magnitude of photon absorption by the sample. For instance, if the absorbance value is large ($\varepsilon c_A l > 2$) then $1-10^{-\varepsilon c_A l} \sim 1$ and the rate can be written as

$$-\frac{dA}{dt} = \phi I_m \frac{S}{V} \qquad (3)$$

which is a zeroth-order reaction. Conversely, if the absorbance of the substance is small ($\varepsilon c_A l < 0.1$) then $1-10^{-\varepsilon c_A l} \sim 1$ and the rate can be written as

$$-\frac{dA}{dt} = 2.303\varepsilon c_A l \phi I_m \frac{S}{V} = constant \cdot c_A \qquad (4)$$

which is a first-order reaction. To determine the rate equation that corresponds to the individual cases illustrated in Scheme 1, the relative absorbances of the chromophore with and without a trap in the reactive sphere will be evaluated. An assumption is made that the experimental path lengths and molar absorptivity of both cases are the same because both species exist in the same sample and, in both cases the absorbing species is the same. Therefore, the relative absorbances will be determined by the relative concentrations of both species. Returning to Figure 3, it is observed that < 1% of the absorbing species is consumed in the initial fast reaction rate. This species, termed Y, is in very low concentration and therefore is predicted to exhibit first-order kinetics, eq 5, where Y_0 is the relative concentration of species Y at time zero and k_2 is a "rate constant" for the photoreaction.[18] (Note that k_2 is equal to $2.303\varepsilon\ l\phi I_m S/V$. To make comparisons of

the "rate constants" possible, the parameters l, I_m, S, and V were kept constant from sample to sample and polymer to polymer.) Integrating eq 4 in terms of concentration of Y as a function of time, t, yields eq 5, where Y_0 is the relative concentration of species Y at time zero and k_2 is the rate constant for the photoreaction.

$$[Y] = Y_0 e^{-k_2 t} \tag{5}$$

The remaining 99% of the photoreactive starting material that reacts at a slower rate, species X, is in high concentration and is predicted to show the usual zeroth-order kinetics.[17] The resulting rate for the disappearance of X is shown in eq 8, where X_0 is the concentration of species X at time, t, zero and k_1 is the corresponding "rate constant." (k_1 is equal to $\phi I_m S/V$.).

$$[X] = [X_0] + -k_1 t \tag{6}$$

By combining equations 5 and 6, a new overall rate equation for the disappearance of A is formed, eq 7. This equation represents the combined contributions to the overall rate for the two cases derived from the Perrin-like model as illustrated in Figure 4.

$$[A] = X_0 + k_1 t + Y_0 e^{-k_2 t} \tag{7}$$

The Perrin-like expression, eq 7, was used to fit the kinetic traces of polymers **1** and **2,** and the results are illustrated as the solid line in Figures 3a and b. It is apparent that the Perrin-like equation is the best fit for the data at both long and short reaction times. At short reaction times, the dominant species contributing to the observed fast reaction rate is the photogenerated radical species where there is a radical trap in the reaction sphere. The Perrin-like model describes the fast reaction kinetics as a first-order exponential. At longer reaction times, the reaction rate is dominated by the relatively

slow reaction that involves migration of a radical trapping species into the reactive sphere of the photogenerated metal radicals. This is described in the Perrin-like model as simple zeroth order kinetics. The next section will investigate the applicability of the Perrin-like model in other polymer systems by analyzing degradation data found in the literature.
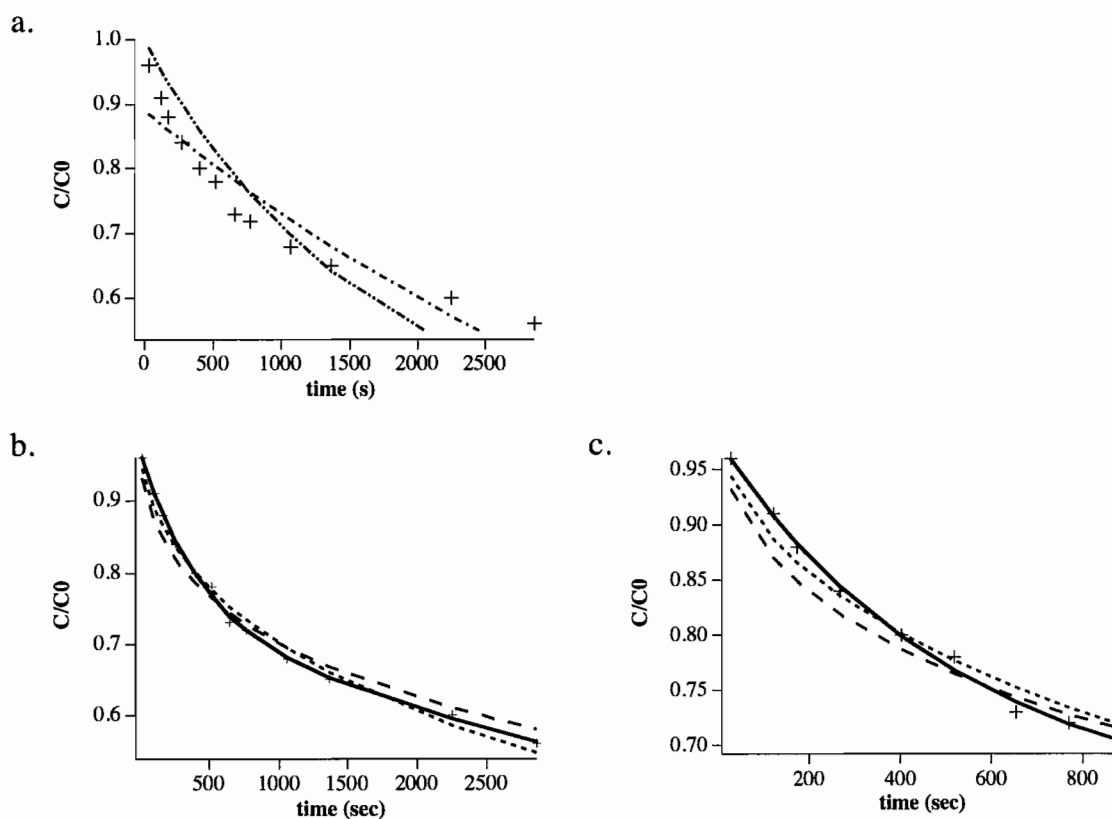
Figure 5. Relative radical concentration as a function of time at 343.5 K following irradiation of polymer **3** (+). The fits are for the 1st order (-·-·-) and 2nd order (-···-··-) equations (a) and simple diffusion (----), diffusion-controlled (----), and Perrin-like (———) fit equations (b). The plot in c shows the initial data in plot b on expanded axes.

6.2.3   *Analysis of a Literature Example Using the Perrin-like Model*

To analyze the versatility of the Perrin-like model to other polymer systems, literature data were fit to eq 7. Figure 5 shows data for the photodegradation of polyoxymethylene, **3**, under gamma irradiation.[3] (The literature data points were obtained using a literature capture method described in the next section of this chapter.) The degradation mechanism of polyoxymethylene is known; upon irradiation, three radical species are formed: $-O-\overset{\bullet}{C}H-$, $-O-\overset{\bullet}{C}H_2$, and $\overset{\bullet}{O}-CH_2-$.[18, 19] The data presented are for the disappearance of the two carbon-centered radicals as monitored by EPR spectroscopy. The kinetic trace for the photodegradation of polymer **3**, like that of polymers **1** and **2**, is biphasic in that there is a fast reaction at short times followed by a slower conversion at extended reaction times.

$$\left(\!\!\sim\!\!O\right)_{\!n}$$

3
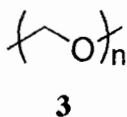
Figure 5a shows the fits of the data for the reaction of polymer **3** to first- and second-order equations (i.e., $C/C_0 = Ae^{-kt}$ and $C/C_0 = (1 + Bt)^{-1}$, respectively). The fits are poor, and therefore these two equations do not accurately represent the reaction mechanism for the degradation of this polymer. Figure 5b shows the fits for the other three models: simple-diffusion, diffusion-controlled, and the Perrin-like model. As was the case with polymers **1** and **2**, it is evident that these three equations more closely fit the data than the first- and second-order equations. Taking a closer look at the initial reaction

rates in Figure 5c, it is apparent that both the simple-diffusion and the diffusion-controlled models overestimate the initial reaction rate. This is similar to the findings reported above for polymers **1** and **2**. The Perrin-like model (eq 7), however, fits the data well at both long and short reaction times and is therefore a suitable model for the photodegradation of this polymer system. The interpretation is that the fast, initial rate is due to reaction of the carbon-centered radicals with another photogenerated radical species or an adjacent abstractable atom such as a hydrogen atom in the reaction sphere, and the slower rate is for the reaction of the carbon-centered radicals involving a diffusive reaction.

Literature Data Capture Method

The original data was 'captured' using pixel conversion.[20] The data image was scanned from the original journal article and opened in previewing software. The cursor was used to locate the pixel coordinates for the data points in the graph as well as the origin and maximums of the x- and y-axes. The pixel values for the data were recorded in an array and converted to the 'original' values, X and Y, using the following previously derived eqs 8 and 9, [20]

$$X = X_{min} + (pX - pX_{min})\frac{X_{max} - X_{min}}{pX_{max} - pX_{min}} \tag{8}$$

$$Y = Y_{min} + (pY_{min} - pY)\frac{Y_{max} - Y_{min}}{pY_{min} - pY_{max}} \tag{9}$$

where X_{min}, Y_{min}, X_{max}, and Y_{max} are the axes origin and extreme values extracted from the plot, pX_{min}, pY_{min}, pX_{max}, and pY_{max} are the corresponding pixel coordinates for the axes,

and pX and pY are the pixel coordinates for the data points of interest. The generated arrays of 'original' data were fit to model equations using IGOR Pro Carbon.

6.2.4 *Fitting Parameters as a Function of Temperature*

The photodegradation rates of polymers **1** and **2** were evaluated as a function of reaction temperature. As in the sections above, the data were fit to first-order, second-order, simple-diffusion, diffusion controlled, and Perrin-like equations. All data were found to be best fit by the Perrin-like model (eq 7). The parameters obtained from the best fit of the data were plotted as a function of irradiation temperature (Figure 6). The parameters Y_0 and X_0 in eq 7 represent the relative concentrations of the photogenerated radical species with and without a radical trapping agent in the reactive sphere, respectively. As shown in Figure 6, Y_0 is small, ranging from 0.5% to 2.5% over the temperature range 25-50 °C. Note also that Y_0 is larger in polymer **1** than in polymer **2**.
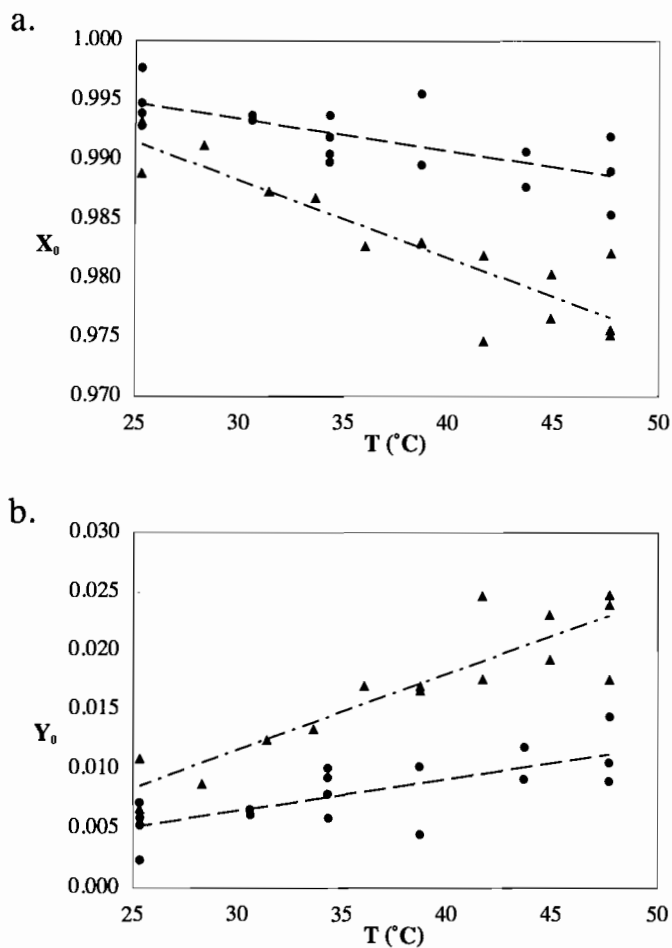
Figure 6. Fitting parameters X_0 and Y_0 from equation 7 as a function of temperature for polymers 1 (▲) and 2 (●).

The relative ratio of X_0 to Y_0 is dependent on the relative concentration of the radical trapping agent to the concentration of the photogenerated radical. The radical trap (chlorine atom) to metal species (molybdenum) ratio is approximately 100:1 for polymer 1 and 9:1 for polymer 2. An increase in radical trap concentration with respect to potential metal radical species will increase the probability of a radical trap being located in the reactive sphere. Therefore, it is predicted that polymer 1 would have a larger

number of photogenerated radicals with a Cl in the reaction sphere than polymer **2**, i.e., $Y_0(\mathbf{1}) > Y_0(\mathbf{2})$. As shown in Figure 6, this is indeed the case. For example, at room temperature, Y_0 for polymer **1** is approximately 0.008 and Y_0 for polymer **2** is 0.005.

For both polymers **1** and **2**, the value of Y_0 increased gradually with an increase in temperature and there was a corresponding decrease in X_0. (Over the temperature range of the experiment, the value of Y_0 for polymers **1** and **2** increased at a rate of 0.065% ± 0.009% K^{-1} and 0.027% ± 0.007% K^{-1}, respectively.) This trend is likely due to an effective increase in the reaction sphere caused by the enhanced kinetic motion of the radicals and the trapping species. This results in a greater likelihood of a radical trapping agent being in the reactive sphere of the photogenerated radical species.

The experimentally determined values for k_1 and k_2 (eq 7) for polymers **1** and **2** as a function of temperature were evaluated. Over this temperature range, the value of k_1 (the rate constant for the zeroth-order (slower) reaction) ranges from 10^{-6} to 10^{-5} s^{-1}, while k_2 (the rate constant for the first-order (faster) reaction) is on the order of 10^{-3} s^{-1}.[b] Restated, the rate constant for the non-diffusive reaction, k_2, is greater than the rate constant for the diffusive reaction, k_1. This result shows that diffusion is the rate-limiting step in the diffusive reaction, as expected.

To extract apparent activation enthalpies and entropies, the data were fit to an Eyring plot (Figure 7) and the resulting values are shown in Table 1.[c] The enthalpies of activation for the non-diffusive process are much smaller than those for the diffusive process for both polymers **1** and **2**, again consistent with rate-limiting diffusion in the diffusive reaction. The entropies of activation for both processes and polymers are all

negative. However, due to the size of the error in the activation entropies, no conclusions can be drawn from the values in Table 1.
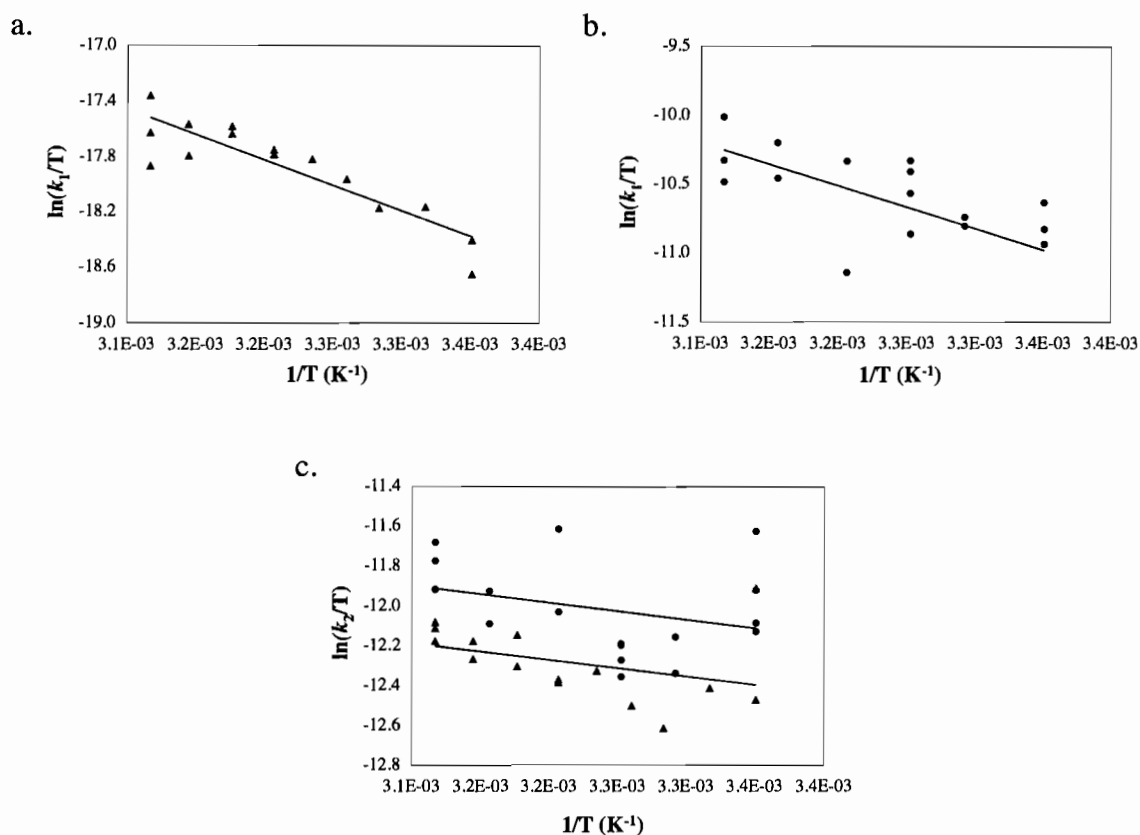
Figure 7. Erying plots for the fitting parameters k_1 and k_2 from equation 7 for polymers **1** and **2**.

Table 1. Apparent enthalpy and entropy of activation values obtained from the Eyring plot of the rate constants, k_1 and k_2, versus temperature for the photodegradation of polymers **1** and **2**.

Polymer	k_1 (diffusive)		k_2 (non-diffusive)	
	$\Delta H^{\ddagger}$ (kcal/mol)	$\Delta S^{\ddagger}$ (kcal/K mol)	$\Delta H^{\ddagger}$ (kcal/mol)	$\Delta S^{\ddagger}$ (kcal/K mol)
1	7 ± 1	-60 ± 40	2 ± 1	-70 ± 40
2	6 ± 2	-50 ± 40	2 ± 1	-70 ± 40

6.3   Conclusions

The photodegradation rate data of two polymer films, a cross-linked poly(vinyl chloride) and a segmented polyurethane, were compared to six kinetics models. It was found that the degradation did not follow simple zeroth-, first-, or second-order kinetics. Two other models, a simple-diffusion and a diffusion-controlled model, were analyzed and found to more closely represent the data than the zeroth-, first-, and second-order equations. However, these two models still overestimated the initial reaction rates. Accordingly, a new kinetics model, the Perrin-like model, was introduced that utilized basic photochemical rate equations and the heterogeneous nature of solid-state polymers. This equation fit the data with excellent accuracy. The model was also compared to the photodegradation rate of an example found in the literature, polyoxymethylene. The Perrin-like model equation was found to be an accurate fit of the literature data presented. An investigation of the effect of temperature on the parameters extracted from the fits to the Perrin-like model, showed that only a few percent of the radical species generated had radical trapping agents in the reactive sphere (Perrin-like environment) and that the majority of metal radicals did not have radical trapping agents in the reactive sphere (diffusive environment). It was also found that apparent $\Delta H^{\ddagger}$ for the photoreaction in the Perrin-like environment was lower than that of the diffusive reaction. It is hypothesized that the rate-limiting step in the diffusive reaction is diffusion of the photogenerated metal radical to the radical trapping agent.

6.4   Endnotes

a.   Polymers **1** and **2** are polymers **PVC-Mo** and **PU-70**, respectively.

b.   Rate coefficients for zeroth- and first-order reactions have units of $M\ s^{-1}$ and s^{-1}, respectively. However, because the data were presented and fit as the relative concentration versus time, the values of k_1 and k_2 both have units of s^{-1}. For the purpose of comparison, k_1 and k_2 will retain the unit s^{-1} and be referred to as rate constants or coefficients.

c.   The activation parameters obtained from photochemical reactions as a function of temperature must be interpreted with caution. See ref. 18, page 12.

CHAPTER VII

CONCLUDING REMARKS

7.1   Chapter Summaries

Sometime during the life of a polymeric material, it is exposed to light and some other variable, such as extreme temperature or mechanical stress. In order to predict the service lifetime of polymeric materials and to design environmentally degradable plastics, it is critical to understand the photochemical degradation reactions of polymers. To control polymer degradation in a prescribed fashion, so that the rate and onset of degradation is both tunable and predictable, it is also necessary to understand how external parameters and specific polymer properties affect degradation rates. This dissertation described the results of degradation experiments that probed several factors that affect polymer photodegradation rates: radical trap concentration, glass transition temperature, irradiation temperature, time-dependent morphology, and tensile stress.

Chapter I outlined what was understood to date about polymer photodegradation mechanisms and how external parameters and polymer properties affect degradation rates. Chapter II introduced a novel class of polymers that incorporated organometallic molybdenum dimers into the polymer backbone. In solution, these polymers are photodegradable in the presence of visible light and a suitable radical trap (i.e. O_2 or CCl_4). In the solid-state, these polymers were shown to degrade in the presence of O_2 or a radical trap built into the polymer chain (i.e. C–Cl units).

Chapters III, IV, and V discussed how parameters affect degradation rates. One unifying theme throughout the experiments is the mobility of the photogenerated radical. When a bond is homolyzed, two radicals are formed and exist initially in a solvent cage. These radicals can either recombine for no net degradation, or they can escape the solvent cage to potentially be trapped by a radical trapping agent. The findings suggest that external influences and intrinsic polymer properties directly affect the mobility of the photogenerated radicals and consequently the ability of the radicals to escape the solvent cage. In Chapter III, for example, polymers with different the glass transition temperatures (T_g) were shown to have significantly different quantum yields. Polymers irradiated below T_g, where polymer mobility is limited, had a slower degradation rate than polymers irradiated above T_g. In fact, polymers irradiated above T_g had degradation efficiencies similar to those in solution. This suggests that photogenerated radicals have the same mobility in solution as in the solid-state above T_g.

The effect of temperature on polymers below T_g was discussed in Chapter IV. It was discovered that quantum efficiency had an exponential dependence on reaction temperature. The activation energies for the photochemical reactions corresponded with the activation energies of the secondary thermal transitions of the polymers. This suggested that polymer molecular motions, to which the photogenerated radical species are a part of, facilitate the escape of the radicals from the 'solvent' cage (increase in k_d) and consequently increasing the photodegradation efficiency.

The final two parameters, time-dependent morphology and tensile stress, were presented in Chapter V. These two studies both involve the formation of crystalline

regions in the solid-state. The results indicate that thermodynamic stability of the polymer affects the efficiency with which photogenerated radicals escape the radical cage. In the case of time-dependent morphology changes, the change in morphology decreased the residual strain induced in the casting process and created thermodynamically stable soft and hard regions which effectively decreased the ability of the photogenerated to escape the cage. In the case of tensile stress, there were two interesting results. First, tensile stress increased the rate of radical escape from the recoil of 'taut' photogenerated radical polymer segments. Second, stress induces crystallinity, which effectively decreased the rate of radical diffusion out of the cage and decreased degradation rates. Restated, thermodynamically stable polymers had slower degradation rates than polymers with residual or applied stress.

Chapter VI evaluated the reaction kinetics of the photodegradation reaction of the metal-metal bond containing polymers. Several model equations were used to fit the experimental data including a variety of diffusion models, however, none of the models properly fit the data. A new kinetic model based on Perrin-like kinetics was presented and found to fit the data accurately.

7.2   Concluding Hypothesis

The experiments preformed using novel metal-metal bond containing polymers suggest that polymer degradation efficiency is strongly influenced by the mobility of the photogenerated radicals. In Chapter III, the effect of glass transition temperature on the degradation of polymers was investigated and it was found that the quantum efficiency was greater above T_g than below T_g. This suggested that polymer molecular was a key

factor. This was further supported in Chapter IV were irradiation temperature was explored. It was hypothesized that the quantum yield was affected by the ability of the photogenerated radicals to escape the radical cage, $k_{cage\ escape}$ (shown in Scheme 1). This was supported by the similarity in the activation energies of the photoreaction and the activation energies of the relevant molecular motions required for radical cage escape.

$$\text{wwM-Mwww} \underset{k_{bonding}}{\overset{k_{homolysis}}{\rightleftharpoons}} \left[\text{wwM}\bullet,\bullet\text{Mwww}\right] \underset{k_{cage\ reformation}}{\overset{k_{cage\ escape}}{\rightleftharpoons}} 2\ \text{wwM}\bullet \overset{\overset{\text{Cl}}{\underset{|}{\text{ww}}}}{\underset{k_{trap}}{\longrightarrow}} 2\ \text{wwM-Cl}$$
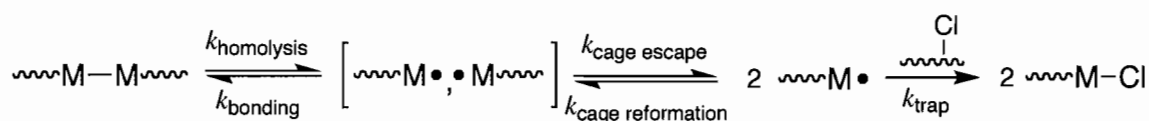
Scheme 1. Photodegradation mechanism of a metal dimer containing polymer illustrating the 'solvent' cage.

Other evidence that molecular motion is key was presented in Chapter V. The experiments on tensile stress and time-dependent morphology demonstrated that degradation efficiencies vary with changes in polymer morphology. Tensile stress has two effects on polymers. It can increase radical-radical separation from the recoil of 'taut' photogenerated radical polymer segments which increases $k_{cage\ escape}$ or it can decrease $k_{cage\ escape}$ from stress-induced crystalline formation. In the later case, the photogenerated radicals were essentially held in place in the crystalline matrix resulting in a decrease in radical separation efficiency. This was also shown in the case of polyurethane that, with time, there was an increase in crystallinity and a corresponding decrease in quantum efficiency.

In summary, it has been shown that the mobility of the photogenerated radicals is the primary contributing factor that influences polymer degradation efficiencies. A decrease in the mobility of the photogenerated radicals decreases the radical separation efficiency and, consequently, the degradation rates decline.

APPENDIX A

MEASURING SOLID-STATE QUANTUM YIELDS: THE CONVERSION OF A

FREQUENCY-DOUBLED Nd:YAG DIODE LASER POINTER MODULE INTO A

VIABLE LIGHT SOURCE

A.1 Introduction

Accurate quantum yield measurements are difficult to obtain for reactions in the

solid-state. The difficulty arises from three problems. First, the surface area of

irradiation must be accurately known so that quantum yield values can be accurately

calculated.[1,2] Second, the samples are not homogeneous following irradiation. As

explained below, this can lead to errors in the calculation of the quantum yield. Third,

light scattering artificially decreases the absorbance of a sample, which leads to errors in

rate measurements and hence the quantum yield.[3-5] (This problem is particularly

prevalent in opaque or non-transparent samples.) Unfortunately, light scattering results

from the intrinsic properties of the sample, and it is difficult to correct by instrumental

methods. Nevertheless, the first two difficulties can be addressed by proper instrument

design, and in this section, we report an irradiation apparatus that circumvents the first

two problems.

With regard to the first problem, it is noted that the quantum yield is defined as

the rate of the reaction divided by the rate of photon absorption, Equation 1.[1,6]

(Equivalently, is the number of molecules reacted divided by the number of photons

absorbed by the reactant.) For solid-state studies, the reaction rates (numerator) are determined by iterative irradiation and degradation monitoring, typically by molecular weight determination, end-group analysis, mechanical testing, etc. However, for these reactions, it is not necessarily trivial to obtain the rate of photon absorption (denominator) because the volume of irradiation must be known. It is important therefore that sample thickness be accurately known and that the surface area of irradiation be measurable and consistent. Obtaining an accurate surface area of irradiation is made complicated when a divergent source such as a high-pressure Hg arc lap is used as the irradiation source. Small translational movement along the path of irradiation may occur during iterative sample replacements. This will produce a change in surface area of irradiation that scales with the square of the distance of translational motion.

$$\Phi = \text{rate of reaction/rate of photon absorption} \tag{1}$$

With regard to the second problem, it is noted that the sample can become inhomogeneous if the light beam is smaller that the surface area of the sample. This leads to inhomogeneity because only the irradiated parts of the sample will have reacted. For example, if the sample is moved from the light beam to the spectrometer for interrogation then upon further irradiation the sample must be returned to precisely the same location as during the previous irradiation so that the exact same region of the sample can be irradiated again. Because solid-state samples can rarely be repositioned exactly, this leads to errors in the Δ(absorbance) measurements and hence to errors in the rate of reaction.

To overcome the problem of obtaining accurate quantum yields in the solid-state, we built a computer-controlled device that simultaneously irradiates and spectroscopically monitors samples in the solid-state. It measures and records the absorbed light intensity as a function of time and also records a reference (unabsorbed) light intensity. A key feature of the apparatus is that the same light beam is used to irradiate and simultaneously monitor the reaction. The films can thus be left in one place, and consequently there are no "positioning errors" associated with these measurements. Another important feature is that a collimated light source (i.e., laser) is used to irradiate the sample, thus reducing errors attributed to inconsistencies in the "area of irradiation" of the sample.

This work is published in volume 78 of the journal Review of Scientific Instruments in 2007. The experiments were performed by J. Harris and myself. C. Dax was critical in the design and assembly of the instrumentation. J. Harris and myself prepared the manuscript with D. Tyler providing editorial assistance.

A.2 Experimental Apparatus

A.2.1 *The Merlin Detection Unit*

An Oriel Merlin radiometry system was used to measure quantum yields. The details of the experimental setup for this system are shown in Figure 1. The major components of this system are (1) an irradiation source, (2) an Oriel 100 mm^2, NIST-calibrated silicon photodiode (Model 70356) detector, (3) an Oriel Merlin radiometry control unit, and (4) a personal computer. The light source could quickly be interchanged between the Nd:YAG (yttrium aluminum garnet) laser and the high-pressure Hg arc lamp

by the addition or removal of a mirror. Light from the source was passed through a sample holder, which rested on a temperature control unit (set to 25.0 ± 0.1 °C for the data herein). Solid samples were mounted in an airtight aluminum casing with glass plates for light transmittance. (A solution sample apparatus consisting of a 1 cm cell holder and a stirring mechanism could also be employed.) Light passing through the sample holder was focused through a lens and a five-blade chopper (Oriel Model 75163) onto the working area of the signal detector head. The signal was chopped at a frequency of 30.0 Hz, to eliminate light fluctuations due to electrical line noise. The photodiodes of the detector have operator selectable transimpedance resistors, which were set to 10^4 gain. Housing the detector inside the insulated, temperature-controlled box minimized errors attributed to the detector's sensitivity to fluctuations in temperature. The data were processed using Merlin radiometer system (Model 70100). The Merlin system contained all the hardware and protocols required for detection of low light levels, lock-in amplification, and digital processing of the signal.
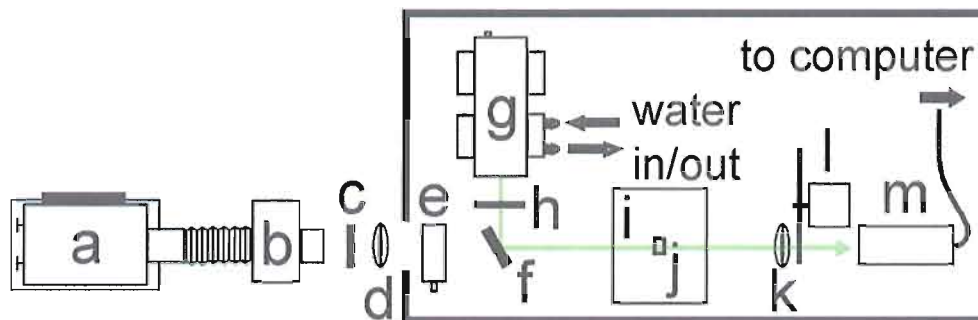
Figure 1. The experimental setup for both liquid and solid state quantum yield measurements using either a Hg arc lamp or Nd:YAG laser as the source. The components of this system are as follows: (a) Hg arc lamp, (b) monochromator, (c) iris, (d) focusing lens, (e) light valve, (f) mirror, (g) Nd:YAG laser, (h) mask for the laser beam, (i) variable temperature mounting plate, (j) sample holder, (k) focusing lens, (l) chopper, and (m) detector.

A.2.2 *Conversion of the Frequency-doubled Nd:YAG Laser Pointer Module into a Viable Irradiation Source*

A 15 mW frequency-doubled Nd:YAG diode laser pointer module (DPSS-5) was purchased from "Beam of Light Technologies."[7] Unmodified, the laser pointer module is inappropriate for quantum yield measurements. (Both λ_{max} and the intensity are temperature sensitive and the system requires cooling for operating times of more than 20 seconds.) In addition, the beam size, profile, and shape of the Nd:YAG laser were inappropriate for solid-state quantum yield measurements and were modified accordingly. The beam size was expanded by replacing the collimating lens included in the module with a 4 inch focal length plano-convex lens placed 2.25 inches away from the nodule (Figure 2). The beam was given a round shape with a top-hat profile by passing it through an 8 mm diameter hole drilled into the aluminum housing that encased the laser. Although the size, shape, and profile of the beam were adjusted during the

conversion process, the key to successfully converting a laser pointer module into a usable irradiation source for quantum yield measurements is the ability to precisely control the temperature of the laser. Precision temperature control of the Nd:YAG laser was achieved in two ways. First, the laser quantum yield measurements were performed inside an insulated box, whose internal temperature was maintained at 25 ± 1 °C (see the schematic in Figure 1). Second, the aluminum housing was kept at a temperature of 25.0 $\pm$ 0.1 °C by combination of both water-cooling and the use of a conventional servo feedback loop used to control a thermoelectric cooler module (see schematic in Figure 2).
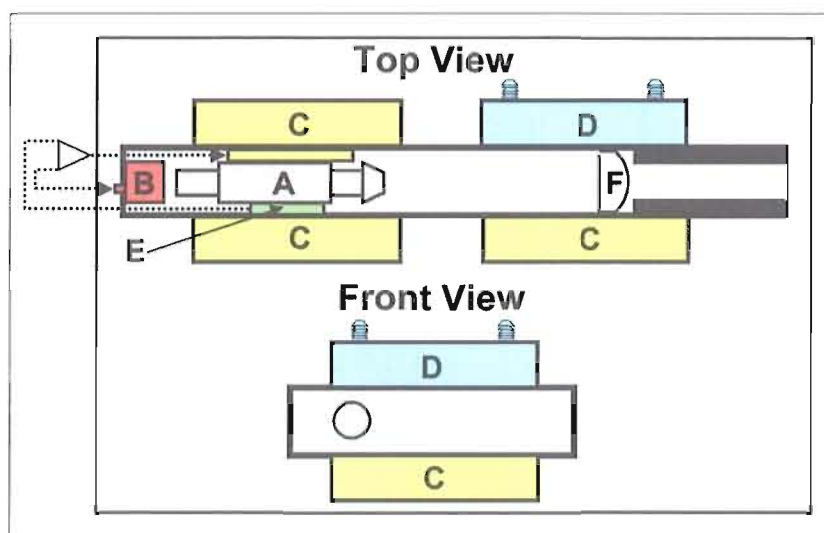
Figure 2. A schematic of the Nd:YAG laser, which consists of (a) the laser module, (b) temperature set, (c) thermoelectric cooler modules, (d) a water cooling module, (e), a thermocouple, and (f) lens.

A.2.3 *The Nd:YAG Laser as a Light Source*

The collimated light source was the Nd:YAG laser discussed in the previous section. Before irradiating the sample, the 8 mm beam was first passed through a mask to

adjust the beam dimensions to a 2×8 mm^2 rectangle. The beam profile is shown in Figure 3(a); $\lambda_{max} = 532.48 \pm 0.01$ nm with a full width at half maximum (FWHM) of 0.79 $\pm$ 0.02 nm. A silvered mirror (New Focus 5103) was used to precisely align the masked beam through the sample and onto the detector (see the schematic in Figure 1).

A.2.4 *The 200 W High-pressure Hg Arc Lamp as a Light Source*

The divergent light source was a 200 W high-pressure mercury arc lamp (Oriel Model 6135). The beam profile is shown in Figure 3(b); $\lambda_{max} = 546.88 \pm 0.00$ nm with a FWHM of 1.17 ± 0.01 nm. The arc lamp was fitted with a quartz-ended IR filter (Oriel Model 77263), a collimating mirror, and a flexible light tube. The other end of the flexible light tube was attached to the slit input of a monochromator (Oriel Model 77250) equipped with a ruled diffraction grating of 1200 lines/mm line density (Oriel Model 77298). The entrance and exit slits were set to 0.2 mm. The exiting light was focused into the insulated box and on the samples using a focusing lens. To reduce fluctuations in beam intensity, the light was attenuated by passing it through a light valve optimized for 546 nm light with an adjustable feedback loop (see the schematic in Figure 1).
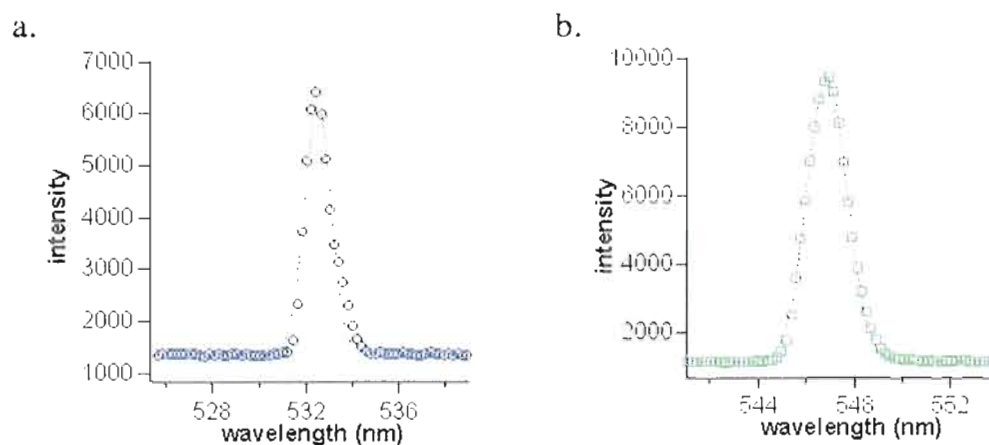
Figure 3. Beam profiles for (a) Nd:YAG laser with λ_{max} = 532.48 ± 0.01 nm and FWHM = 0.79 ± 0.02 nm, and (b) high-pressure mercury arc lamp with λ_{max} = 546.88 ± 0.00 nm and FWHM = 1.17 ± 0.01 nm. The beam intensities are (a) $1.6 \times 10^{-3} \pm 2 \times 10^{-6}$ and (b) $2.4 \times 10^{-4} \pm 3 \times 10^{-6}$ W. The beam profiles were obtained by reflecting the beam off a white surface onto an Ocean Optics USB4000 spectrometer and analyzed using Igor Carbon Pro fitting program.

A.3   Experiments and Discussion

A.3.1 *Reagents*

All manipulations were carried out in the absence of water and atmospheric oxygen using standard glove box techniques. The light sensitive nature of the samples required that their preparation and storage be under darkroom conditions. Films of polymer **1** (Figure 4) were prepared using the method described in the literature.[8]

1
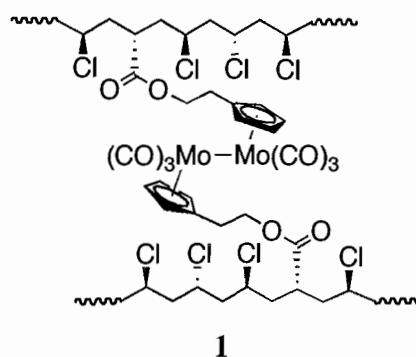
Figure 4. The structure of polymer **1** used in the photochemical degradation studies.

A.3.2 *Results of the Solid-state Experiments*

The photochemical reaction of polymer **1** is shown in Scheme 1.[9] The reaction was monitored by the disappearance of the Mo–Mo chromophore at 546 nm (using the Hg arc lamp) or at 532 nm (using the Nd:YAG laser). The reaction was allowed to proceed to 1%–3% completion. The quantum yields were calculated using standard methods:[1] Φ (Hg arc lamp) = 0.06 and Φ (Nd:YAG) = 0.07. Figure 5 compares data acquired during the irradiation of polymer **1** using the Nd:YAG laser and the high-pressure Hg lamp. Note that the intensity of the Nd:YAG laser ($1.6 \times 10^{-3} \pm 2 \times 10^{-6}$ W) is greater than the intensity of the Hg arc lamp ($2.4 \times 10^{-4} \pm 3 \times 10^{-6}$ W) (Figure 3). The benefit of using a source that produces higher intensity light is that less time is needed to achieve the same percent conversion. For the experiments in Figure 5, 86 minutes were needed for 1% conversion of polymer **1** using the Hg arc lamp, while only 25 minutes were needed for 1% conversion using the Nd:YAG laser. These values correspond to a reaction rate of 5.3 M/min for the laser and 2.3 M/min for the arc lamp.[a]
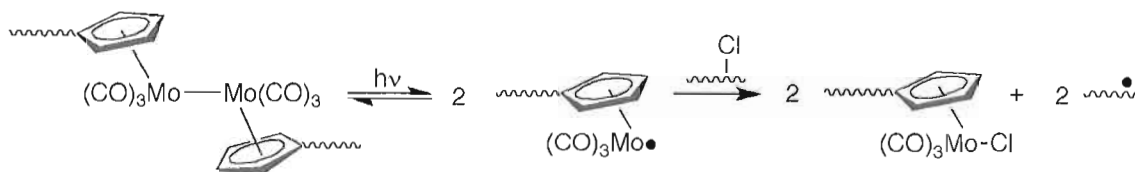
Scheme 1. The photochemical reaction of polymer **1**.
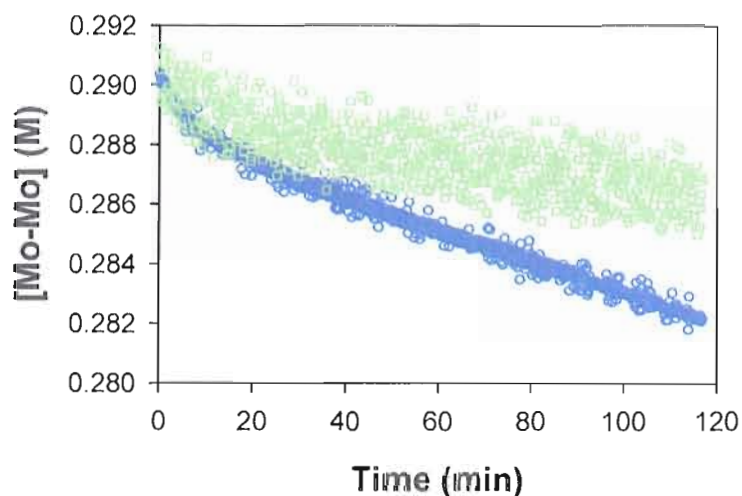
Figure 5. Irradiation of a polymer containing the chromophore unit $Cp(CO)_3Mo–$ $Mo(CO)_3Cp$ using the Nd:YAG laser (represented with circles) at $\lambda = 532$ nm and the attenuated Hg arc lamp (represented with squares) at $\lambda = 546$ nm.

Figure 5 also illustrates an improvement in the signal-to-noise [Nd:YAG laser source (S/N = 1150); Hg arc lamp (S/N = 190)]. The improvement is a result of the increased stability of the irradiation source from proper temperature control. The increased signal-to-noise ratio allows for a more accurate determination of the reaction rate and can be directly compared by the significant improvement in the coefficient of determination from R^2(Hg arc lamp) = 0.42 to R^2(Nd:YAG) = 0.98.

Other concomitant benefits of using the Nd:YAG laser as an irradiation source should also be noted. (1) The Nd:YAG laser is more cost effective than a traditional

high-pressure Hg arc lamp. The cost of the frequency-doubled Nd:YAG diode laser

pointer module (DPSS-5; Beam of Light Technologies) is $55, while the cost of a

replacement bulb (200 W Hg bulb from Oriel) for a high-pressure mercury arc lamp is

$193. (2) The useful lifetime of the Nd:YAG laser is greater than that of the high-

pressure Hg arc lamp for quantum yield measurements. Although an accurate lifetime of

the Nd:YAG crystal has yet to be determined, the laser thus far has lasted for 1500 hours

of irradiation. (Note, the only change over the 1500 hours has been a slow decrease in

beam intensity from 1.6×10^{-3} to 1.2×10^{-3} W.) In comparison, the useful lifetime of a

high-pressure Hg arc lamp bulb for solid-state quantum yield measurements is

approximately 200 hours.[10] (After about 200 hours, the arc path begins to move, which

results in intensity fluctuations and renders it useless for these types of experiments.) (3)

The replacement and disposal of the Nd:YAG laser module are easy and safe.

Replacement of the laser module requires the removal of the old module from the

circuitry, the removal of the stock lens from the new laser module, and the attachment of

the new laser module to the circuitry. The used laser module can be disposed of safely in

the trash. In contrast, replacement of Hg arc lamp bulb involves the handling of high-

pressure bulbs that contain toxic mercury. Thus before a mercury bulb can be properly

disposed of, it is necessary to discharge the high pressures and mercury form the bulb.

A.4   Summary

The design of our modified Nd:YAG diode laser/computer-controlled device

allows us to circumvent two of the main problems associated with traditional solid-state

quantum yield measurements. First, errors attributed to inconsistencies in the "area of

irradiation" of the ample were eliminated by the collimated nature of the laser beam.

Second, using the same beam of light to both irradiate and monitor the sample, this

allowing the sample to remain stationary during the experiment, eliminated "positioning

errors". The inclusion of the Nd:YAG laser in the computer-controlled device allows for

faster data acquisition times with an improved signal-to-noise ratio. Overall, the

improvements allow a significant reduction in errors associated with solid-state quantum

yield measurements.[b]

A.5   Endnotes

a.   Note that the differences in the reaction times and reaction rates are also dependent on the molar absorptivity of the chromophore (ε_{546} = 1615 L mol/cm and ε_{532} = 1995 L mol/cm), so the values cannon be compared directly.

b.   One disadvantage of the laser is that it provides only one wavelength for irradiation. The mercury arc lamp is an indispensable part of the system if other irradiation wavelengths are needed.

APPENDIX B

SYNTHESES AND PREPARATION OF PHOTOCHEMICALLY REACTIVE

SPECIES USED IN THE DEGRADATION STUDIES

B.1   Materials

All manipulations were carried out using standard Schlenk techniques or in a

Vacuum Atmospheres Co. glove box under a nitrogen atmosphere. Unless otherwise

noted, HPLC grade solvents were deoxygenated by passage through columns of alumina

and copper oxide under an argon atmosphere. $(\eta^5\text{-}C_5H_4CH_2CH_2OH)_2Mo_2(CO)_6$ was

prepared as previously described.[1,2] Hypol 2000 was donated by the W. R. Grace Co. It

was stored at 5 °C and deoxygenated with a nitrogen purge before use. Hypol 2000 is a

toluene diisocyanate-endcapped, branched poly(ethylene glycol) (ca. 6.7 wt %

isocyantate) with an $M_n \sim 2,000$ and an equivalent weight of 625 g/equiv of isocyanate.

Poly(ethylene glycol) (PEG-1000) (Mn $\sim$ 1,000) was obtained from Aldrich and

deoxygenated with a nitrogen purge before use. Carboxylated poly(vinyl chloride) ($M_n \sim$

220,000 and 1.8 wt % carboxyl content) was purchased from Aldrich. Thionyl chloride

(Fluka, 99%) was stored in a desiccator.   1-(Chloromethyl)-2,4-diisocyanatobenzene

(97%) was obtained from Aldrich, stored in the drybox, and used as received. 1,4-

Butanediol (98%; Aldrich) was distilled under reduced pressure and stored under

nitrogen in the drybox. Tolylene 2,4-diisocyanate terminated poly(propylene glycol) (3.6

wt % isocyanate; $M_n \sim 2,300$) was obtained from Aldrich. Dibutyltin diacetate (DBTA;

Aldrich) was stored in the refrigerator in the dark. Carbon tetrachloride was prepared in a

nitrogen atmosphere by distillation over phosphorus pentoxide and then filtered though a

silica plug.

B.2   Characterization Instruments

Infrared spectra were recorded on a Nicolet Magna 550 FT-IR spectrometer with

OMNIC software. Thermal transitions were determined using a TA Dynamic

Mechanical Analyzer Q800 with an oscillating frequency of 0.1 s^{-1} or a TA 2920 DSC

instrument with a heating rate of 10 °C/min. The modulus measurements were carried

out at room temperature using an Instron 4444 mechanical tester and are reported as

stress (MPa)/% strain. Molecular weights were determined either by a Knauer vapor

pressure osmometer (VPO) (at 45 °C with THF as the solvent) or A Waters 515 HPLC

pump with HR3 and HR4 stryragel columns and a Waters 410 Differential Refractometer

gel permeation chromatograph (GPC) unit (molecular weight are respect to polystyrene

standards in THF). Oxidation states of molybdenum were obtained by Dratos His X-ray

photoelectron spectroscopy (XPS) using the monochromatized Al source (200 W). The

vacuum in the main chamber was $< 3 \times 10^{-9}$ Torr during data acquisition. To achieve

optimal signal-to-noise ratios and peak widths, high-resolution spectra were acquired at

20 eV pass energy. The binding energies were referred to the C 1s peak at 285.0 eV.

B.3 Synthesis of $[(\eta^5\text{-}C_5H_4CH_2CH_2OH)(CO)_3Mo]_2$.[1,2]

B.3.1 *Synthesis of Sodium Cyclopentadiene.*

Freshly cut sodium (2.105 g, 0.092 mol) was added to 80 mL of nitrogen-purged dicyclopentadiene at room temperature in a 500 mL three-neck flask equipped with a magnetic stir bar, reflux condenser, N_2 inlet, and a stopper. On heating, the solution turned blue and then sodium sand formed. The mixture was heated for 6 hrs at 160 °C. A white precipitate was observed as well as dihydrogen evolution. The remaining cyclopentadiene was filtered off the white product. The product was washed with four 100 mL portions of hexanes and dried under vacuum. Yield: 8.017 g (99%). ^{1}H NMR (d_6-DMSO, 300 MHz): δ 5.3 (s, 5H).

B.3.2 *Synthesis of Cyclopentadienylethanol.*

Sodium cyclopentadiene (4.5 g, 0.051 mol) was added to 30 mL of nitrogen-purged THF in a 100 mL Schlenk flask equipped with a magnetic stir bar and rubber stopper in the drybox; the solution was brown/red. The reaction flask was removed from the drybox and immersed in an ice-water bath. Ethylene oxide (3 mL, 0.06 mol) was measured out in a graduated cylinder that was cooled in an ice-water bath and 7 mL of nitrogen-purged, 0 °C THF was added. The ethylene oxide/THF mixture was cannulated into the reaction flask over a 1 hr period; the solution was a burgundy color. The solution was stirred at 0 °C for 2 hrs and then allowed to warm to room temperature. 1.0 M HCl was added until the pH was acidic; the solution would temporarily change to orange/red upon addition of the acid. All subsequent steps were preformed in air. The suspension

was transferred to a 1000 mL separatory funnel. 50 mL of water and 50 mL of ether were added to the funnel. The water layer was removed and the ether layer was washed three times with 100 mL of water. The water extracts were combined and washed three times with 100 mL of ether. The ether layers were combined and dried with Na_2SO_4. The ether was vacuumed off to leave a brown/red oil. The product was vacuum distilled. ^1H NMR (CDCl$_3$) m 6.19 – 6.47 (m, 3H, alkenyl C$_5$H$_5$); 3.80 (q, 2H, -C$\underline{H}_2$OH); 3.01 (s, 1H, allylic C$_5$H$_5$); 2.95 (s, 1H, allylic C$_5$H$_5$); 2.68 (m, 2H, C$_5$H$_5$C$\underline{H}_2$).

B.3.3 *Synthesis of 2-(1-Methoxy-1-methyl-ethoxy)-ethyl-cyclopentadiene.*

Was prepared according to the literature.

B.3.4 *Synthesis of (η^5-C$_5$H$_4$CH$_2$CH$_2$OH)$_2$Mo$_2$(CO)$_6$.*

Was prepared according to the literature.

B.4 Synthesis of the polyurethane copolymer of Hypol-2000 and (C$_5$H$_4$CH$_2$CH$_2$OH)$_2$Mo$_2$(CO)$_6$ (Hypol-Mo).

Hypol 2000 (0.400 g, 0.640 mmol of –NCO) and (η^5-C$_5$H$_4$CH$_2$CH$_2$OH)$_2$Mo$_2$(CO)$_6$ (0.185 g, 0.185 g, 0.0640 mmol of –OH) were added, under nitrogen, to a 100 mL Schlenk flask containing 33 mL of THF and equipped with a magnetic stirbar and condenser. DBTA (0.020 mL; 0.075 mol) was syringed into the mixture, which was then refluxed for 8 h. The reaction was monitored by IR spectroscopy. The reaction was stopped when the isocyanate band at 2273 cm^{-1} had

disappeared. Absolute ethanol (0.5 mL) was added to destroy any unreacted isocyanate groups. The solution was stirred for 0.5 h while cooling. Hexane (50 mL) was cannulated into the cooled solution to precipitate the polymer, which was isolated by decanting the solution and then drying under vacuum. M_n (VPO, THF) = 7900 g/mol.

B.5 Synthesis of the polyurethane copolymer of Hypol-2000, PEG-1000 and $(C_5H_4CH_2CH_2OH)_2Mo_2(CO)_6$ (Hypol-PEG-Mo).

Hypol 2000 (0.422 g, 0.675 mmol of –NCO) was placed in a 100 mL Schlenk flask equipped with a magnetic stir bar and condenser and then degassed, followed by a nitrogen purge. $(\eta^5\text{-}C_5H_4CH_2CH_2OH)_2Mo_2(CO)_6$ (0.087 g, 0.300 mmol of –OH) and poly(ethylene glycol) (PEG-1000; 0.188 g, 0.375 mmol of –OH) were deoxygenated under nitrogen and then dissolved in 30 mL of freeze-pump-thawed, dry THF and cannulated into the Schlenk flask containing Hypol 2000. DBTA (0.020 mL, 0.075 mol) was added to the reaction solution, and the solution was refluxed for 8 h, at which time the isocyanate band at 2273 cm^{-1} had disappeared in the infrared in the infrared spectrum. Absolute ethanol (0.5 mL) was added to destroy any unreacted isocyanate groups, and the solution was stirred for 0.5 h while cooling. Hexane (50 mL) was cannulated into the cooled solution to precipitate the polymer, which was isolated by decanting the solution and then drying under vacuum. M_n (VPO, THF) = 13500 g/mol.

B.6   Synthesis of Acyl-substituted Poly(vinyl chloride) (PVC-COCl).

Using Schlenk techniques, carboxylated poly(vinyl chloride) (PVC-COOH; 2.0 g,

0.8 mmol of –COOH) was dissolved in 150 mL THF in a 3-neck round bottom flask

fitted with a stir bar, Schlenk adapter, addition funnel, reflux condenser, and a drying

tube for scrubbing acid. Thionyl chloride (1.5 mL, 2.45 g, 20.6 mmol) dissolved in 50

mL THF was added to the addition funnel. The reactants were slowly combined over 1 h

and then brought to reflux for 36 h. The solution resulting solution was clear orange and

became more viscous when vacuum concentrated. Hexanes (50 mL) were added and a

white precipitant of the polymer formed. The hexanes were cannulated off and the

polymer was washed three times with 50 mL portions of hexanes. The residual solute

was removed by vacuum and the remaining white solid polymer was dried under vacuum

for 2 days. IR (KBr pellet): ν(C=O) 1775 (s) and 1731 (m) cm^{-1}.

B.7   Synthesis and preparation of poly(vinyl chloride) crosslinked with

$(C_5H_4CH_2CH_2OH)_2Mo_2(CO)_6$ **(PVC-Mo).**

In a drybox under a red light, PVC-COCl (0.4 g, 0.11 mmol of –COCl) was

dissolved in THF in a round bottom flask containing a stir bar. $(\eta^5$-

$C_5H_4CH_2CH_2OH)_2Mo_2(CO)_6$ (0.04 g, 0.14 mmol of –OH) were dissolved in 40 mL THF

and slowly added by pipette to the reaction flask, followed by addition of 1 mL of

triethylamine. After two days, the salt precipitate was removed by filtration. The

remaining clear, red solvent was concentrated by vacuum, poured into a Teflon-coated

mold, left for 24 h, then placed under a vacuum for two days. IR (polymer film):

ν(C=O) 1770 (s) and 1731 (m) cm^{-1}; ν(C≡O) 2004 (m), 1951 (s), and 1907 (s) cm^{-1}.

Modulus = 1300 $\pm$ 100 MPa (using a grip separation speed of 5 mm/min). T_g = 65 $\pm$ 4 °C.

B.8   Synthesis and Preparation of the polyurethane copolymers of TDI, TDI-PPG, 1,4-butanediol and $(C_5H_4CH_2CH_2OH)_2Mo_2(CO)_6$ (PU-XX).

1-(Chloromethyl)-2,4-diisocyanatobenzene, tolylene 2,4-diisocyantae terminated poly(propylene glycol), (η^5-$C_5H_4CH_2CH_2OH)_2Mo_2(CO)_6$, and 1,4-butanediol were added, under nitrogen, to a 150 mL Schlenk flask containing 50 mL of THF and equipped with a magnetic stirbar and condenser (reagent quantities expressed in Table 1). DBTA (0.020 mL, 0.075 mmol) was syringed into the reaction mixture and the solution was refluxed for 8 h. Absolute ethanol (0.1 mL) was added, and the solution was stirred for 30 min while cooling. The solution was cast onto a Teflon surface and the solvent allowed to evaporate under an inert atmosphere for 2 days, after which time the film was thoroughly dried under vacuum. The polymer films were insoluble in all common organic solvents and consequently, M_n could not be determined by VPO or GPC.

Table 1. The starting material quantities for the polyurethane series **PU-XX**.

Polymer	TDI (g, mmol -NCO)	TDI-PPG (g, mmol -NCO)	Mo Dimer (g, mmol -OH)	1,4-butanediol (g, mmol -OH)
PU-35	0.136, 0.700	0.817, 0.700	0.029, 0.100	0.086, 1.90
PU-50	0.089, 0.850	0.992, 0.850	0.024, 0.850	0.073, 0.850
PU-60	0.113, 1.08	0.840, 0.720	0.026, 0.090	0.077, 1.71
PU-70	0.208, 2.00	1.00, 0.857	0.041, 0.143	0.122, 2.72
PU-90	0.376, 3.60	0.467, 0.400	0.057, 0.200	0.171, 3.80

B.9   Preparation of PVC Embedded with Cp′$_2$Mo$_2$(CO)$_6$ (Mo in PVC).

In a drybox, PVC-COOH (0.4 g) was dissolved in 20 mL THF. Cp'$_2$Mo$_2$(CO)$_6$ (40 mg, 0.08 mmol) was dissolved in 5 mL THF and added to the polymer solution. The excess solvent was concentrated by vacuum, poured into a Teflon-coated mold, left for 24 hr to evaporate slowly then placed under vacuum for two days. $T_g = 72 \pm 3$ °C. Modulus = 1200 ± 50 MPa. The microcrystallinity of the Cp'$_2$Mo$_2$(CO)$_6$ in the PVC matrix could not be determined by DSC. Crystallization phases were observed at approximately 170 and 215 °C in the samples of raw PVC, Cp'$_2$Mo$_2$(CO)$_6$, and a mixture of the two. These peaks have not yet been identified, but there presence in all three samples prevents drawing any conclusion as to whether the Cp'$_2$Mo$_2$(CO)$_6$ dispersed in PVC contains any microcrystalline regions of Cp'$_2$Mo$_2$(CO)$_6$.

B.10   Preparation of Cp′$_2$Mo$_2$(CO)$_6$ Solution (Mo in Soln).

In a drybox, Cp′$_2$Mo$_2$(CO)$_6$ (30 mg, 0.06 mmol) and CCl$_4$ (10 mL, 15.9 g, 0.1

mol) were added to a 100 mL volumetric flask and diluted with hexane to the mark. The

solution was 6 mM in Cp′$_2$Mo$_2$(CO)$_6$ and 1 M in radical trapping agent (CCl$_4$).

REFERENCES

Chapter I

1. Schnabel, W., *Polymers and Light: Fundamentals and Technical Applications.* Wiley-VCH: Weinheim, 2007.

2. West, R.; Maxka, J. *ACS Symposium Series* **1988,** *360*, 6-20.

3. West, R. *J. Org. Chem.* **1986,** *300*, 327-346.

4. Hofer, D.; Miller, R. D.; Willson, C. G. *Proc. SPIE-Int. Soc. Opt. Eng.* **1984,** *469*, 16-23.

5. Ishikawa, M.; Nate, K. *ACS Symp. Ser.* **1988,** *360*, 209-223.

6. Maneerat, C.; Hayata, Y. *Trans. ASABE* **2008,** *51*, 163-168.

7. Kijchavengkul, T.; Auras, R.; Rubino, M.; Ngouajio, M.; Fernandez, R. T. *Chemosphere* **2008,** *71*, 1607-1616.

8. Scott, G. *Trends Polym. Sci. (Cambridge, U. K.)* **1997,** *5*, 361-368.

9. Lamont, W. J. J. *Vegetable Production Using Plasticulture*; Asian and Pacific Region, Food & Fertilizer Technology Center: 1999, 1999.

10. Tyler, D. R. *Coord. Chem. Rev.* **2003,** *246*, 291-303.

11. Yamashita, T.; Tomitaka, H.; Kudo, T.; Horie, K.; Mita, I. *Polym. Deg. Stab.* **1993,** *39*, 47-54.

12. Dan, E.; Guillet, J. E. *Macromolecules* **1973,** *6*, 230-235.

13. Shimada, S.; Hori, Y.; Kashiwabara, H. *Polymer* **1981,** *22*, 1377-1384.

14. Hori, Y.; Shimada, S.; Kashiwabara, H. *J. Polym. Sci., Polym. Phys. Ed.* **1984,** *22*, 1407-1415.

15. Yoshioka, T.; Saitoh, N.; Okuwaki, A. *Chem. Lett.* **2005,** *34*, 70-71.

16.   Nakatani, H.; Matsuoka, H.; Suzuki, S.; Taniike, T.; Liu, B.; Terano, M. *Macromol. Symp.* **2007,** *257*, 112-121.

17.   Boxhammer, J. *Polymer Testing* **2001,** *20*, 719-724.

18.   Feller, R. L.; Curran, M.; Colaluca, V.; Bogaard, J.; Bailie, C. *Polym. Degrad. Stab.* **2007,** *92*, 920-931.

19.   Tyler, D. R. *Macromolecules Containing Metal and Metal-Like Elements* **2006,** *6*, 77-109.

20.   Grassie, N.; Scott, G., *Polymer Degradation and Stabilization.* Cambridge University Press: New York, 1985.

21.   Guillet, J., *Polymer Photophysics and Photochemistry: An Introduction to the Study of Photoprocesses in Macromolecules.* Cambridge University Press: New York, 1985.

22.   Sommazzi, A.; Garbassi, F. *Prog. Polym. Sci.* **1997,** *22*, 1547-1605.

23.   Scott, G.; Gilead, D.; Editors, *Degradable Polymers: Principles and Applications.* Chapman & Hall: New York, 1995.

24.   Hartley, G. H.; Guillet, J. E. *Macromolecules* **1968,** *1*, 413-417.

25.   Hartley, G. H.; Guillet, J. E. *Macromolecules* **1968,** *1*, 165-170.

26.   Kaczmarek, H. *Curr. Top. Polym. Res.* **2005,** 71-124.

27.   Roy, P. K.; Surekha, P.; Rajagopal, C.; Choudhary, V. *J. Appl. Polym. Sci.* **2008,** *108*, 2726-2733.

28.   Amin, M. U.; Scott, G. *Eur. Polym. J.* **1974,** *10*, 1019-1028.

29.   Mellor, D. C.; Moir, A. B.; Scott, G. *Eur. Polym. J.* **1973,** *9*, 219-225.

30.   Grassie, N.; Scott, G., *Polymer Degradation and Stabilisation.* Cambridge University Press: New York, 1985.

31.   Xu, J.; Shi, W.; Gong, M.; Yu, F.; Yan, L. *J. Appl. Polym. Sci.* **2005,** *97*, 1714-1724.

32.   Matsukawa, K. *J. Photopolym. Sci. Technol.* **2005,** *18*, 203-210.

33.   Hwu, J. R.; King, K. Y. *Chem.-Eur. J.* **2005,** 11, 3805-3815.

34.   Gonsalves, K.; Zhan-Ru, L.; Rausch, M. D. *J. Am. Chem. Soc.* **1984,** *106*, 3862-3863.

35.   Gonsalves, K. E.; Lenz, R. W.; Rausch, M. D. *Appl. Organomet. Chem.* **1987,** *1*, 81-93.

36.   Pittman, C. U., Jr. *J. Polym. Sci., Polym. Chem. Ed.* **1968,** *6*, 1687-1695.

37.   Tenhaeff, S. C.; Tyler, D. R. *Organometallics* **1991,** *10*, 1116-1123.

38.   Tenhaeff, S. C.; Tyler, D. R. *Organometallics* **1991,** *10*, 473-482.

39.   Tenhaeff, S. C.; Tyler, D. R. *Organometallics* **1992,** *11*, 1466-1473.

40.   Shultz, G. V.; Tyler, D. R. Preparation of Photoreactive Polymers by ADMET Polymerization of $(Cp(CH_2)_8CH=CH_2)_2Mo_2(CO)_6$ Macromolecules, to be submitted for publication.

41.   Geoffroy, G. L.; Wrighton, M. S., *Organometallic Photochemistry*. Academic Press: New York, 1979.

42.   Meyer, T. J.; Caspar, J. V. *Chem. Rev. (Washington, D. C.)* **1985,** *85*, 187-218.

43.   Shirai, M.; Suyama, K.; Okamura, H.; Tsunooka, M. *J. Photopolym. Sci. Technol.* **2002,** *15*, 715-730.

44.   Rivaton, A.; Gardette, J.-L.; Mailhot, B.; Morlat-Therlas, S. *Macromol. Symp.* **2005,** *225*, 129-146.

45.   Horie, K.; Mita, I. *Adv. Polym. Sci.* **1989,** *88*, 77-128.

46.   Khemani, K. C., *Degradable Polymers and Materials: Principles and Practice*. American Chemical Society: Washington DC, 2006; Vol. 939.

47.   Allen, N. S. *Photochemistry* **2003,** *34*, 197-266.

48.   Pospisil, J.; Pilar, J.; Billingham, N. C.; Marek, A.; Horak, Z.; Nespurek, S. *Polym. Degrad. Stab.* **2006,** *91*, 417-422.

49.   Le Huy, H. M.; Bellenger, V.; Paris, M.; Verdu, J. *Polym. Degrad. Stab.* **1991,** *35*, 171-179.

50. O'Donnell, B.; White, J. R. *J. Mater. Sci.* **1994,** *29*, 3955-3963.

51. Adam, W.; Bronstein, I.; Trofimov, A. V.; Vasil'ev, R. F. *J. Am. Chem. Soc.* **1999,** *121*, 958-961.

52. Braden, D. A.; Parrack, E. E.; Tyler, D. R. *Coord. Chem. Rev.* **2001,** *211*, 279-294.

53. Covert, K. J.; Askew, E. F.; Grunkemeier, J.; Koenig, T.; Tyler, D. R. *J. Am. Chem. Soc.* **1992,** *114*, 10446-10448.

54. Male, J. L.; Lindfors, B. E.; Covert, K. J.; Tyler, D. R. *J. Am. Chem. Soc.* **1998,** *120*, 13176-13186.

55. Mishra, R.; Tripathy, S. P.; Fink, D.; Dwivedi, K. K. *Radiat. Eff. Defects Solids* **2004,** *159*, 569-573.

56. Mishra, R.; Tripathy, S. P.; Fink, D.; Dwivedi, K. K. *Radiat. Meas.* **2005,** *40*, 754-757.

57. Celina, M.; Gillen, K. T.; Assink, R. A. *Polym. Degrad. Stab.* **2005,** *90*, 395-404.

58. Audouin, L.; Girois, S.; Achimsky, L.; Verdu, J. *Polym. Degrad. Stab.* **1998,** *60*, 137-143.

59. Balzani, V.; Carassiti, V., *Photochemistry of Coordination Compounds.* Academic Press: New York, 1970.

60. Thominette, F.; Verdu, J. *Polym. Prepr. (Am. Chem. Soc., Div. Polym. Chem.)* **1994,** *35*, 971-972.

61. O'Donnell, B.; Qayyum, M. M.; Tong, L.; White, J. R. *Polym. Prepr. (Am. Chem. Soc., Div. Polym. Chem.)* **1993,** *34*, 211-212.

62. O'Donnell, B.; Qayyum, M. M.; Tong, L.; White, J. R. *Plast., Rubber Compos. Process. Appl.* **1994,** *21*, 297-307.

63. Tong, L.; White, J. R. *Plast., Rubber Compos. Process. Appl.* **1996,** *25*, 226-236.

64. O'Donnell, B.; White, J. R. *Polym. Degrad. Stab.* **1994,** *44*, 211-222.

65. Busfield, W. K.; Monteiro, M. J. *Materials Forum* **1990,** *14*, 218-223.

66. Baumhardt-Neto, R.; De Paoli, M. A. *Polym. Degrad. Stab.* **1993,** *40*, 59-64.

67. Baumhardt-Neto, R.; De Paoli, M. A. *Polym. Degrad. Stab.* **1993**, *40*, 53-58.

68. Schoolenberg, G. E.; Vink, P. *Polymer* **1991**, *32*, 432-7.

69. Benachour, D.; Rogers, C. E. *ACS Symposium Series* **1981**, *151*, 263-74.

70. Igarashi, M.; DeVries, K. L. *Polymer* **1983**, *24*, 769-782.

71. Huvet, A.; Philippe, J.; Verdu, J. *Eur. Polym. J.* **1978**, *14*, 709-713.

72. Busfield, W. K.; Taba, P. *Polym. Degrad. Stab.* **1996**, *51*, 185-196.

73. Igarashi, M.; DeVries, K. L. *Polymer* **1983**, *24*, 1035-1041.

74. Plotnikov, V. G. *Doklady Akademii Nauk SSSR* **1988**, *301*, 376-379.

75. Shlyapnikov, Y. A.; Kiryushkin, S. G.; Marin, A. P., *Antioxidative Stabilization of Polymers*. Taylor and Francis: Bristol, PA, 1996.

76. Dogue, L. J.; Mermilliod, N.; Genoud, F. *J.Polym. Sci., Part A: Polym. Chem.* **1994**, *32*, 2193-2198.

77. Popov, A. A.; Blinov, N. N.; Vorob'eva, N. S.; Zaikov, G. E.; Karpova, S. G. *Kinetika i Kataliz* **1981**, *22*, 139-145.

78. Rabek, J. F., *Photostabilization of Polymers*. Elsevier: New York, 1990.

79. Zhurkov, S. N.; Zakrevskii, V. A.; Korsukov, V. E.; Kuksenko, V. S. *J. Polym. Sci., Polym. Phys. Ed.* **1972**, *10*, 1509-1520.

80. Chen, R.; Yoon, M.; Smalley, A.; Johnson, D. C.; Tyler, D. R. *J. Am. Chem. Soc.* **2004**, *126*, 3054-3055.

81. Tyler, D. R. In *Macromolecules Containing Metal and Metal-like Elements*, Aziz, A. S.; Carraher, J., C. E. ; Pittman, J., C. U.; Sheats, J.; Zeldin, M., Eds. John Wiley: New York, 2005; Vol. 6.

82. Zweifel, H.; Ed., *Plastics Additives Handbook, 5th Ed.* Hanser: Cincinnati, 2001.

83. Audouin, L.; Langlois, V.; Verdu, J.; de Bruijn, J. C. M. *J. Mater. Sci.* **1994**, *29*, 569-583.

84. Fraisse, F.; Morlat-Therias, S.; Gardette, J. L.; Nedelec, J. M.; Baba, M. *J. Phys. Chem. B* **2006,** *110*, 14678-14684.

85. Bigger, S. W.; Delatycki, O. *J. Polym. Sci., Part A: Polym. Chem.* **1987,** *25*, 3311-3323.

86. Sarkas, H. W.; Kwan, W.; Flom, S. R.; Merritt, C. D.; Kafafi, Z. H. *J. Phys. Chem.* **1996,** *100*, 5169-5171.

87. Ivanov, V. B.; Zhuravlev, M. A. *Polym. Photochem.* **1986,** *7*, 55-64.

88. Freitas, A. R.; Vidotti, G. J.; Rubira, A. F.; Muniz, E. C. *Polym. Degrad. Stab.* **2005,** *87*, 425-432.

89. Seguchi, T.; Tamura, N. *J. Phys. Chem.* **1973,** *77*, 40-44.

90. Waite, T. R. *Phys. Rev.* **1957,** *107*, 463-470.

91. Waite, T. R. *J. Chem. Phys.* **1958,** *28*, 103-106.

92. Waite, T. R. *J. Chem. Phys.* **1960,** *32*, 21-23.

93. Shimada, S.; Hori, Y.; Kashiwabara, H. *Polymer* **1977,** *18*, 25-31.

Chapter II

1. Pittman, C. U., Jr. *J. Polym. Sci., Polym. Chem. Ed.* **1968,** *6*, 1687-1695.

2. Pittman, C. U., Jr.; Rausch, M. D. *Pure Appl. Chem.* **1986,** *58*, 617-622.

3. Gonsalves, K.; Zhan-Ru, L.; Rausch, M. D. *J. Am. Chem. Soc.* **1984,** *106*, 3862-3863.

4. Gonsalves, K. E.; Lenz, R. W.; Rausch, M. D. *Appl. Organomet. Chem.* **1987,** *1*, 81-93.

5. Knobloch, F. W.; Rauscher, W. H. *J. Polym. Sci.* **1961,** *54*, 651-656.

6. Tenhaeff, S. C.; Tyler, D. R. *Organometallics* **1991,** *10*, 473-482.

7. Tyler, D. R. *Coord. Chem. Rev.* **2003,** *246*, 291-303.

8.   Tenhaeff, S. C.; Tyler, D. R. *Organometallics* **1992,** *11*, 1466-1473.

9.   Tenhaeff, S. C.; Tyler, D. R. *Organometallics* **1991,** *10*, 1116-1123.

10. Steigman, A. E.; Goldman, A. S.; Leslie, D. B.; Tyler, D. R. *J. Chem. Soc., Chem. Commun.* **1984,** 632-633.

11. Werfel, F.; Minni, E. *J. Physics C: Solid State Phys.* **1983,** *16*, 6091-6100.

12. Xie, G.; Jiang, Z. *Chin. Sci. Bull.* **2000,** *45*, 1562-1564.

13. Chen, R.; Yoon, M.; Smalley, A.; Johnson, D. C.; Tyler, D. R. *J. Am. Chem. Soc.* **2004,** *126*, 3054-3055.

14. Chen, R.; Tyler, D. R. *Macromolecules* **2004,** *37*, 5430-5436.

Chapter III

1.   Grassie, N.; Scott, G., *Polymer Degradation and Stabilisation.* Cambridge University Press: New York, 1985.

2.   Guillet, J., *Polymer Photophysics and Photochemistry: An Introduction to the Study of Photoprocesses in Macromolecules.* Cambridge University Press: New York, 1985.

3.   Hamid, S. H., *Handbook of Polymer Degradation.* 2nd Ed.; M. Dekker: New York, 1992.

4.   Rabek, J. F., *Mechanisms of Photophysical Processes and Photochemical Reactions in Polymers.* Wiley: New York, 1987.

5.   Geuskens, G. *Compr. Chem. Kinet.* **1975,** *14*, 333-424.

6.   Huvet, A.; Philippe, J.; Verdu, J. *Eur. Polym. J.* **1978,** *14*, 709-713.

7.   Cunliffe, A. V.; Davis, A. *Polym. Degrad. Stab.* **1982,** *4*, 17-37.

8.   Tenhaeff, S. C.; Tyler, D. R. *Organometallics* **1991,** *10*, 1116-1123.

9.   Tenhaeff, S. C.; Tyler, D. R. *Organometallics* **1991,** *10*, 473-482.

10. Tenhaeff, S. C.; Tyler, D. R. *Organometallics* **1992,** *11*, 1466-1473.

11. Nieckarz, G. F.; Tyler, D. R. *Inorganica Chimica Acta* **1996,** *242*, 303-310.

12. Nieckarz, G. F.; Litty, J. J.; Tyler, D. R. *J. Organomet. Chem.* **1998,** *554*, 19-28.

13. Tyler, D. R. *Coord. Chem. Rev.* **2003,** *246*, 291-303.

14. Chen, R.; Yoon, M.; Smalley, A.; Johnson, D. C.; Tyler, D. R. *J. Am. Chem. Soc.* **2004,** *126*, 3054-3055.

15. Chen, R.; Tyler, D. R. *Macromolecules* **2004,** *37*, 5430-5436.

16. Krisyuk, B. E.; Popov, A. A.; Zaikov, G. E. *Vysokomol. Soedin., Seriya A* **1980,** *22*, 329-334.

17. Male, J. L.; Lindfors, B. E.; Covert, K. J.; Tyler, D. R. *J. Am. Chem. Soc.* **1998,** *120*, 13176-13186.

18. Daglen, B. C.; Harris, J. D.; Dax, C. D.; Tyler, D. R. *Rev. Sci. Instrum.* **2007,** *78*, 074104/1-074104/4.

19. Gonsalves, K.; Zhan-Ru, L.; Rausch, M. D. *J. Am. Chem. Soc.***1984,** *106*, 3862-3863.

20. Gonsalves, K. E.; Lenz, R. W.; Rausch, M. D. *Appl. Organomet. Chem.***1987,** *1*, 81-93.

21. Knobloch, F. W.; Rauscher, W. H. *J. Polym. Sci.* **1961,** *54*, 651-656.

22. Nguyen, P.; Gomez-Elipe, P.; Manners, I. *Chem. Rev. (Washington, D. C.)* **1999,** *99*, 1515-1548.

23. Manners, I. *Coord. Chem. Rev.***1994,** *137*, 109-129.

24. Manners, I. *Adv. Organomet. Chem.* **1995,** *37*, 131-168.

Chapter IV

1.   Mishra, R.; Tripathy, S. P.; Fink, D.; Dwivedi, K. K. *Radiat. Eff. Defects Solids* **2004,** *159,* 569-573.

2.   Mishra, R.; Tripathy, S. P.; Fink, D.; Dwivedi, K. K. *Radiat. Meas.* **2005,** *40,* 754-757.

3.   Celina, M.; Gillen, K. T.; Assink, R. A. *Polym. Degrad. Stab.* **2005,** *90,* 395-404.

4.   Yamashita, T.; Tomitaka, H.; Kudo, T.; Horie, K.; Mita, I. *Polym. Degrad. Stab.* **1993,** *39,* 47-54.

5.   Audouin, L.; Girois, S.; Achimsky, L.; Verdu, J. *Polym. Degrad. Stab.* **1998,** *60,* 137-143.

6.   Chen, R.; Tyler, D. R. *Macromolecules* **2004,** *37,* 5430-5436.

7.   Meyer, T. J.; Caspar, J. V. *Chem. Rev. (Washington, DC)* **1985,** *85,* 187-218.

8.   Male, J. L.; Lindfors, B. E.; Covert, K. J.; Tyler, D. R. *J. Am. Chem. Soc.* **1998,** *120,* 13176-13186.

9.   Guillet, J., *Polymer Photophysics and Photochemistry: An Introduction to the Study of Photoprocesses in Macromolecules.* Cambridge University Press: New York, 1985.

10.   Dan, E.; Guillet, J. E. *Macromolecules* **1973,** *6,* 230-235.

11.   Lorand, J. P. *Prog. Inorg. Chem.* **1972,** *17,* 207-325.

12.   Balzani, V.; Carassiti, V., *Photochemistry of Coordination Compounds.* Academic Press: New York, 1970.

13.   Fried, J. R., *Polymer Science and Technology.* 1st ed.; Prentice Hall PTR: Upper Saddle River, New Jersey, 1995.

Chapter V

1.   Hepburn, C., *Polyurethane Elastomers*. 2nd ed.; Elsevier Science Publishers: Great Britain, 1992.

2.   Wilkes, G. L.; Bagrodia, S.; Humphries, W.; Wildnauer, R. *J. Polym. Sci., Polym. Lett. Ed.* **1975,** *13*, 321-327.

3.   White, J. R.; Rapoport, N. Y. *Trends Polym. Sci. (Cambridge)* **1994,** *2*, 197-202.

4.   Chen, R.; Tyler, D. R. *Macromolecules* **2004,** *37*, 5430-5436.

5.   Chen, R.; Tyler, D. R. *ACS Symposium Series* **2006,** *928*, 429-442.

6.   Chen, R.; Yoon, M.; Smalley, A.; Johnson, D. C.; Tyler, D. R. *J. Am. Chem. Soc.* **2004,** *126*, 3054-3055.

7.   De Haseth, J. A.; Andrews, J. E.; McClusky, J. V.; Priester, R. D., Jr.; Harthcock, M. A.; Davis, B. L. *Appl. Spectrosc.* **1993,** *47*, 173-179.

8.   Heintz, A. M.; Duffy, D. J.; Nelson, C. M.; Hua, Y.; Hsu, S. L.; Suen, W.; Paul, C. W. *Macromolecules* **2005,** *38*, 9192-9199.

9.   Elwell, M. J.; Ryan, A. J.; Grunbauer, H. J. M.; Lieshout, H. C. *Polymer* **1996,** *37*, 1353-1361.

10.   Sheth, J. P.; Klinedinst, D. B.; Pechar, T. W.; Wilkes, G. L.; Yilgor, E.; Yilgor, I. *Macromolecules* **2005,** *38*, 10074-10079.

11.   Vandenbelt, J. M.; Henrich, C. *Appl. Spectrosc.* **1953,** *7*, 171-176.

12.   Spectral Database for Organic Compounds SDBS Page. http://riodb01.ibase.aist.go.jp/sdbs/cgi-bin/direct_frame_top.cgi (accessed Jul 2008).

13.   McHale, J. L., *Molecular Spectroscopy*. 1st ed.; Prentice Hall: Upper Saddle River, NJ, 1999.

14.   Pimentel, G. C.; McClellan, A. L., *The Hydrogen Bond*. 1st ed.; W. H. Freeman & Co.: San Francisco, 1960.

15.   Shlyapnikov, Y. A.; Kiryushkin, S. G.; Marin, A. P., *Antioxidative Stabilization of Polymers*. Taylor and Francis: Bristol, PA, 1996.

16.   Dogue, L. J.; Mermilliod, N.; Genoud, F. *J. Polym. Sci., Part A: Polym. Chem.*
        1994, *32,* 2193-2198.

17.   Popov, A. A.; Blinov, N. N.; Krisyuk, B. E.; Karpova, S. G.; Neverov, A. N.;
        Zaikov, G. Y. *Vysokomol. Soedin., Seriya A* **1981,** *23,* 1510-1517.

18.   Rabek, J. F., *Photostabilization of Polymers.* Elsevier: New York, 1990.

19.   Krimm, S.; Folt, V. L.; Shipman, J. J.; Berens, A. R. *J. Polym. Sci.* **1963,** *Pt. A1,*
        2621-2650.

20.   Tasumi, M.; Shimauouchi, T. *Spectrochim. Acta* **1961,** *17,* 731-754.

Chapter VI

1.   Rivaton, A.; Gardette, J.-L.; Mailhot, B.; Morlat-Therlas, S. *Macromol. Symp.*
        2005, *225,* 129-146.

2.   Hwu, J. R.; King, K. Y. *Chem.--Eur. J.* **2005,** *11,* 3805-3815.

3.   Shimada, S.; Hori, Y.; Kashiwabara, H. *Polymer* **1981,** *22,* 1377-1384.

4.   Dogue, L. J.; Mermilliod, N.; Genoud, F. *J. Polym. Sci., Part A: Polym. Chem.*
        1994, *32,* 2193-2198.

5.   Seguchi, T.; Tamura, N. *J. Phys. Chem.* **1973,** *77,* 40-44.

6.   Waite, T. R. *Phys. Rev.* **1957,** *107,* 463-470.

7.   Waite, T. R. *J. Chem. Phys.* **1958,** *28,* 103-106.

8.   Waite, T. R. *J. Chem. Phys.* **1960,** *32,* 21-23.

9.   Shimada, S.; Hori, Y.; Kashiwabara, H. *Polymer* **1977,** *18,* 25-31.

10.   Hori, Y.; Shimada, S.; Kashiwabara, H. *J. Polym. Sci., Polym. Phys. Ed.* **1984,** *22,*
        1407-1415.

11.   Bond, G. C., *Metal-Catalysed Reactions of Hydrocarbons.* Springer: Uxbridge,
        2005; p 209 - 255.

12.   McAuley, K. B.; MacGregor, J. F.; Hamielec, A. E. *AIChE J.* **1990,** *36*, 837-850.

13.   Ebewele, R. O., *Polymer Science and Technology.* Chapman & Hall: 2000.

14.   Rabek, J. F., *Photodegradation of Polymers Physical Characteristics and Applications.* Springer: New York, 1996.

15.   Perrin, F. *Compt. Rend.* **1924,** *178*, 1978-1980.

16.   Turro, N. J., *Modern Molecular Photochemistry.* Addison-Wesley Publishing Co.: Reading, Mass., 1978; p 628.

17.   Balzani, V.; Carassiti, V., *Photochemistry of Coordination Compounds.* Academic Press: New York, 1970.

18.   Yoshida, H.; Ranby, B. *J. Polym. Sci., Part A: Gen. Pap.* **1965,** *3*, 2289-302.

19.   Rabek, J. F., *Polymer Photodegradation: Mechanisms and Experimental Methods.* Chapman & Hall: London, 1995.

20.   Aymard, C.; Shirts, R. B. *J. Chem. Educ.* **2000,** *77*, 1230-1232.

Appendix A

1.   Balzani, V.; Carassiti, V., *Photochemistry of Coordination Compounds.* Academic Press: New York, 1970.

2.   Nighswander-Rempel, S. P. *J. Fluoresc.* **2006,** *16*, 483-485.

3.   Kang, Q.; Gao, B. Y.; Hu, J.; Shen, D. *Adsorption* **2005,** *11*, 519-527.

4.   Salinaro, A.; Emeline, A. V.; Zhao, J.; Hidaka, H.; Ryabchuk, V. K.; Serpone, N. *Pure Appl. Chem.* **1999,** *71*, 321-335.

5.   Thennadil, S. N.; Martens, H.; Kohler, A. *Appl. Spectrosc.* **2006,** *60*, 315-321.

6.   Crosby, G. A.; Demas, J. N. *J. Phys. Chem.* **1971,** *75*, 991-1024.

7.   Beam of Light Technologies. http://www.z-bolt.com (accessed Jul 2008).

8.   Chen, R.; Tyler, D. R. *Macromolecules* **2004,** *37*, 5430-5436.

9.   Chen, R.; Yoon, M.; Smalley, A.; Johnson, D. C.; Tyler, D. R. *J. Am. Chem. Soc.* **2004,** *126*, 3054-3055.

10. Patterson, P. L. *J. Opt. Soc. Am.* **1972,** *62*, 627-633.

Appendix B

1.   Tenhaeff, S. C.; Tyler, D. R. *Organometallics* **1991,** *10*, 1116-1123.

2.   Covert, K. J.; Askew, E. F.; Grunkemeier, J.; Koenig, T.; Tyler, D. R. *J. Am. Chem. Soc.* **1992,** *114*, 10446-10448.